National Library of Canada
Bibliothèque nationale du Canada

Canadian Theses Service
Service des thèses canadiennes

Ottawa, Canada
K1A 0N4

NOTICE

The quality of this microform is heavily dependent upon the quality of the original thesis submitted for microfilming. Every effort has been made to ensure the highest quality of reproduction possible.

If pages are missing, contact the university which granted the degree.

Some pages may have indistinct print especially if the original pages were typed with a poor typewriter ribbon or if the university sent us an inferior photocopy.

Previously copyrighted materials (journal articles, published tests, etc.) are not filmed.

Reproduction in full or in part of this microform is governed by the Canadian Copyright Act, R.S.C. 1970, c. C-30.

AVIS

La qualité de cette microforme dépend grandement de la qualité de la thèse soumise au microfilmage. Nous avons tout fait pour assurer une qualité supérieure de reproduction.

S'il manque des pages, veuillez communiquer avec l'université qui a conféré le grade.

La qualité d'impression de certaines pages peut laisser à désirer, surtout si les pages originales ont été dactylographiées à l'aide d'un ruban usé ou si l'université nous a fait parvenir une photocopie de qualité inférieure.

Les documents qui font déjà l'objet d'un droit d'auteur (articles de revue, tests publiés, etc.) ne sont pas microfilmés.

La reproduction, même partielle, de cette microforme est soumise à la Loi canadienne sur le droit d'auteur, SRC 1970, c. C-30.

Canada

SPECIFYING TOLERANCE LIMITS FOR CONSTRUCTION IMPERFECTIONS IN REINFORCED CONCRETE COOLING TOWER SHELLS

by

ANGELOS ALEXANDRIDIS

A thesis
presented to the University of Ottawa
in fulfillment of the
thesis requirement for the degree of
PH.D.
in
CIVIL ENGINEERING

OTTAWA, Ontario, 1987

© Angelos Alexandridis, Ottawa, Canada, 1987.

Permission has been granted to the National Library of Canada to microfilm this thesis and to lend or sell copies of the film.

The author (copyright owner) has reserved other publication rights, and neither the thesis nor extensive extracts from it may be printed or otherwise reproduced without his/her written permission.

L'autorisation a été accordée à la Bibliothèque nationale du Canada de microfilmer cette thèse et de prêter ou de vendre des exemplaires du film.

L'auteur (titulaire du droit d'auteur) se réserve les autres droits de publication; ni la thèse ni de longs extraits de celle-ci ne doivent être imprimés ou autrement reproduits sans son autorisation écrite.

ISBN 0 315 46702 9

UNIVERSITÉ D'OTTAWA
UNIVERSITY OF OTTAWA

ABSTRACT

A comparison of maximum tolerances for meridional imperfection in cooling tower shells was made between the recently standardized guidelines of ACI 334 and the two published criteria of Croll and Al-Dabbagh. The comparison, based on the analysis of two shells having similar profile to the Ardeer tower and conforming to the steel requirements of the ACI guidelines, revealed significant differences between the predicted imperfection forces near the centre of the imperfection and the maximum permissible radial deviations at various levels in the two shells.

Based on the classical theory of thin elastic shells, a closed form solution was developed for imperfection forces occurring in the vicinity of a meridional imperfection having the form of a Cosine curve. This solution closely agrees with the results obtained from a finite element analysis. Furthermore, comparison of the forces calculated from the closed form solution and those calculated using Croll and Al-Dabbagh showed the closed form solution to more closely approximate the forces from the finite element analysis over the whole range of possible imperfection lengths.

The closed form solution pertaining to an elastic shell was further generalized to include the effect of vertical cracking which renders the shell orthotropic and also, the redistribution of forces from circumferential membrane to meridional bending which occurs during yielding of the circumferential steel. Assuming that a cooling tower shell can safely strain in the circumferential direction to twice the yield strain of steel while retaining sufficient bending resistance in the meridional direction to prevent a progressive type failure, a set of tolerance limits was derived for predicting the maximum permissible radial deviation at any level in a cooling tower shell. Unlike the recommended tolerances of the ACI, the derived tolerance limits relate to the geometry and the stresses in the shell. When compared to the published limitations of Croll and Al-Dabbagh, the derived limits of tolerance, which allow the shell to yield circumferentially, generally permit larger radial deviations in the more critically stressed zones near the base of a cooling tower shell. Furthermore, unlike Croll and Aldabbagh, the derived tolerance limits permit imperfections of very short length characteristic of a kink in the perfect meridian.

ACKNOWLEDGEMENTS

In connection with this thesis, the author wishes to express his sincere appreciation to the following individuals:

To Professor N. J. Gardner for his helpfull advice and encouragement as supervisor of this thesis

To his entire family for their continuous patience and understanding

To Miss Susan Saydeh for her humour and good nature

LIST OF TABLES

LIST OF FIGURES

NOMENCLATURE

A_1 to A_9	coefficients pertaining to the circumferential strain for the orthotropic yielded shell, equation (7-14)
B_1 to B_4	real arbitrary constants, equation (6-5)
C_1 to C_3	coefficients for symmetric and anti-symmetric terms, equation (6-7)
E	Young's modulus
F	statically equivalent load for slope imperfection, equation (3-7b)
H	imperfection length, Figure 4=1
J_0 to J_3	parameters as defined on page 75
K	shell bending stiffness defined on page 31
L	imperfection wavelength, Figure 4-1
M_θ, M_ϕ	bending moment per unit length, Figure 3-4
N_θ, N_ϕ, $N_{\theta\phi}$	in-plane stress resultant per unit length, Figure 1-2
p	minimum circumferential steel ratio, equation (5-5a)
P	statically equivalent load for curvature imperfection, equation (3-7a)
P_x, P_y, P_z	force per unit area acting on shell, Figure 1-2
Q_ϕ	shear force per unit length, Figure 3-4
r_1, r_2, r_3, r_0	shell radii, Figure 1-1
r_3	distance to the shell axis measured along the projection of the local tangent, Firure 3-5
R	cylindrical radius

S	meridional distance conveniently measured from the centre of an imperfection, Figures 3-1, 3-5
t	shell thickness
U	coefficients pertaining to the circumferential strain for the orthotropic, elastic shell, equation (7-13)
W	normal component of displacement, Figure 3-5
Z	vertical ordinate in shell of revolution
α	shell parameter as defined on page 87, 111
α'	overstress factor in the vertical steel, equation (4-5b)
β	coefficient pertaining to imperfection bending moment defined in equations (6-12a), (7-6a) and plotted in Figures 6-8, 7-3
Γ	coefficient pertaining to imperfection circumferential force defined in equations (6-12b), (7-6b) and plotted in Figures 6-8, 7-3
δ	symbol denoting change
Δ	radial deviation, Figure 4-1
ϵ	direct strain
η	overstress factor in the vertical steel, equation (7-20b)
λ	shell parameter as defined on page 71, 111
λ'	perturbation factor defined on page 124
μ_1, μ_2	coefficients in equations (6-12), (7-6)
ν	Poisson's ratio
ξ	function defining meridional deviation with respect to the perfect meridian, Figure 3-1
ξ_i	imperfection height, Figure 4-1
ρ	reinforcing steel ratio

χ	meridional rotation, Figure 3-5
Ψ	coefficient pertaining to imperfection force increase associated with the P-Δ effect, defined on page 90 and plotted in Figure 6-9
θ (subscript)	circumferential direction
ϕ (subscript)	meridional direction
* (superscript)	membrane solution
p (superscript)	perfect shell
y (superscript)	yielded shell

CONTENTS

Chapter I

INTRODUCTION

1.1 THIN SHELLS

A shell is a surface structure the surface of which has curvature in one or two directions. If the thickness is much smaller than all other dimensions, the shell is more specifically termed a thin shell.

In general, shells are classified according to their geometry or method by which they are generated. In the case of doubly curved surfaces, shells having both principal radii of curvature on the same side of the surface, as in the case of a dome, are referred to as having a positive curvature, otherwise the shell is said to have a negative curvature as is the case for the hyperboloid of revolution.

An important class of shells are generated by revolving a plane curve about an axis in its plane. Such shells are referred to as shells of revolution. The generating curve is called the meridian and its plane the meridian plane. The radii of principal curvature are those of the meridian denoted r_1 and the distance along the normal from the axis of revolution to the surface denoted r_2 , Figure 1-1 . For the

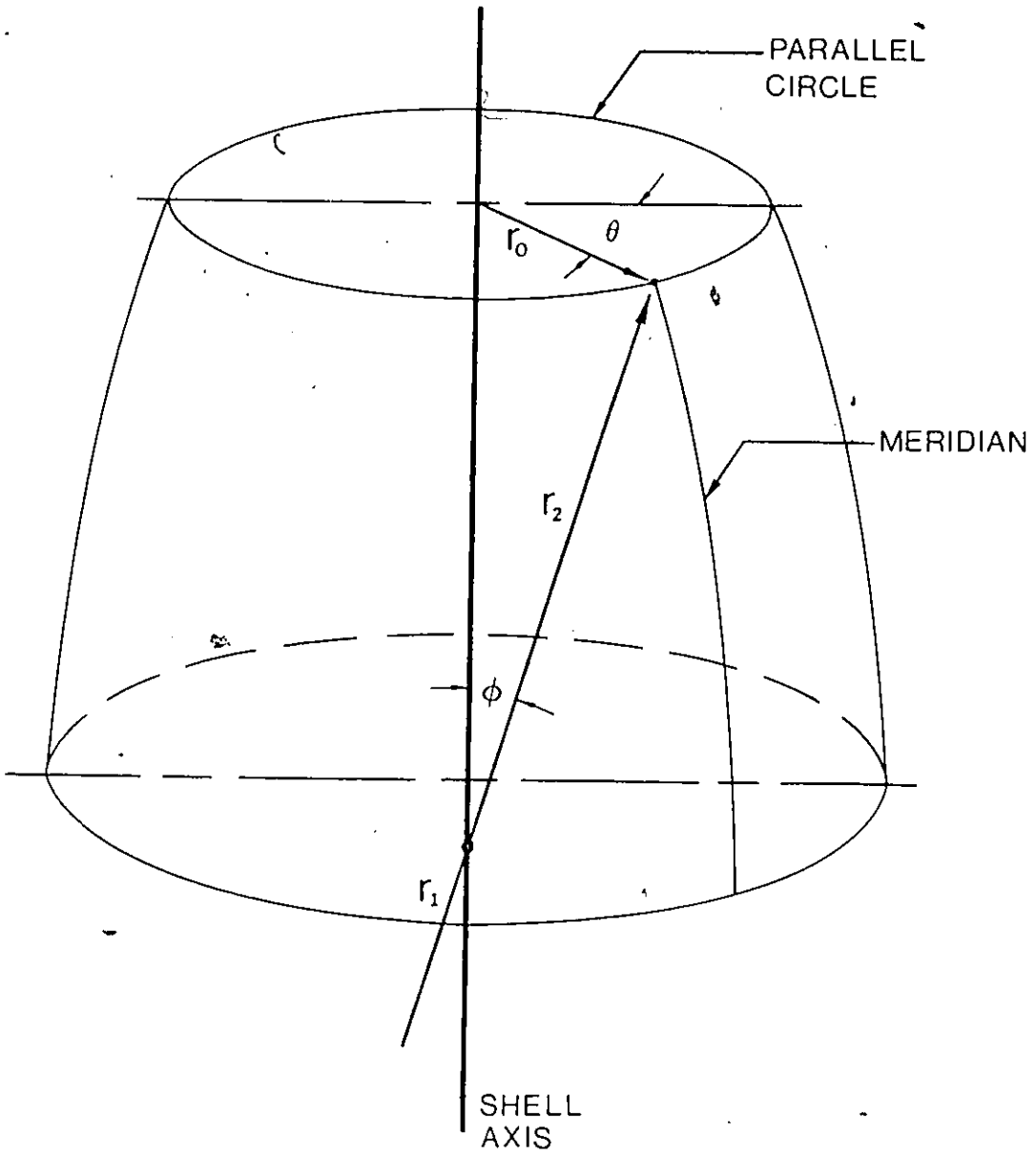

Figure 1-1 Shell of revolution

hyperboloid of revolution r_1 and r_2 lie on opposite sides of the surface.

Ideally, thin shells resist external loads through the development of in-plane or membrane forces. For example, doubly curved shells having positive curvature, such as a dome, transmit loads to the supports primarily by compressive arching forces whereas negative curvature shells, such as the hyperbolic shell of revolution, also utilize in-plane shear as a prime mechanism for resisting external loads.

The stress resultants corresponding to the membrane theory are illustrated in Figure 1-2. The condition for static equilibrium yields three independent equations rendering these resultants determinate. These equilibrium equations, though not presented here, can be found in any standard textbook for shell theory (1,2,3). It should be noted that these equations satisfy equilibrium but in general violate compatibility and boundary conditions. Consequently, membrane action may not be sufficient to fully describe the true behaviour of a shell and bending terms must be included in the analysis to restore compatibility. Bending can be induced by abrupt changes in loading or shell geometry while the extent of significant bending depends on the particular shell geometry.

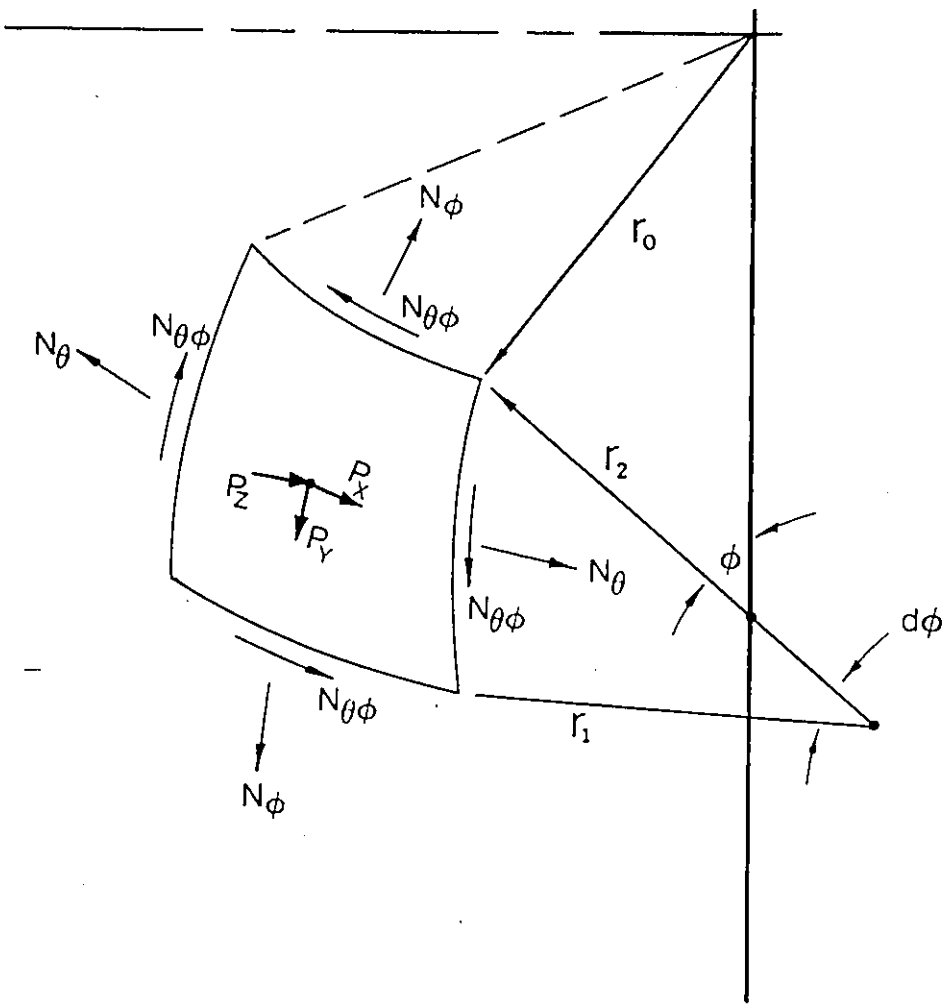

Figure 1-2 Membrane forces for a shell of revolution

1.2 HYPERBOLIC COOLING TOWER

Recent decades have seen increased use of shell like forms in structural engineering. Of particular interest to the civil engineer is the cooling tower used to dissipate excess heat during the generation of electricity or certain industrial processes. Although in the past, such heat was given up directly into naturally occurring bodies of water, the associated thermal pollution has made the cooling tower a desirable alternative.

Cooling towers can be classified as wet or dry. Wet cooling towers achieve cooling by evaporation while dry cooling towers cool by conduction and convection in much the same way as an automobile radiator. For economic reasons, wet-type cooling towers are more beneficial although in the case of nuclear power plants the dry-type are preferred in order to minimize the loss of radio active cooling water to the surrounding environment.

Cooling towers can further be classified as natural-draught or mechanical-draught. In a mechanical-draught tower, air is forced through by large driven fans. Such towers are smaller and less expensive to build than natural-draught ones, but their operating costs are comparably higher. Present trends are towards larger, hyperbolic, natural-draught towers similar to the one illustrated in Figure 1-3. Here, warm water is sprayed over baffles which encourages

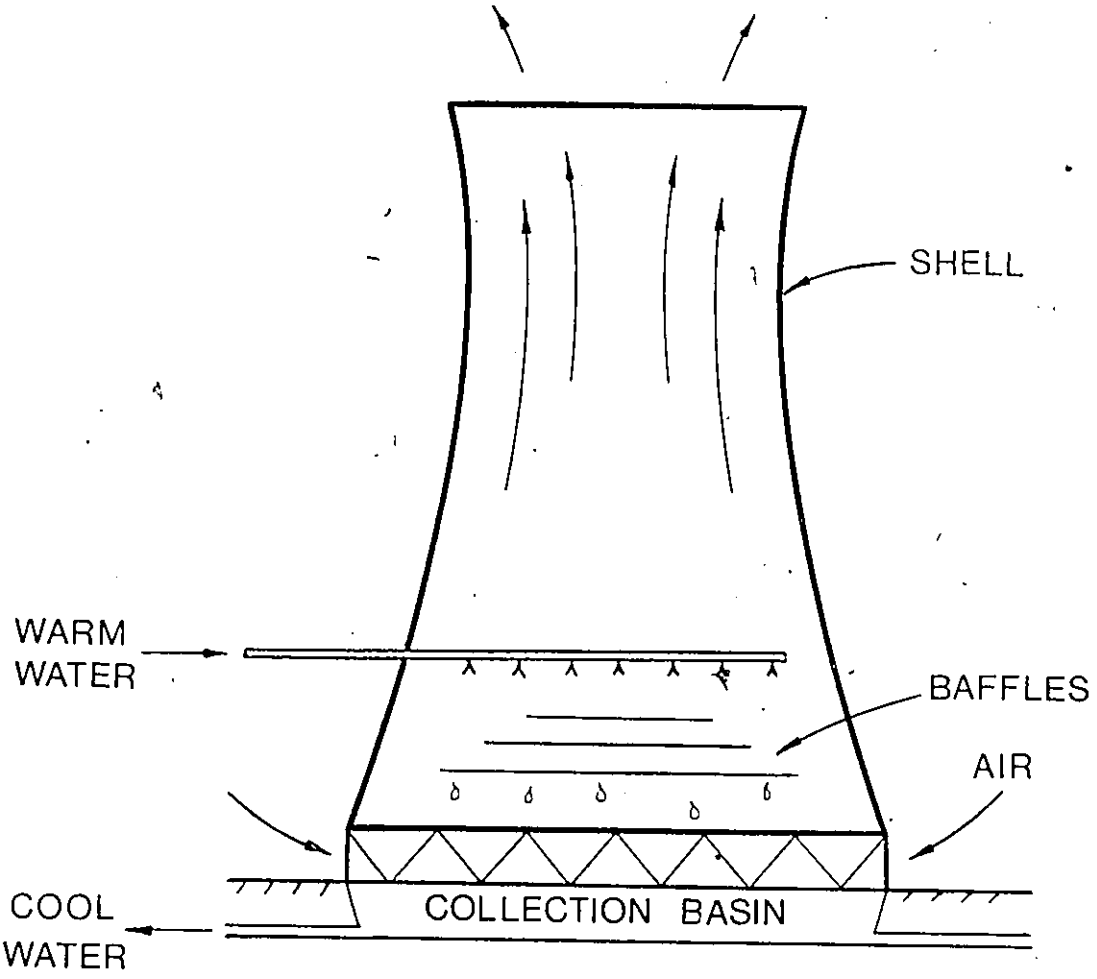

Figure 1-3 Wet, natural-draught cooling tower

evaporation and is then allowed to drip down to a collection basin. Outside air is naturally drawn in at the base of the tower to replace the warmer, less dense air which rises out of the tower.

1.3 CONSTRUCTION OF COOLING TOWER SHELLS

Natural-draught cooling towers are comprised of a number of structural units such as the shell, supporting columns or truss, foundation, fill support system and cold water basin. In consideration of its size and with the present trend towards fewer but larger towers, the shell requires particular attention. The demand for dry-type cooling of power generating plants has led to shell heights exceeding 160 m (525 ft) and recently, heights of 200 m (656 ft) or more have been considered giving rise to unique problems of construction and design.

To date, cooling tower shells have been successfully constructed from :

(1) Reinforced concrete using climbing formwork.

(2) Steel cable network acting as a veil and supported by a central pylon.

(3) Reinforced concrete precast elements.

(4) Steel.

However, not all of these alternatives have proved to be economical solutions. In a 1980 publication (4), Zerna and

Mungan have reported that in Germany, steel construction has not found wide application and the use of precast elements has proved uneconomical because of the requirement for special mounting equipment and methods. Similarly, the use of a cable network is uneconomical because of the large foundation associated with the central pylon and cable anchors, and because the cables inherently resist only tensile force. The report concluded that with increasing height, reinforced concrete using climbing formwork constitutes the most suitable solution.

Zerna and Mungan further reported that for cooling tower shells of reinforced concrete, the use of circumferential stiffening rings becomes economically desirable beyond a certain size in order to provide adequate buckling resistance. This latter conclusion was based on some numerical studies of fictitious cooling tower shells and is somewhat uncertain as no ring stiffened cooling tower with a large number of rings had at the time been built.

In North American practice, The American Concrete Institute (5) recommends adequate stiffening of the top and the base of the shell. Should additional stiffness be needed to improve the buckling characteristics, preferance is given to a gradual thickening of the shell wall so as to avoid local stress disturbances. The following investigation therefore, deals with the conventional reinforced concrete cooling tower shell having no intermediate stiffening rings.

1.4 DESIGN OF REINFORCED CONCRETE COOLING TOWER SHELLS

In the design of cooling tower shells, the size and shape are normally dictated by thermodynamic considerations pertaining to the cooling demands of the tower. The minimum shell thickness is determined on the basis of preventing local or overall buckling while the steel reinforcement is chosen so as to conform to the stresses arising from the various external load combinations which are likely to occur during its service life.

During its operational lifespan, a cooling tower shell must adequately resist forces due to gravity, wind and possibly earthquake. Additional loads resulting from internal suction and thermal gradients during operation must also be considered.

Presently, much emphasis is placed on wind action which appears to have stemmed from the well publicized failure of three cooling tower shells at Ferrybridge (6,7), England, in 1965. These towers, standing 114 metres (374 ft) high and having 12.7 cm (5 in) thick shells collapsed during severe wind conditions. A study concerning the cause of failure (8) found vertical tower stresses sensitive to minor changes in the assumed wind load. This is illustrated in Figure 1-4 for the case of one isolated tower. where, for the windward side of the tower, a condition of meridional tension exists at wind speeds exceeding 80 MPH (129 Km/h). Such stress sensi-

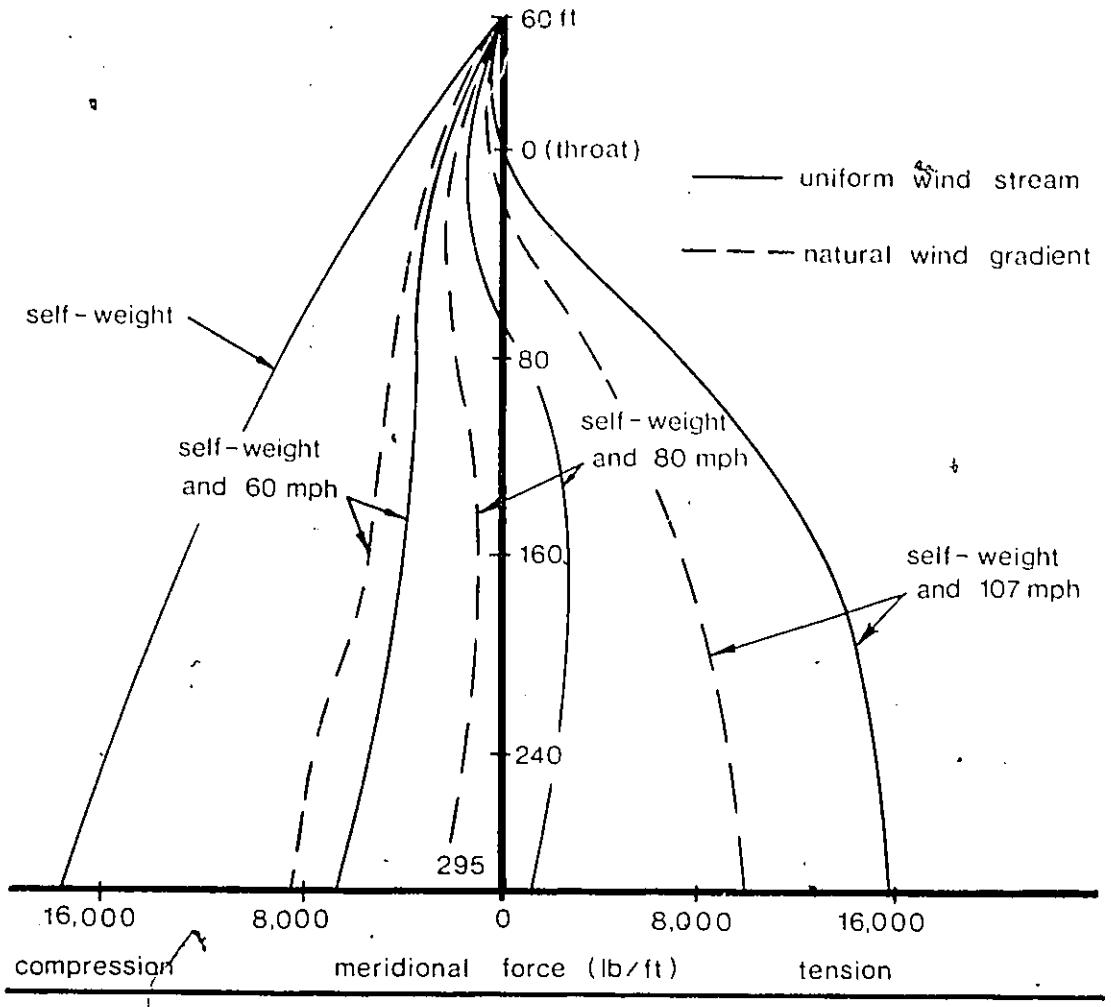

Figure 1-4 Variation in the maximum meridional force in the wall of the Ferrybridge tower for different wind velocities

tivity arises because, meridional compression is resisted by the combined action of steel and concrete, but tension being the difference between the downward force of self weight and the upward lift of the wind is resisted only by the steel. An underestimation of the overturning action of the wind therefore, leads to a critical condition of vertical tension.

In general, wind forces on a cooling tower can be described as

$$q_{z\theta} = q_z \bar{G} H_\theta \qquad (1\text{-}1)$$

where q_z describes the vertical pressure profile, H_θ a function of the circumferential distribution and $\bar{G}$ a gust response factor depending on the dynamic response of the structure to turbulence (5,9). The circumferential pressure distribution can be described in terms of angle increments with respect to the windward meridian by the symmetrical Fourier series

$$H_\theta = \sum A_n \cos(n\theta) \qquad (1\text{-}2)$$

Niemann (10), reported a set of coefficients for H_θ obtained from measurements on a full scale hyperbolic cooling

HARMONIC n	COEFFICIENT A_n	* COEFFICIENT A_n
0	−.3923	−.11670
1	.2602	−.27918
2	.6024	−.61978
3	.5046	−.50927
4	.1064	−.09167
5	−.0948	.11794
6	−.0186	.03333
7	.0468	−.04474
8		−.00833
9		−.00972
10		−.01356
11		−.11597
12		−.01667

Table 1-1 Fourier coefficients for calculating circumferential wind variation (* Including internal suction)

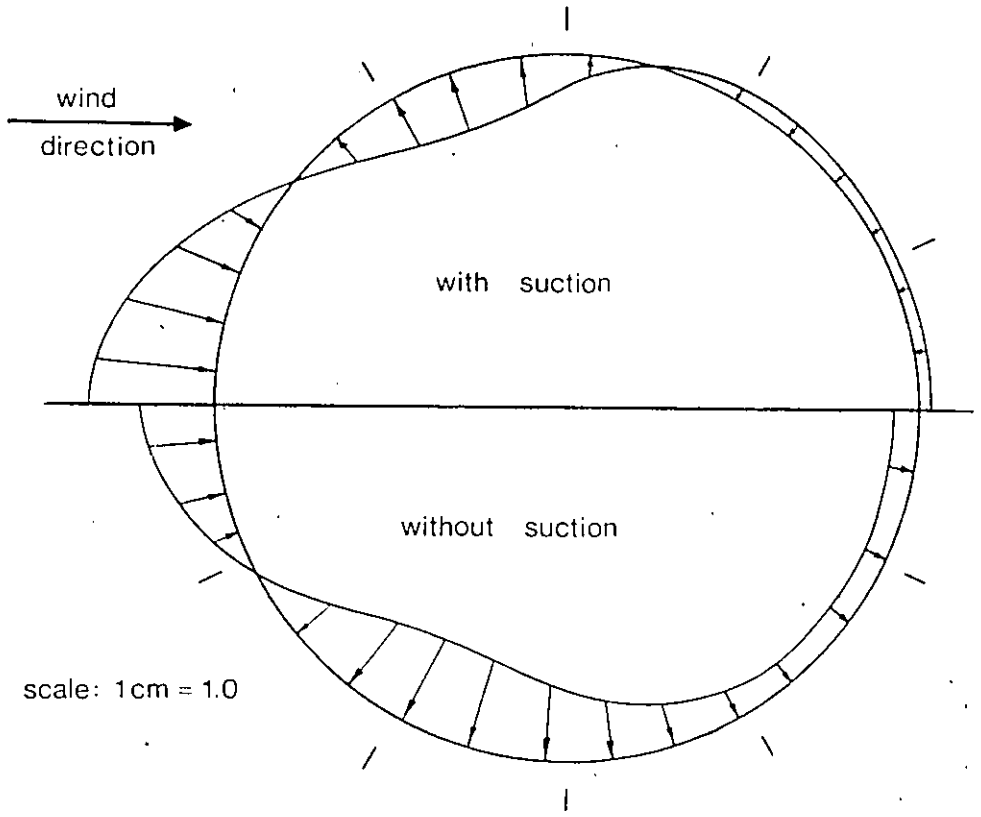

Figure 1-5 Normalized circumferential pressure distribution

tower. The coefficients A_n , corresponding to the first eight harmonics of equation (1-2) are tabulated in Table 1-1 and the corresponding normalized variation illustrated in Figure 1-5. Furthermore, the International Association for Shell and Spatial Structures (11) has recommended an internal suction coefficient of 0.5 be algebraically added to all external pressure coefficients H_θ.

Present practice is to analyze cooling tower shells in accordance with recognized theories for the bending of thin elastic shells taking due account of the design geometric profile, thickness variations and support conditions. However, the ACI does endorse analyses based on the membrane theory provided realistic boundary conditions are considered and local bending (upper and lower edges) is accounted for by an appropriate method. It is commonly assumed that concrete remains uncracked, homogeneous and isotropic.

This method of analysis briefly described is valid under the assumption that computed deformations fall within the limits of the applied theory and that the shell geometry suffers only negligible imperfections. Otherwise, both the bending effects and the calculated buckling resistance may be significantly different from reality.

Chapter II

IMPERFECT COOLING TOWER SHELLS

2.1 COOLING TOWER IMPERFECTIONS

Beginning in the early 1950's, numerous publications appeared discussing both analytical and numerical techniques relevant to the analysis of the hyperbolic cooling tower shell. These reports based their developments on relatively simple and ideal shapes giving no consideration to imperfections that result from the best of construction practices. Even though imperfections exist in all structures, cooling tower shells are more difficult to build than most structures and hence must be considered more prone to errors of construction due to their large size and relative thinness.

2.2 IMPORTANCE OF COOLING TOWER IMPERFECTIONS

The importance of construction imperfections is yet unclear and has resulted on occasions in different points of view. Zerna, Kratzig and Mungan (12) investigating German cooling tower practice reported the results of a survey along 48 meridians and more than 100 lifts for the Mulheim-Karlich tower. The maximum deviation of the wall thickness was found to be about 10% and the largest amplitude of radi-

al deviation 3.2 cm (1.3 in). Their conclusions generalized that such low values can be tolerated and need not be considered in cooling tower design.

Kemp and Croll (13) analyzing the Ardeer tower collapse suggested that erection procedures had led to errors of 30 to 60 cm (12 to 24 in) in the horizontal radius. Given the known sensitivity of stresses to changes in shell profile, it was concluded that more work is necessary to assist the engineer responsible for making judgements as to the admissible constructional tolerances.

In North America, the 1984 ACI guidelines for reinforced concrete cooling tower shells acknowledge the adverse effect of construction deformities and specify that imperfections either be accounted for in the analysis of the shell or be checked against field tolerances during the construction phase. However, there is some ambiguity as to what field tolerances to use. The recommended tolerances of the ACI appear somewhat arbitrary in that they represent typical values based on a survey of tower manufacturers. The accompanying commentary does little to clarify this point.

2.3 ARDEER TOWER COLLAPSE

The consequences of shell imperfections on cooling tower safety was demonstrated by the collapse of an industrial cooling tower at Ardeer, Scotland (14) and recently, by the collapse of a fourth tower at Ferrybridge, England (15,16).

In the case of the Ardeer tower, failure came as a surprise because this tower's design incorporated the recommendations of improved practice following the earlier failures at Ferrybridge. According to the article in New Civil Engineer, the wind speed at the time of collapse was below speeds the tower had previously withstood. Because, numerous other towers also incorporated the same recommendations emphasizing the importance of wind action, interest was shown in determining the cause of the collapse so as to modify existing design practices and prevent failures of a similar type. In particular, consideration was given as to how deviations from the specified shape affected the theoretical stress distributions.

In a report published by the Imperial Chemical Industries Limited (17), details of calculations carried out for the Committee of Inquiry investigating the Ardeer collapse were presented. These calculations indicated that hoop tensions developed in the vicinity of the greatest imperfection could be resisted by the concrete up to the design wind speed of 120 MPH (193 Km/h). However, if vertical cracking

were to occur across this imperfection, as was observed to have occurred in the Ardeer tower, failure of the circumferential steel at the level of imperfection would be anticipated at a lower wind speed of between 60 and 80 MPH (97 and 129 km/h). In actuality, collapse occurred at an estimated wind speed of 70 to 80 MPH (113 to 129 km/h).

Although other possibilities for the collapse were investigated, the Ardeer committee concluded that the presence of surface imperfections played a major role in the tension failure of the circumferential reinforcement. As a consequence, it was recommended that 'further studies of the effects of geometrical imperfections on the stresses in cooling towers are required to enable rational procedures to be developed for specifying the permissible tolerances in shape and the related minimum percentages of circumferential reinforcement'.

2.4 STANDARDIZED CONSTRUCTION TOLERANCE LIMITS

Despite the lack of research and recognized publications on which to base any design recommendations, the British Standards Institute (18) in 1975 proposed the following guidelines:

(1) The maximum error in meridional slope should not exceed 1% .

(2) The maximum error in horizontal radius in conjunction with (1) should not exceed 50 mm (2 in) excluding survey inaccuracies.

(3) The reinforcement in both directions should not be less than 0.20% of the gross concrete area.

Similar tolerance limits were proposed in 1984 by the American Concrete Institute (5) :

(1) A slope deviation per lift of 1.3 to 1.7 percent.

(2) A radius deviation of 2 in (50 mm).

(3) A Wall thickness deviation of -0.5 in (13 mm).

(4) Reinforcement in each direction should not be less than 0.35% of the gross cross-sectional area of the concrete.

It is emphasized that these design recommendations are based largely on intuition and do not appear to take account of the particular shell characteristics. Further, the specified minimum steel percentage of the BSI is significantly lower than the value adopted by the ACI.

Chapter III

IMPERFECTION FORCES-THEORETICAL BACKGROUND

3.1 EFFECT ON MEMBRANE STRESS RESULTANTS

In most cases, the assumption of membrane action is insufficient to predict the true elastic behaviour of a shell since external loads will cause flexure or bending. However, for shell problems where symmetry of form and loading prevails, the membrane theory can lead to reasonably accurate results. Such would be the case, for example, where a closed cylindrical shell is subjected to external pressure or a vertically standing cylinder resists its own weight. Although limited in scope, such cases offer a simple yet intuitive approach to understanding the nature of stresses arising from geometrical imperfections.

In shells of revolution where the loading is axisymmetric, the stress resultant $N_{\theta\phi}$ must vanish as it would produce unsymmetrical deformation about the main axis. The remaining two stress resultants N_θ, N_ϕ can readily be calculated through the condition of static equilibrium.

By considering axial equilibrium, N_ϕ is given by

$$N_\phi \left(\frac{2\pi r_o^2}{r_2}\right) = \int_0^\phi 2\pi r_o \left(P_Y r_1 \sin\phi + P_Z r_1 \cos\phi\right) d\phi \qquad (3\text{-}1a)$$

while N_θ can be found from the radial equilibrium equation

$$\frac{N_\phi}{r_1} + \frac{N_\theta}{r_2} + P_Z = 0 \qquad (3\text{-}1b)$$

An arbitrary imperfection will in some way distort the meridian of the perfect shell. In studying the consequences of such a meridional imperfection, a small deviation may be expressed as a function $\xi(S)$ measured normal to the perfect meridian as shown in figure 3-1.

In general, this imperfection will affect the geometry of the perfect shell as well as the stress resultants. The changes, denoted here by the symbol δ, are found by differentiating equations (3-1)

$$\frac{\delta N_\phi}{r_2} + N_\phi \delta\left(\frac{1}{r_2}\right) = 0 \qquad (3\text{-}2a)$$

$$\frac{\delta N_\phi}{r_1} + N_\phi \delta\left(\frac{1}{r_1}\right) + \frac{\delta N_\theta}{r_2} + N_\theta \delta\left(\frac{1}{r_2}\right) = 0 \qquad (3\text{-}2b)$$

where changes in the circumferential radius r_o have been ignored. By geometry

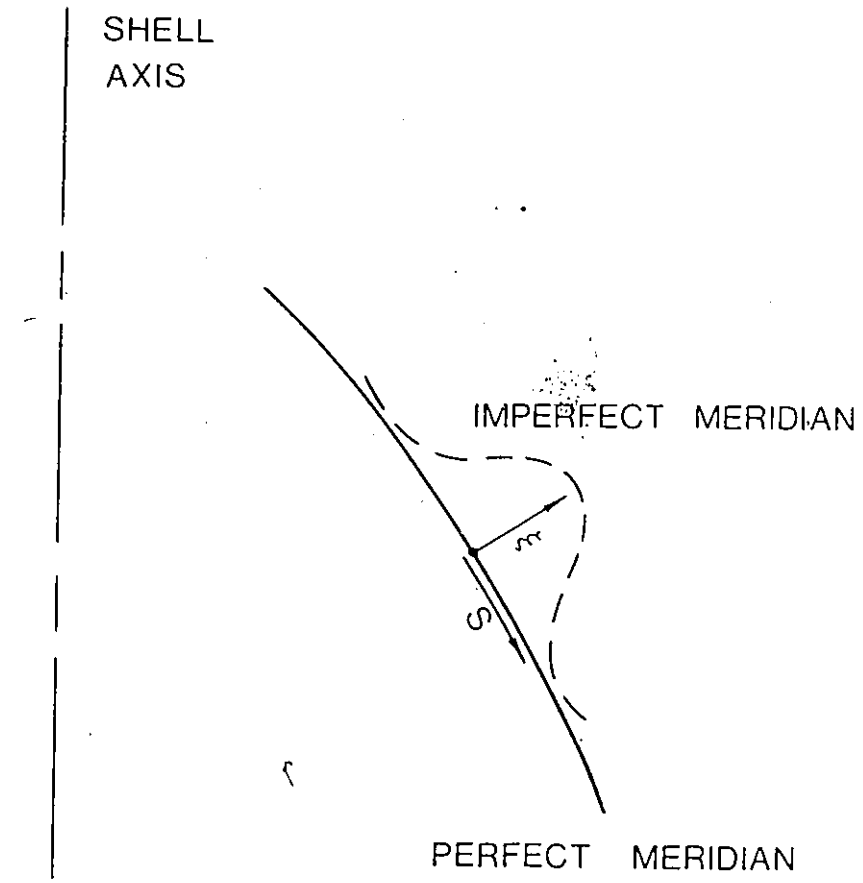

Figure 3-1 Specification of meridional imperfection

$$\delta\left(\frac{1}{r_1}\right) \cong -\frac{d^2\xi}{dS^2} \qquad (3\text{-}3a)$$

$$\delta\left(\frac{1}{r_2}\right) \cong -\frac{d\xi/dS}{r_3} - \frac{\xi}{r_2^2} \qquad (3\text{-}3b)$$

For small imperfections, it is reasonable to assume that the slope $d\xi/dS$ and the height of the imperfection ξ are negligible quantities so that the changes $\delta(\frac{1}{r_2})$ may be ignored with little error introduced. Substituting this result into equations (3-2) leads to the conclusion

$$\delta N_\phi = 0 \qquad (3\text{-}4a)$$

$$\delta N_\theta = r_2 N_\phi \frac{d^2\xi}{dS^2} \qquad (3\text{-}4b)$$

Hence, the consequence of a meridional imperfection is to have no effect on the meridional force N_ϕ whereas the circumferential force N_θ is influenced - the degree of this influence being governed by the magnitude of N_ϕ and the severity of the imperfection as given by the curvature $d^2\xi/dS^2$.

Although an approximation, the foregoing conclusion has been substantiated in practice. Flugge (1), used the membrane theory to examine the effects of axisymmetric discontinuities in the meridional curvature of a hemispherical

dome. Although the imperfections considered were small in comparison to the over-all dimensions of the shell, the actual radius of curvature of the middle surface in the region of the imperfection differed significantly from the theoretical curvature used in computing the perfect membrane forces. The results of Flugge's membrane analysis indicated that the meridional forces were not visibly different from those of an exact hemisphere while the circumferential forces deviated markedly in the vicinity of the imperfections.

However, Flugge reported that such stress concentrations were not important since when bending action is included, the circumferential force would then make 'only a feeble attempt to follow .... the high (stress) peaks' that are predicted by the membrane analysis. In a later section of his book, it was similarly suggested that deviations of the order of magnitude of the wall thickness in cylindrical shells 'are not a matter of great concern'.

In a subsequent publication, Soare (19) considered imperfections in the meridian of a hyperbolic cooling tower shell subjected to non-axisymmetric loading, Figure 3-2. Like Flugge, Soare's analysis neglected bending action and assumed that external loads arising from self weight, seismic action and wind action were fully resisted by membrane forces. Some results of his analysis, for the case of wind load, are illustrated in Figure 3-3.

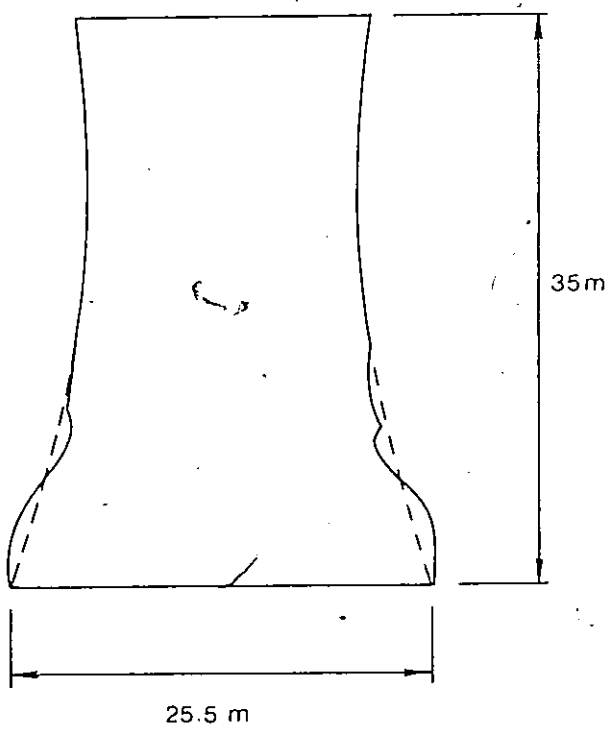

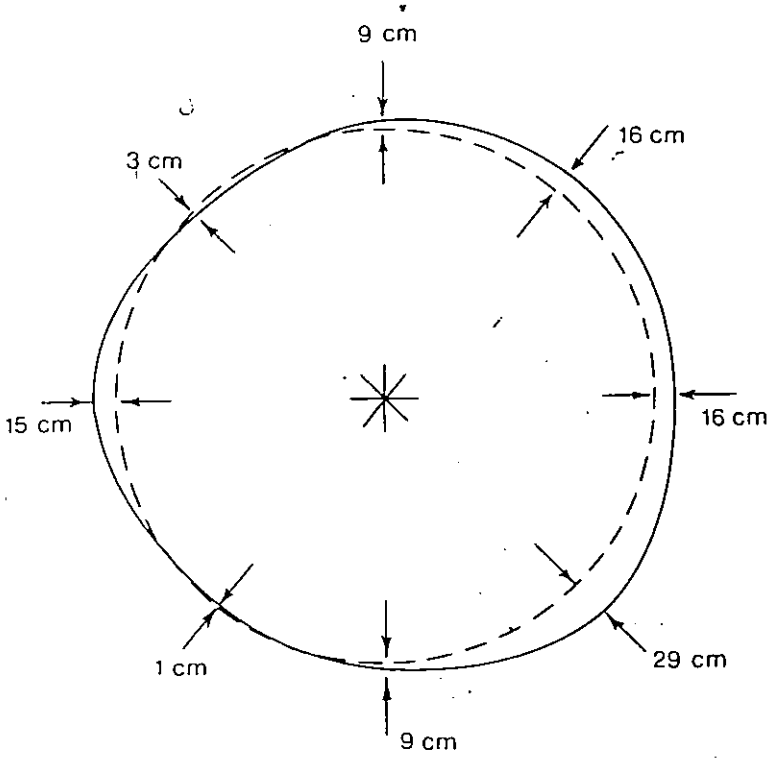

(a) Typical meridional section (b) Typical parallel section

Figure 3-2 Soare's imperfect cooling tower shell

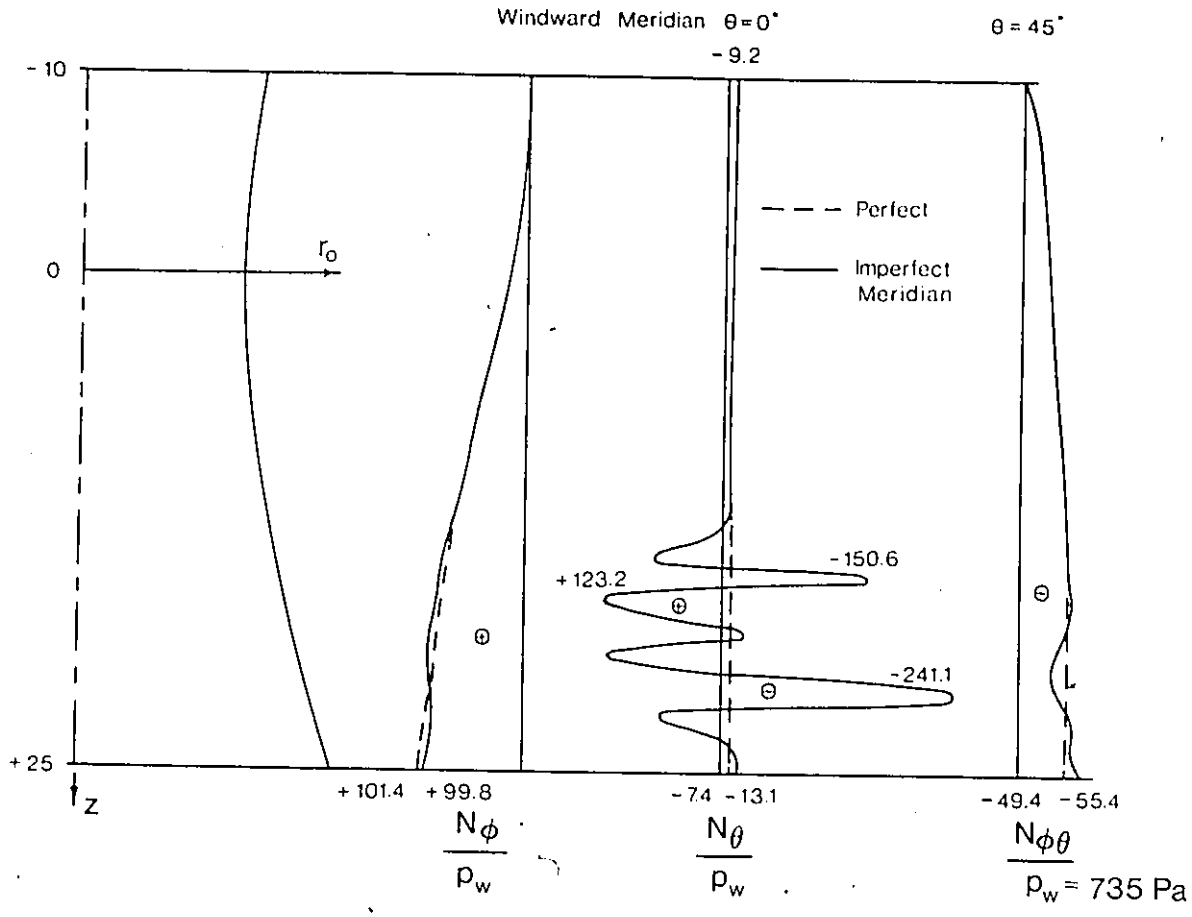

Figure 3-3 Results of Soare's membrane analysis for wind load

Contrary to Flugge's earlier conclusions, Soare emphasized that for the cooling tower shell considered, having imperfections of the same order as the wall thickness, little variation for the meridional and shearing forces result while the circumferential forces are strongly influenced. More importantly, the circumferential tensions induced could be of a greater magnitude than the maximum meridional compression occurring in the tower during the overturning action of the wind (a mode of failure which at the time was not incorported in the design process). However, it appears that this finding could not make any design impact since Soare's use of the membrane theory raised the question as to whether the inclusion of bending terms could in fact eliminate the high stress peaks as was claimed by Flugge. To this effect, Soare offered little insight, allowing Flugge's earlier ascertion to be invoked.

3.2 INCLUSION OF BENDING TERMS

Calladine (20), has examined the effect of imperfections when bending action is included for shells of revolution subjected to axisymmetric load. For such a shell, the stress resultants acting on any small element are shown in Figure 3-4.

In classical shell theory, the radial distances r_0, r_1 and r_2 along with the angular distances θ and ϕ completely

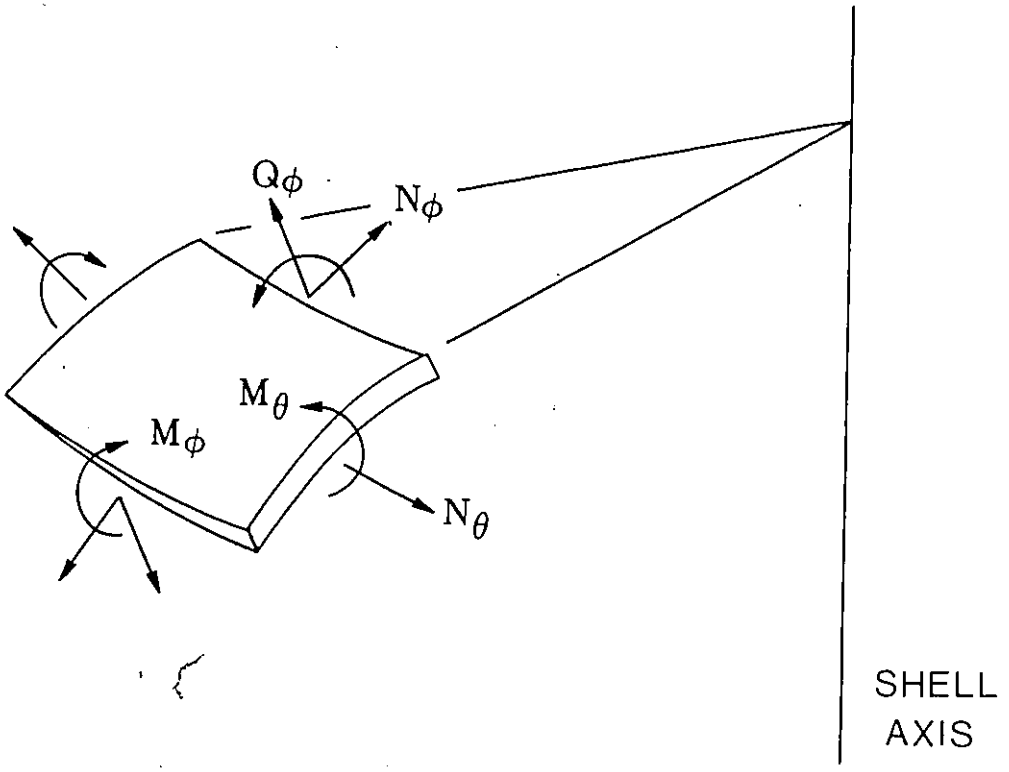

Figure 3-4 Stress resultants for symmetrically loaded thin shell of revolution

define the geometry of the problem. By introducing the variable r_3 (the distance to the shell axis measured along the projection of the local tangent) and the variable S (the distance along the meridian from some arbitrary reference point), Figure 3-5, Calladine restated the classical equations for thin shells of revolution in a simplified form. For reference in subsequent chapters, these equations are presented here as

$$\frac{dU}{dS} = N_\theta^* - N_\theta \qquad (3\text{-}5a)$$

$$\frac{U}{r_3} = N_\phi^* - N_\phi \qquad (3\text{-}5b)$$

$$\frac{dM_\phi}{dS} + \left[\frac{M_\phi - M_\theta}{r_3}\right] = \frac{U}{r_2} \qquad (3\text{-}5c)$$

representing the condition of equilibrium and

$$L(\chi) - \left[\frac{v\chi}{r_1}\right] = \frac{U}{K} \qquad (3\text{-}6a)$$

$$L(U) + \left[\frac{vU}{r_1}\right] = Pr_2 - \chi Et \qquad (3\text{-}6b)$$

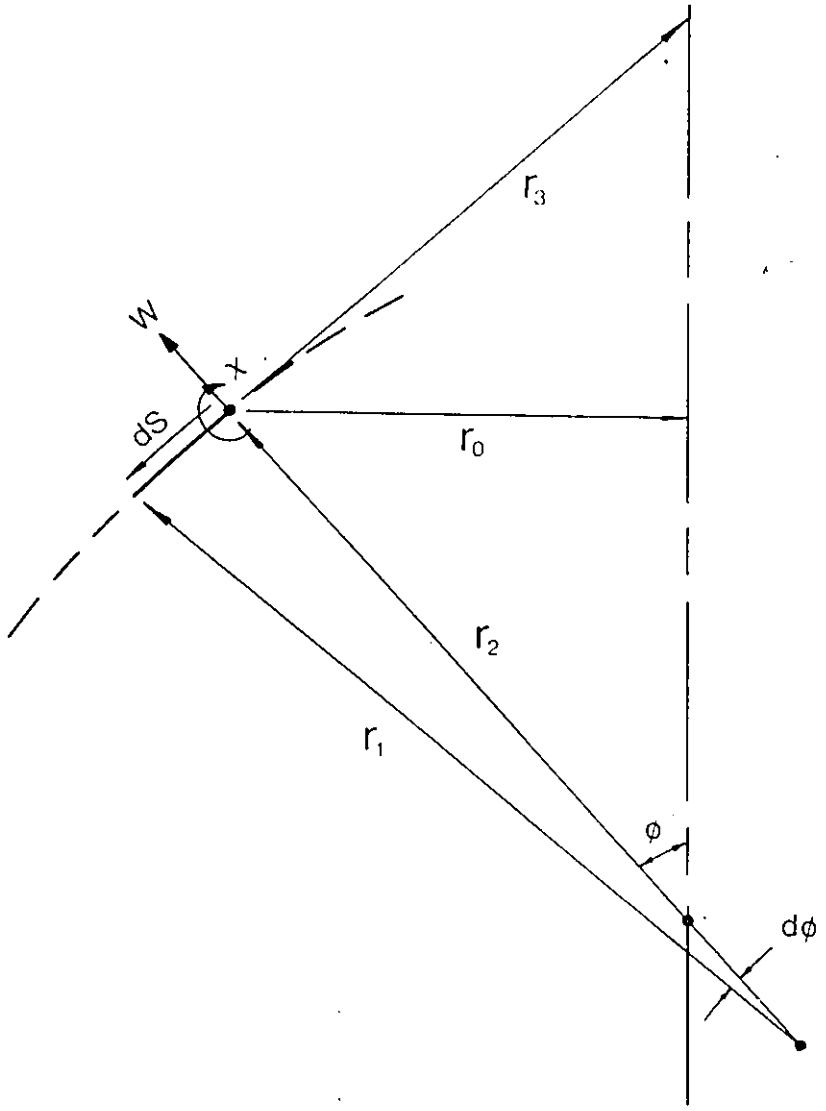

Figure 3-5 Calladine's geometry of meridian

representing the force displacement relations in which

$$U = r_2 Q_\phi$$

$$K = Et^3/12(1-\nu^2)$$

$$L(\ldots) = r_2\left[\frac{d^2}{dS^2}(\ldots) + \frac{1}{r_3}\frac{d}{dS}(\ldots) - \frac{1}{r_3^2}(\ldots)\right]$$

$$P = \frac{dN_\theta^*}{dS} - \nu\frac{dN_\phi^*}{dS} + \left[\frac{(1+\nu)}{r_3}(N_\theta^* - N_\phi^*)\right]$$

In these equations, the loading of the shell enters indirectly through the membrane stress resultants N_θ^* and N_ϕ^*.

In applying this simplified theory to several imperfection forms, Calladine generalized Flugge's earlier conclusions that the effect of meridional imperfections is most marked in terms of changes in N_θ and M_ϕ, with little change in N_ϕ. Further, for cylindrical shells, these force changes are the same as those arising when the cylinder is loaded so that the circumferential force under membrane action is the same as in the imperfect shell. This statically equivalent load is given by the pressure P for a curvature imperfection or the line load F for a slope imperfection according to

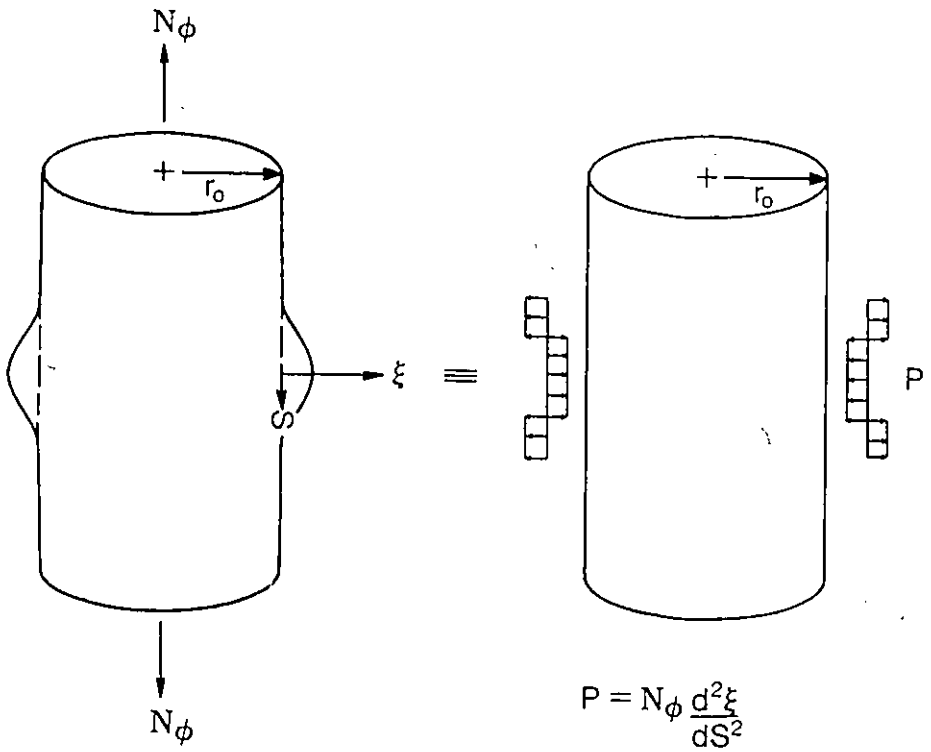

Figure 3-6 Statically equivalent load for meridional curvature imperfection

$$P = N_\phi \frac{d^2\xi}{dS^2} \qquad (3\text{-}7a)$$

$$F = N_\phi \frac{d\xi}{dS} \qquad (3\text{-}7b)$$

This load when applied to the perfect cylinder will be resisted by circumferential forces if membrane action is assumed or by a combination of circumferential forces and meridional moments if bending action is included. It is important to note that the meridional force N_ϕ governs directly the magnitude of stress changes for a given meridional imperfection. Figure 3-6 illustrates Calladine's statically equivalent load for the case of a curvature imperfection.

3.3 IMPERFECT CYLINDER UNDER AXIAL LOAD

It is useful to think in terms of the physical meaning of the imperfection problem through some particular simplified case. The effect of an axisymmetric imperfection can be demonstrated through the imperfect cylinder of Figure 3-7.

If N_ϕ is the meridional stress resultant in the perfect cylinder, then the out-of-balance moment $N_\phi \cdot \xi$ that would be generated could be carried in two ways; by developing meri-

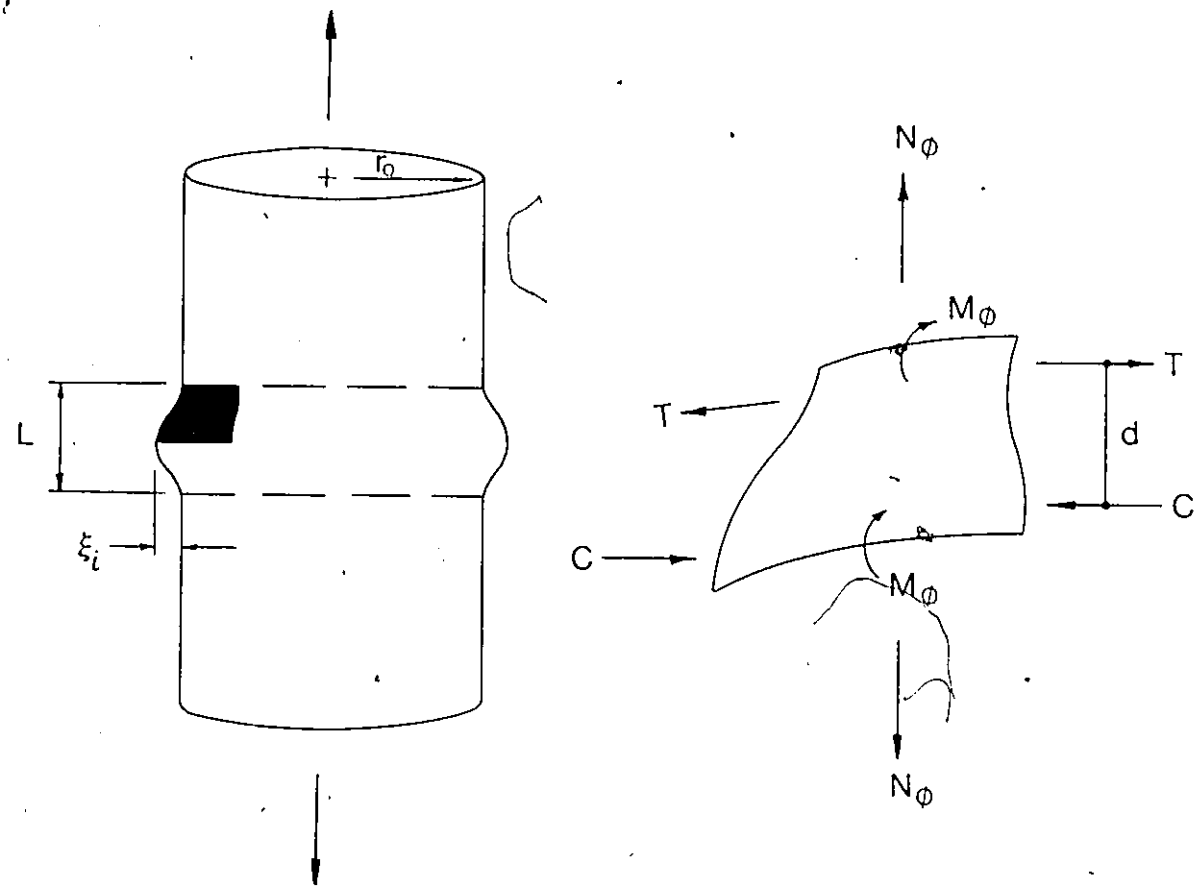

Figure 3-7 Static consideration for out-of-balance moments

dional moments M_ϕ and/or by the meridional components of moment $T \cdot d$ which result from adjacent bands of circumferential tension T and compression C. If the membrane stiffness is large in relation to the bending stiffness, the shell has a tendency to resist the out-of-balance moment through membrane stresses where the contribution $T \cdot d$ is substantially greater than M_ϕ. This is the case when the product of the shell's thickness and radius, $r \cdot t$, is small. When the imperfection length approaches some small value, the moment $T \cdot d$ can no longer be resolved so as to resist the out-of-balance moment. Consequently, a state of equilibrium is reached where the meridional moments M_ϕ dominate.

Chapter IV

SPECIFYING TOLERANCE LIMITS FOR COOLING TOWER SHELLS

Having recognized the detrimental effect of construction imperfections on cooling tower safety, the Committee of Inquiry investigating the Ardeer collapse recommended the development of a rational procedure for specifying maximum imperfection tolerances. Since their report was released in 1974, two studies have been published in which tolerance criteria are proposed for meridionally imperfect cooling tower shells, Figure 4-1:

(1) Croll's Limitation

Croll and Kemp (21), extended an earlier study of the role of imperfections in the Ardeer collapse (13,22) to a consideration of tolerance limits for meridional imperfection. In their study, it was assumed that for cooling tower shells, membrane stiffness dominates so that the out-of-balance moments induced by imperfections are resisted predominantly by circumferential forces.

The change in meridional curvature associated with an idealized imperfection composed of three piece-wise continuous circular arcs as shown in Figure 4-2, can be approximat-

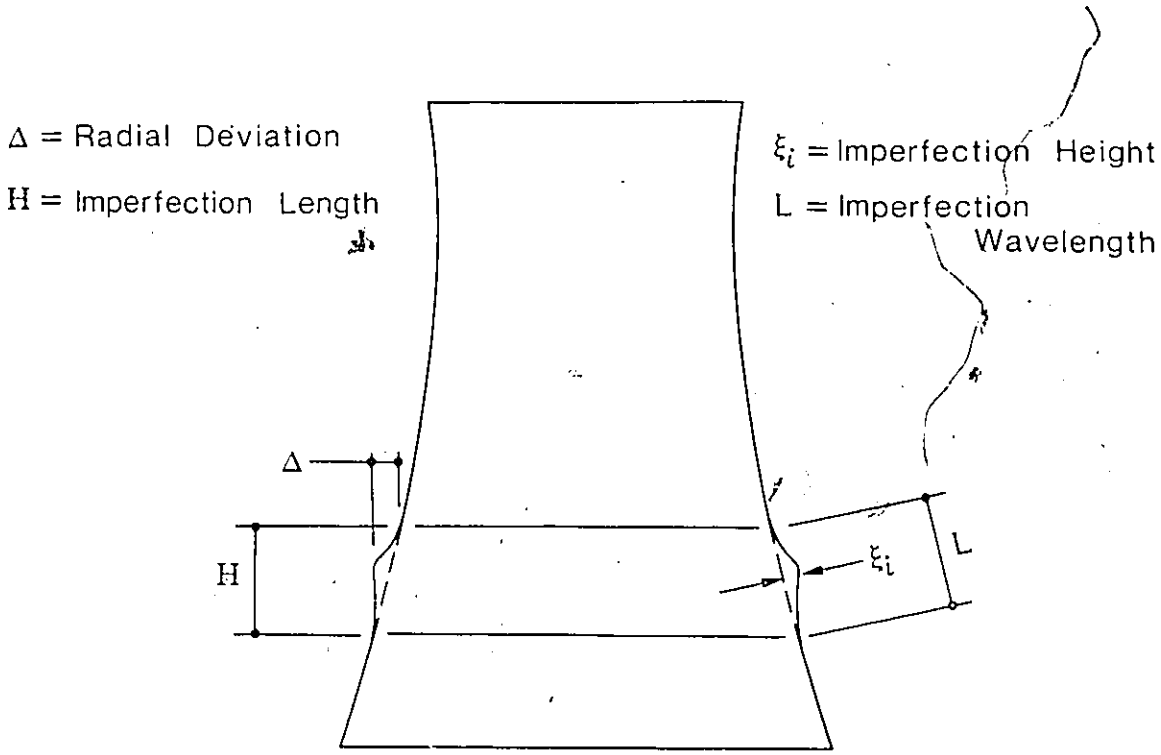

Figure 4-1 Notation for axisymmetric meridional imperfection

ed by $1/r = 16\Delta/H^2$ when $\Delta << H/2$. Based on Calladine's statically equivalent load, Croll and Kemp represented the effect of this imperfection as

$$P = N_\phi \frac{d^2\xi}{dS^2} = 16 N_\phi \frac{\Delta}{H^2}$$

This pressure was allowed to manifest itself as a hoop force according to the simple ring hoop force prediction found in basic strength of materials theory

$$\delta N_\theta = -16 N_\phi r_o \frac{\Delta}{H^2}$$

This expression was generalized to include imperfections whose profiles consist of any three piece-wise, continuous, 2nd order arcs as

$$\delta N_\theta = -24 N_\phi r_o \frac{\Delta}{H^2} \qquad (4\text{-}1)$$

The total circumferential stress resultant N_θ^i occurring in the imperfect shell is then given by the sum of the perfect circumferential stress resultant N_θ and the change δN_θ

$$N_\theta^i = N_\theta - 24 N_\phi r_o \frac{\Delta}{H^2}$$

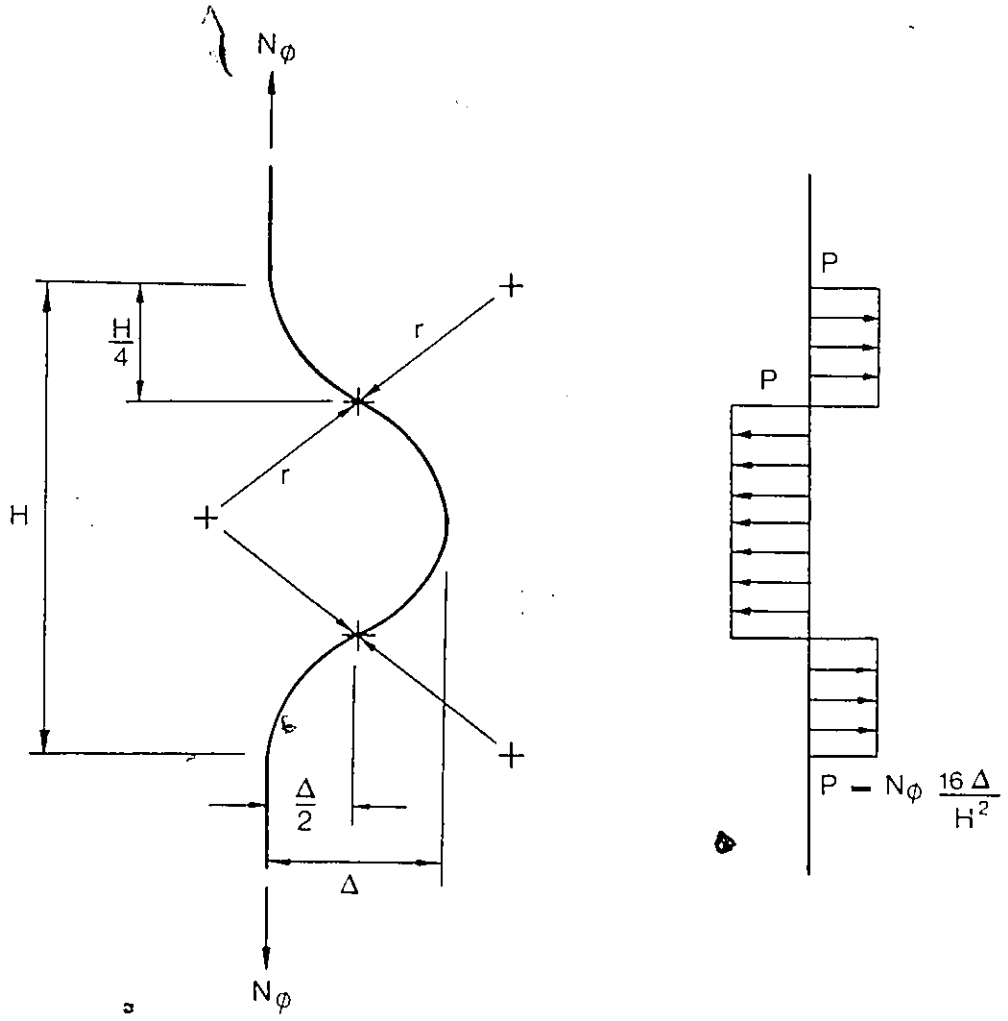

Figure 4-2 Croll's representation of a curvature imperfection

Croll and Kemp suggested this total force be limited to the value N_θ^y at which the circumferential reinforcement yields and obtained the curvature tolerance

$$+\frac{\Delta}{H^2} < \frac{(N_\theta - N_\theta^Y)}{24 N_\phi r_o} \qquad (4\text{-}2)$$

(2) Al-Dabbagh's Limitation

Al-Dabbagh and Gupta (23), applying the equivalent load method to a conical imperfection composed of three slope discontinuities as illustrated in Figure 4-3, showed the changes in circumferential force and meridional moment for each discontinuity to be

$$\delta N_\theta = -\frac{Et N_\phi}{8K^3 D r_o} e^{-kx} (\sin kx + \cos kx) \frac{d\xi}{ds} \qquad (4\text{-}3a)$$

$$\delta M_\phi = \frac{N_\phi}{4K} e^{-kx} (\sin kx + \cos kx) \frac{d\xi}{ds} \qquad (4\text{-}3b)$$

where

E = Young's Modulus

ν = Poisson's Ratio

t = shell thickness

$k = (3(1-\nu^2)/r_o^2 t^2)$

$D = Et^3/12(1-\nu^2)$

x = meridional distance from point of discontinuity

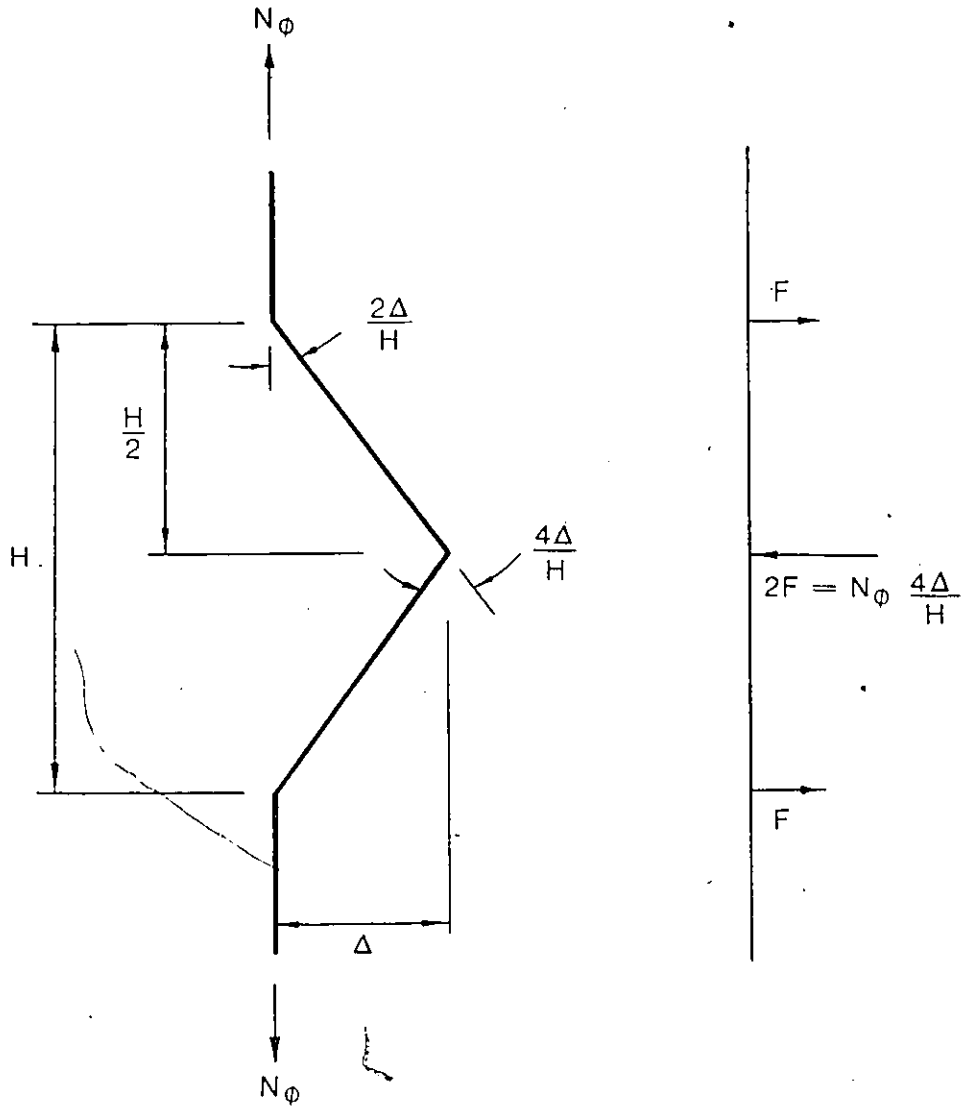

Figure 4-3 Al-Dabbagh's representation of a slope imperfection

Superposing the effects of each discontinuity, the maximum imperfection forces occurring at the middle discontinuity of the imperfection become

$$\delta N_\theta = -2.7\sqrt{\frac{r_o}{t}}\,\frac{\Delta}{H}\,N_\phi \qquad (4\text{-}4a)$$

$$\delta M_\phi = 0.92\sqrt{r_o t}\,\frac{\Delta}{H}\,N_\phi \qquad (4\text{-}4b)$$

Assuming that the circumferential forces should not exceed the capacity of the horizontal reinforcement while simultaneously permitting an overstress α' in the vertical steel, the following slope tolerances were proposed

$$\frac{\Delta}{H} < \frac{p f_Y}{2.7 N_\phi}\sqrt{\frac{t^3}{r_o}} \qquad \text{(horizontal steel)} \qquad (4\text{-}5a)$$

$$\frac{\Delta}{H} < 0.43\,\alpha'\sqrt{\frac{t}{r_o}} \qquad \text{(vertical steel)} \qquad (4\text{-}5b)$$

where p signifies the minimum circumferential steel ratio and f_y the steel yield stress.

Chapter V

COMPARISON OF PUBLISHED LIMITS OF TOLERANCE

In American practice, an engineer required to specify a maximum tolerance for meridional imperfections has a choice from atleast three criteria on which to base an evaluation:

(1) The empirical guidelines of the ACI 334 simultaneously limit circumferential and meridional imperfections the effects of which are very different.

(2) The tolerances published by Croll and Al-Dabbagh refer specifically to deviations of the meridian and account for the size of the tower and the stresses at the level of imperfection.

In specifying an acceptable limit of tolerance, T(,H), two approaches are possible:

(1) The equations (4-1) or (4-4) can be incorporated directly into the design process. Thus, the maximum imperfection forces calculated at any level in the tower can be superposed with those forces obtained from an analysis of the perfect shell. In this way, the imperfect shell, when constructed, should adequately resist

all internal forces provided that construction errors are within the specified tolerance.

(2) Alternatively, a maximum imperfection tolerance, calculated from equations (4-2) or (4-5), could be permitted without the shell having been explicitly designed for it. This is justified on the basis that the shell has some reserve capacity for resisting the local force disturbances arising from the imperfection and prevent overall collapse from an equilibrium point of view.

To determine whether the published criteria of Croll and Al-Dabbagh, and those corresponding to the ACI yield similar acceptable tolerances for meridional imperfection, a comparison was made based on the analyses of two cooling tower shells. Both shells were idealized forms of the Ardeer tower. The first shell, Figure 5-1, had a minimum shell thickness of 15.3 cm (6.0 in) with gradual increases to 70.0 cm (27.6 in) and 55.0 cm (21.7 in) to model the lintel and cornice beams respectively. To allow a comparison to be made, the second shell had dimensions exactly twice those of the first and is representative of the larger towers currently being considered. The equations describing the two meridional curves were obtained by substituting the corresponding geometric data of each shell into the general equation of a hyperbola and are given as

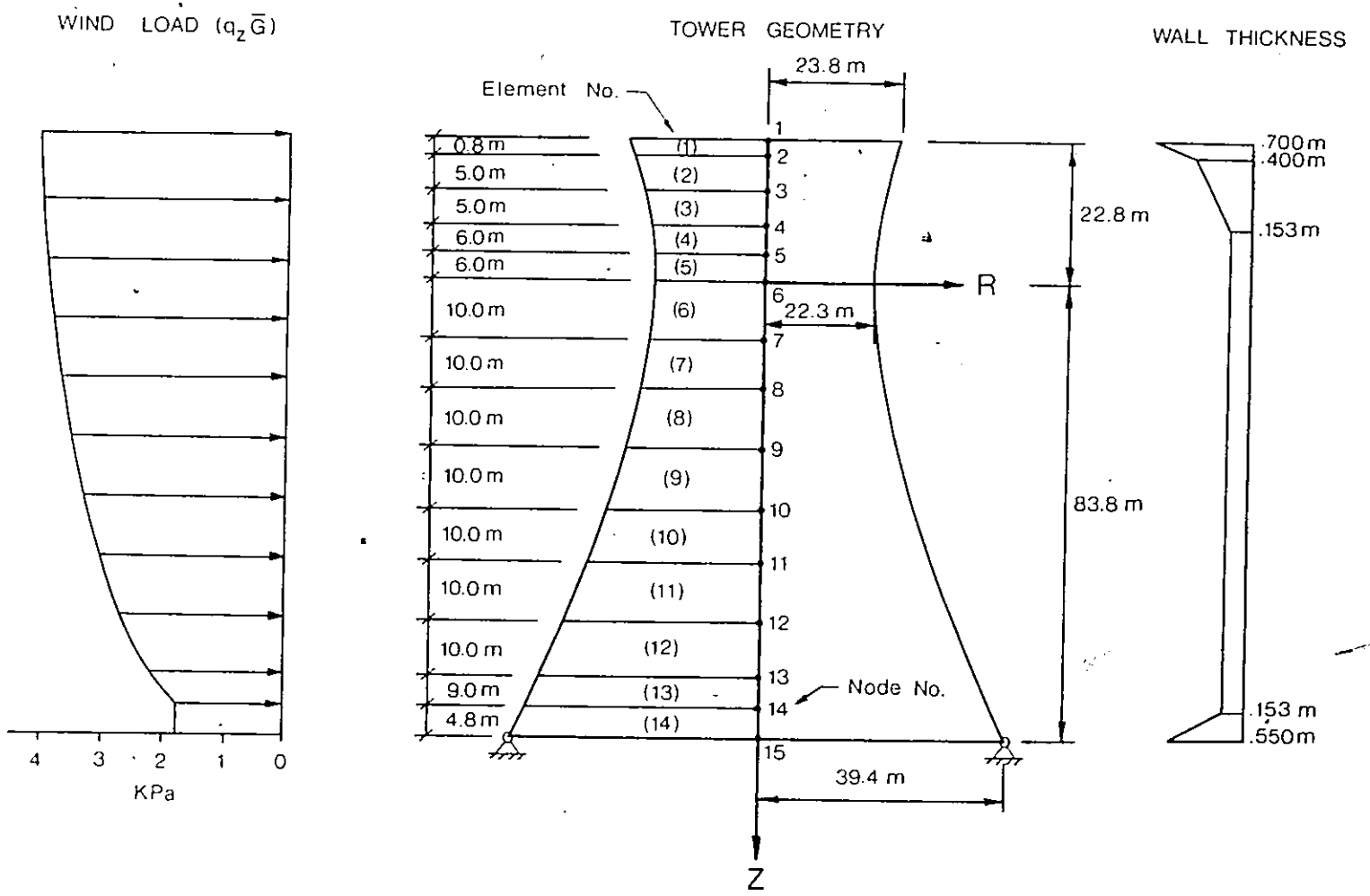

Figure 5-1 Geometry, wind load and wall thickness for the smaller of the two cooling tower shells

SHELL 1: $R^2 + 39\ R - .245283\ Z^2 - 1366.99 = 0$

SHELL 2: $R^2 + 78\ R - .245283\ Z^2 - 5467.96 = 0$

where R = R(Z) is the radius of the shell at vertical coordinate Z.

Bending and twisting moments as well as in-plane forces were evaluated using the SHORE 111 computer program developed at Washington University (24). SHORE 111 is a finite element program for the linear static and dynamic analysis of arbitrarily loaded thin to moderately thick elastic shells of revolution. The meridional curve of a shell may have any quadratic shape. Further, discontinuous meridian curves are permissible making it possible to accurately model axi-symmetric imperfections of the type considered in this report by means of a series of second order curve approximations. A shell is discretized using a series of high-precision curved rotational shell elements. The thickness of these elements may vary linearly along the meridian while the shell material may be specified as isotropic or, single or multi-layer orthotropic.

Through written communication with Dr. H. S. Lew, U.S. Department Of Commerce, National Bureau Of Standards, the validity and accuracy of SHORE 111 in the analysis of a cooling tower shell has been demonstrated. In a comparison with the SAP IV finite element program, SHORE 111 was found

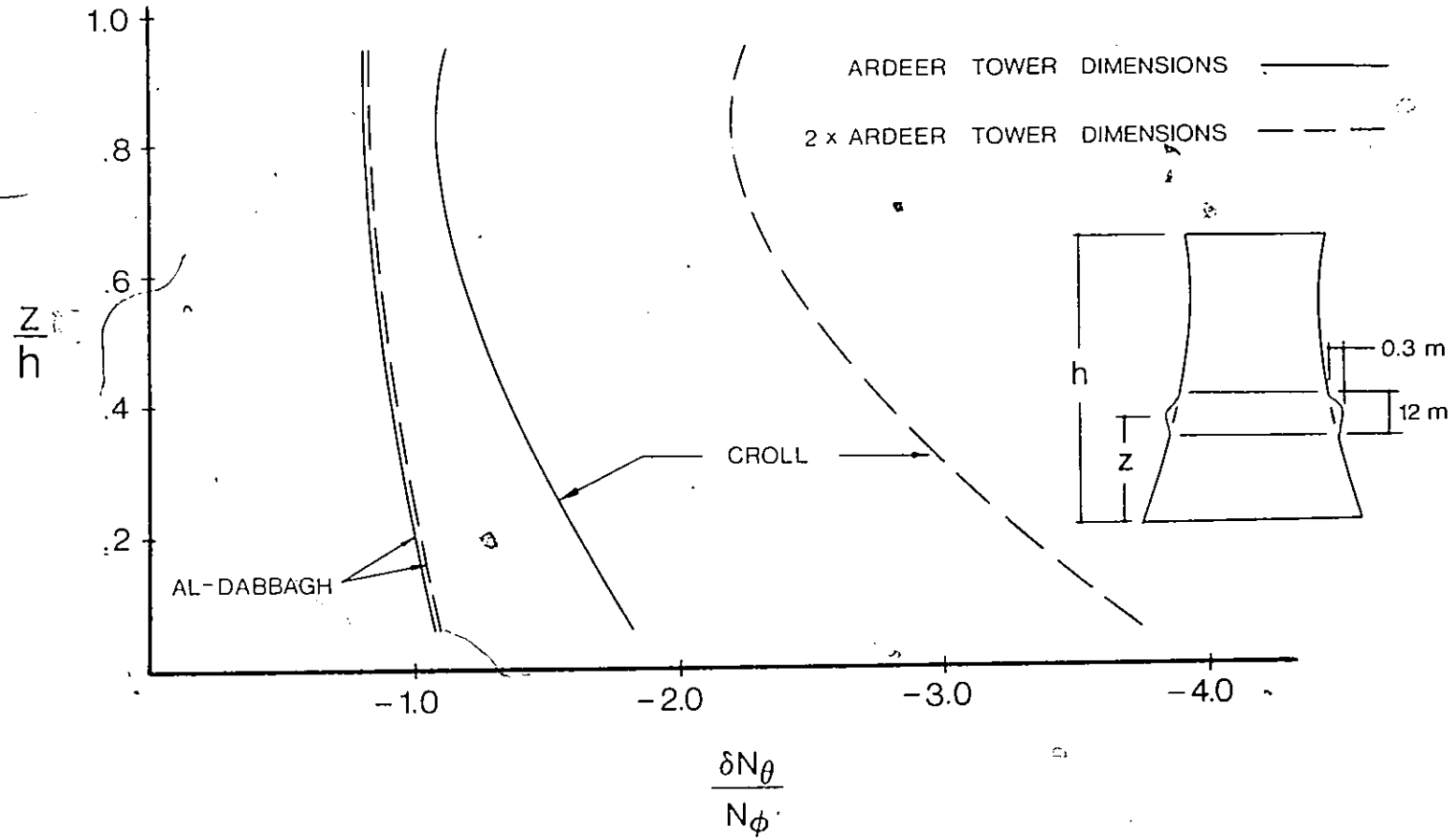

Figure 5-2a Circumferential force changes predicted by Croll and Al-Dabbagh for the two cooling tower shells

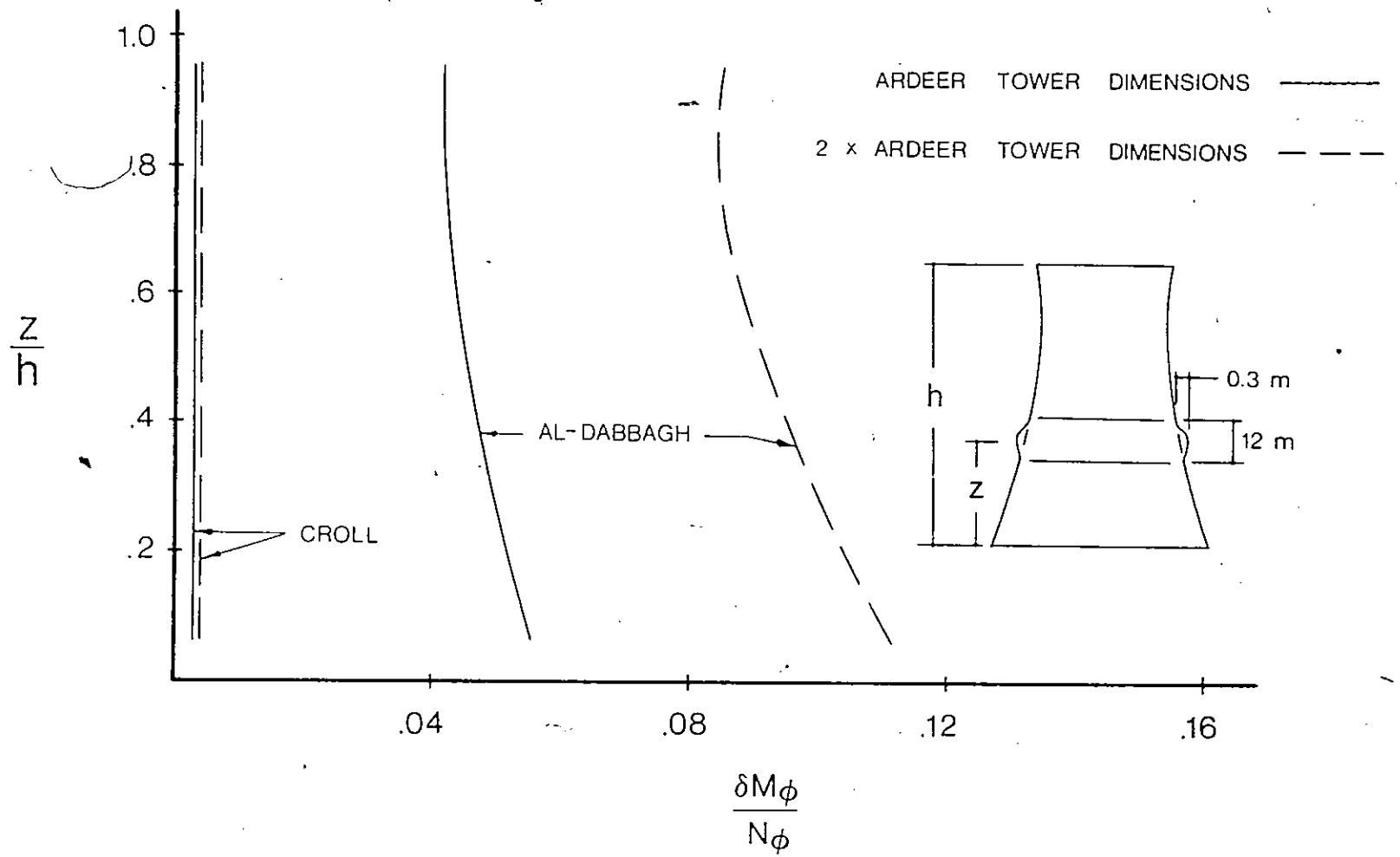

Figure 5-2b Meridional moment changes predicted by Croll and Al-Dabbagh for the two cooling tower shells

to yield stress distributions of similar shape while peak stresses and moments agreed to within a few percent. Furthermore, because SHORE 111 includes transverse shear deformation, a SHORE analysis can be considered a better approximation of the stress levels in a cooling tower shell.

For the present analysis, the entire shell was modelled using fourteen doubly curved ring elements with the assumption of linear elastic response, homogeneity and isotropy. Both wind and gravity loads were considered. To model the wind forces (including suction), the pseudostatic method described in chapter 1 was employed for a wind speed of 190 Km/h (120 mi/h). Although in reality boundary conditions conform to a discrete system of supporting columns, the simplifying assumption of a circumferentially continuous hinged base was made. Several preliminary computer runs on various support restraints indicated the membrane stress resultants remain virtually unchanged over much of the shell.

Figures 5-2, illustrate the force changes δN_θ and δM_ϕ per unit driving force N_ϕ which would occur at different levels in the two shells. These force changes were computed using the equations (4-1) and (4-4) for an imperfection characterized by length H = 12 m (39.4 ft) and radial deviation Δ = 0.3 m (1.0 ft). This is characteristic of the largest imperfection found to exist in the Ardeer tower.

Figures 5-3, show the radial deviation Δ tolerated at varying heights Z in the two shells for an imperfection having length H = 12 m (39.4 ft). Figures 5-4, give the radial deviation Δ for a region near the base of each shell as length H varies from 0 m to 25 m (82.0 ft). These curves were evaluated using equations (4-2) and (4-5), and are based on a uniform distribution of circumferential steel having steel ratio 0.35 percent in conformity with present ACI practice (the original Ardeer tower analysis required approximately half this steel quantity). The yield stress of steel was taken as 340 MPa (49,400 psi).

From Figures 5-2, the following observations are made concerning the force changes due to the imperfection:

(1) Croll and Al-Dabbagh predict increases in circumferential force, δN_θ, of the same order of magnitude as the meridional force N_ϕ in the perfect shell. Since N_θ for the perfect shell is small and generally one order of magnitude less than N_ϕ, the increase δN_θ (assumed to be tensile) will govern the required strength and steel quantity in the circumferential direction. As example, considering the maximum force values at a level 44 m (147 ft) from the base of the smaller shell, $N_\theta = -8.16 \times 10^4$ N/m and $N_\phi = -1.12 \times 10^6$ N/m. Using the lesser conservative value given by Al-Da-

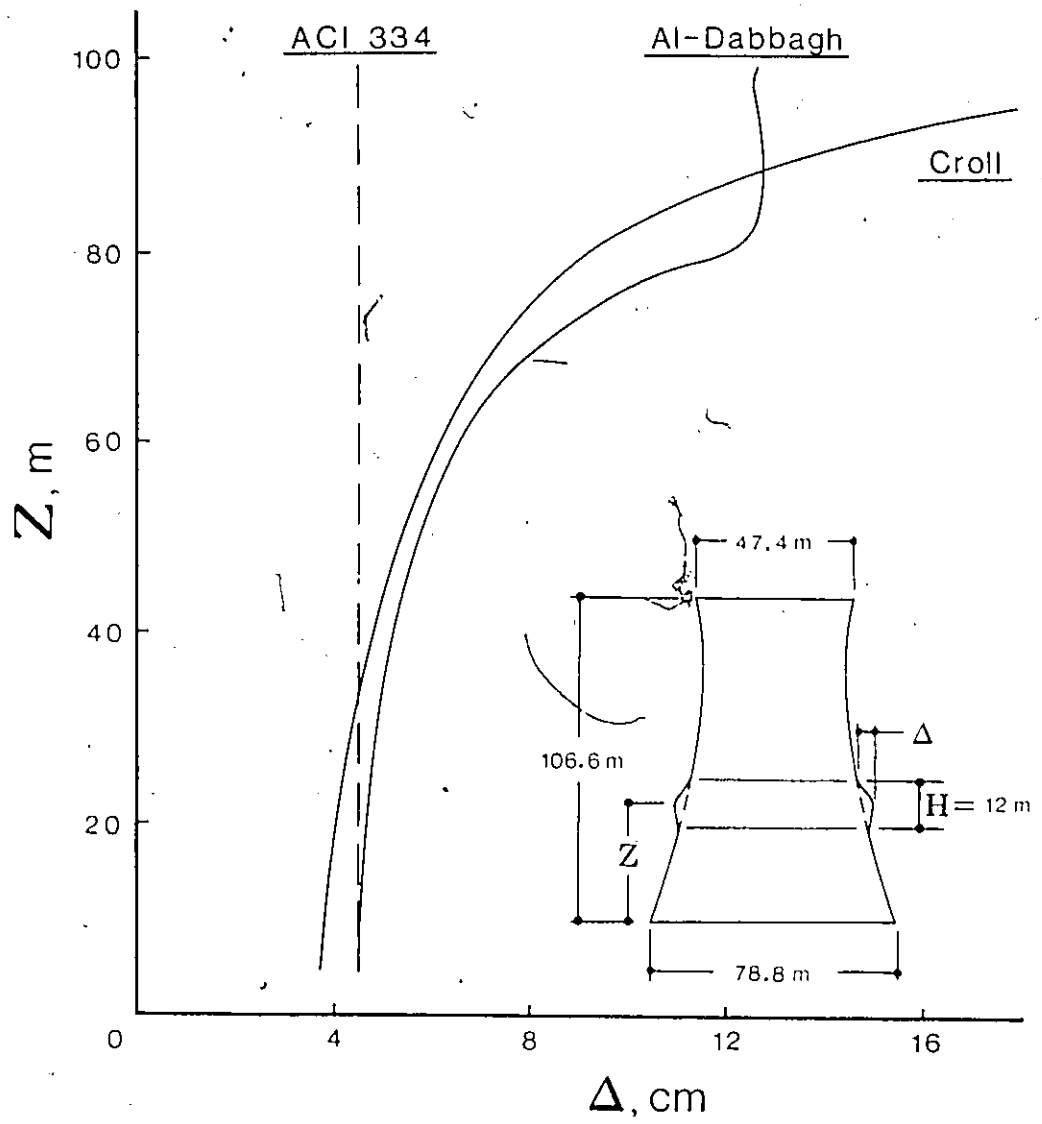

Figure 5-3a Maximum tolerable radial deviation at varying levels in the smaller shell

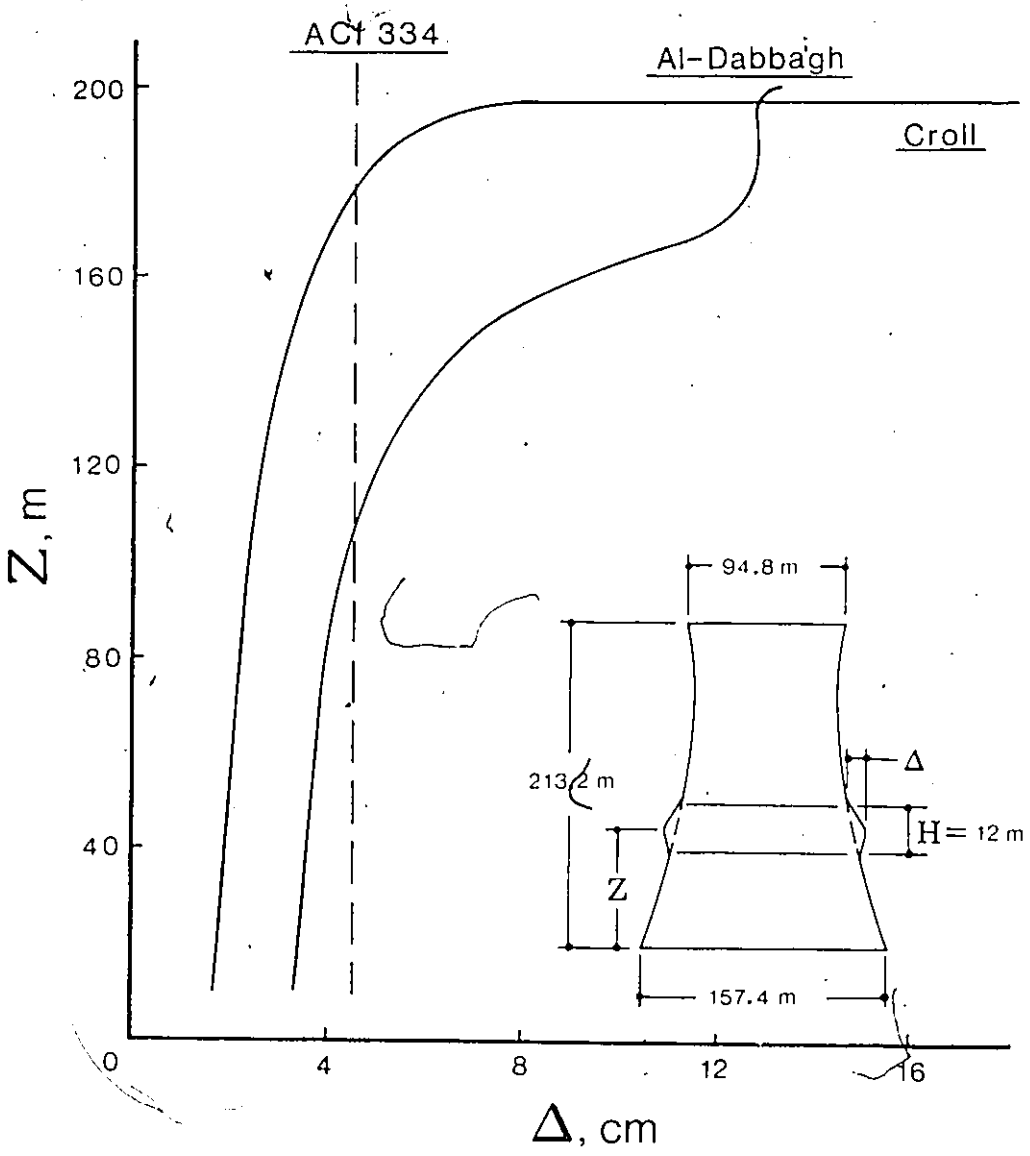

Figure 5-3b Maximum tolerable radial deviation at varying levels in the larger shell

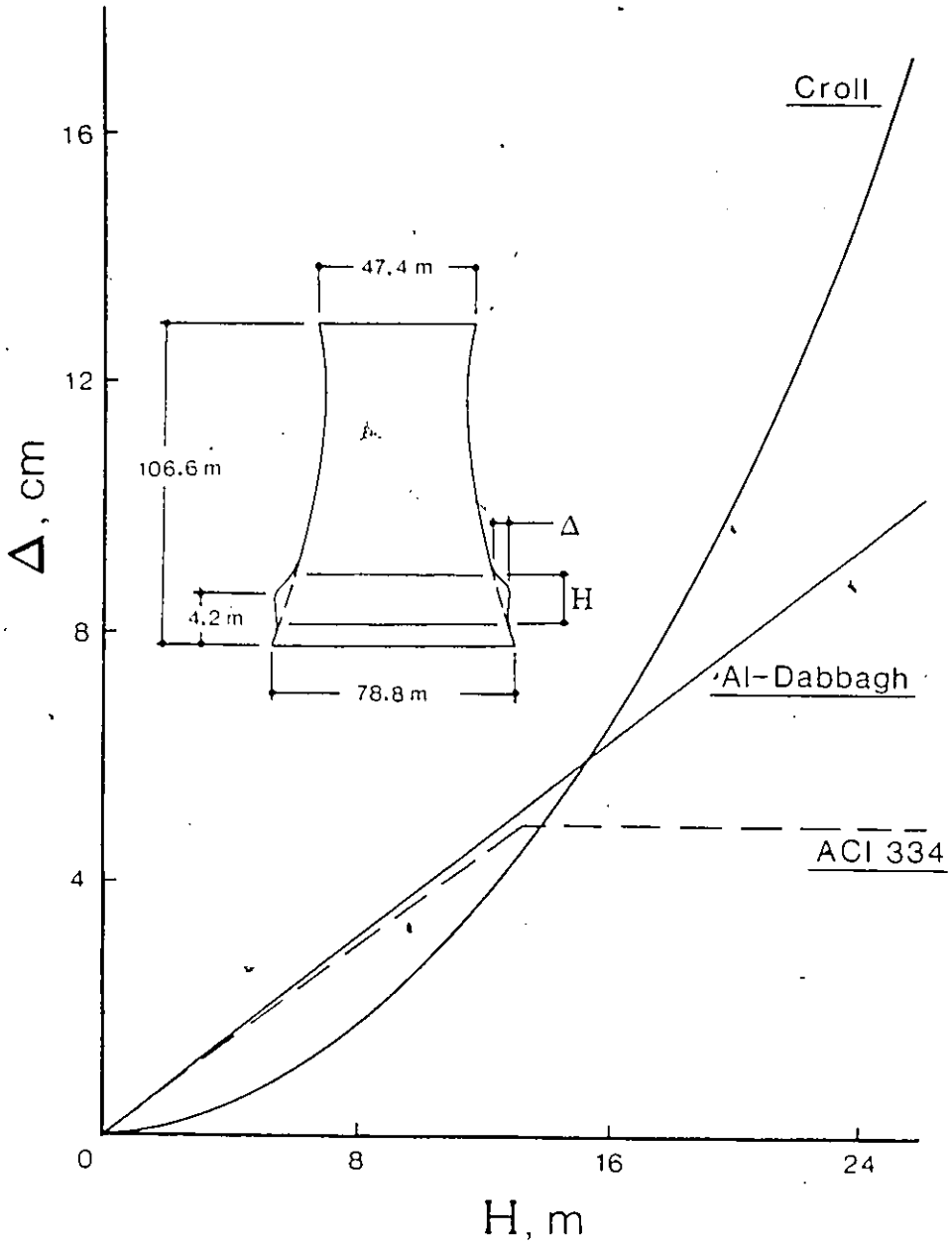

Figure 5-4a Maximum tolerable radial deviation for varying imperfection length near the base of the smaller shell

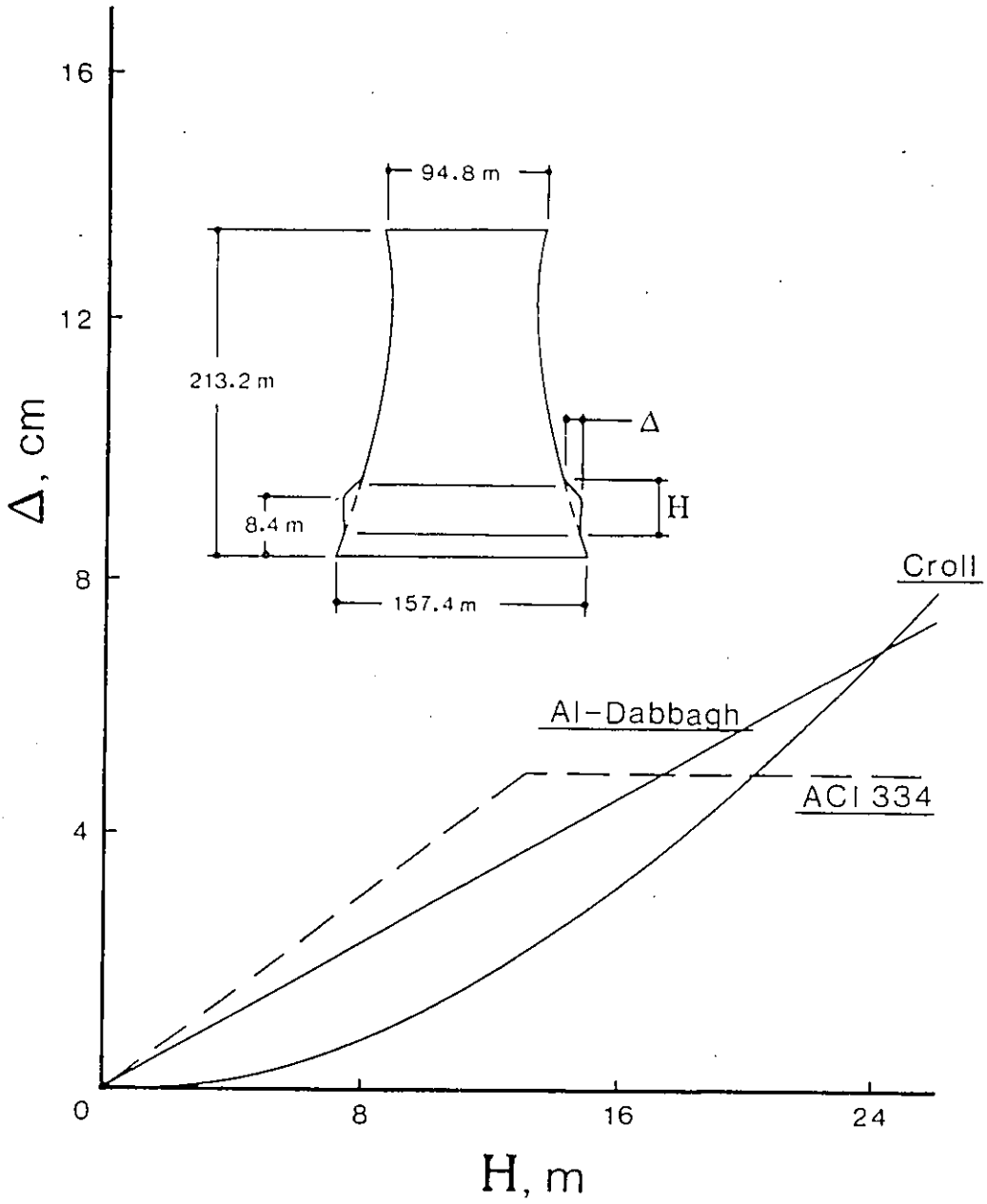

Figure 5-4b Maximum tolerable radial deviation for varying imperfection length near the base of the larger shell

bbagh, $\delta N_\theta = (-.90)(-1.12 \times 10^6) = 1.01 \times 10^6$ N/m. The hoop steel ratio necessary to resist this force prior to yielding is 1.94%. This represents approximately five times the minimum steel ratio specified by the present ACI guidelines and ten times that provided in the actual construction of the Ardeer tower.

(2) Croll, having assumed that the out of equilibrium moment generated by a meridional imperfection is resisted by the shell's membrane action, inherently yields larger increases in circumferential force. Near the base of the smaller shell, Figure 5-2a, Croll's increase in circumferential force is double that of Al-Dabbagh. This difference appears more pronounced as tower dimensions increase. Thus, near the base of the larger shell, δN_θ according to Croll is four times greater than that of Al-Dabbagh.

(3) In contrast to Croll's membrane solution, Al-Dabbagh also predicts an increase in meridional moment, δM_ϕ. The importance of this moment is shown by considering again the smaller shell 44 m (147 ft) from its base. The maximum tensile meridional force on the windward meridian is $N_\phi = 9.30 \times 10^5$ N/m. From Figure 5-2b, $\delta M_\phi = (.048)(9.30 \times 10^5 \text{N/m}) = 4.50 \times 10^4$ N m/m. Assuming the vertical steel to be in two layers a distance 0.8t appart, the proportion of the steel stress induced by this moment is approximately 44%. Considering that

meridional stresses are the most critical in a cooling tower shell during the overturning action of the wind, this example indicates how in the presence of meridional imperfection, the contribution made by meridional bending can be significant and should therefore not be ignored.

From Figures 5-3 and 5-4, the following observations can be made concerning the maximum limits of tolerance:

(1) The ACI guidelines, which do not consider the magnitude of the stresses at the level of imperfection, show no variation in tolerance throughout the shell height. The result is a conservative tolerance of radial deviation for the upper less stressed levels of both shells. In the region above the shell's throat, Figure 5-3a, the ACI permitted radial deviation of 4.5 cm (1.77 in) is approximately one third the 12.8 cm (5.04 in) allowed by Croll and Al-Dabbagh. The converse is true for the higher stressed regions near the base of each shell where the ACI guidelines appear to be non conservative. In particular, near the base of the larger shell, Figure 5-3b, Croll permits a radial deviation only one third that of the ACI.

(2) From Figures 5-3, the tolerances set by Croll and Al-Dabbagh become more stringent as tower dimensions in-

crease. In contrast, the ACI shows no difference in permissible radial deviation between the two shells.

(3) The three criteria demonstrate similar trends by permitting larger radial deviations for the longer imperfection lengths. However, for the shorter lengths the ACI guidelines provide non conservative tolerances. This is evident in Figure 5-4b where for H = 13 m (42.7 ft), the ACI permits a 5.0 cm (1.97 in) deviation compared to 3.4 cm (1.34 in) and 2.0 cm (0.79 in) by Al-Dabbagh and Croll respectively. Further, the ACI provides seemingly conservative tolerances for the longer imperfection lengths. In Figure 5-4a for H = 25 m (82.0 ft), Croll and Al-Dabbagh permit radial deviations of 17.2 cm (6.77 in) and 10.1 cm (3.98 in) compared to 5.0 cm (1.97 in) tolerated by ACI. A similar observation holds true for the larger shell of Figure 5-4b if proportionately longer imperfection lengths in relation to the shell's size are considered.

(4) In Figures 5-3, the tolerances of Croll and Al-Dabbagh display a consistent trend over most of the shell height. Excepting a region above the shell throat where Al-Dabbagh's criteria limits radial deviation so as to prevent meridional bending failure, Croll's limitation is the more conservative. This observation holds for a wide range of imperfections lengths that would normally be encountered in practice - up to

about 15 m (56.0 ft), Figure 5-4a. However, above the throat, significant differences do arise between these two limitations as shown by Figure 5-3b. Al-Dabbagh's 12.7 cm (5.0 in) contrasts the 4.5 cm (1.77 in) tolerance set by Croll. Given that radial deviations are likely to be of the order of the wall thickness (in this case 30.6 cm), differences as high as 27% of this value should not be dismissed as insignificant.

The above observations concerning meridional imperfections in cooling tower shells can be summarized as follow:

(1) In relation to the maximum imperfection forces that are predicted by Croll and Al-Dabbagh:

(a) the increase in circumferential force is of the same order of magnitude as the meridional force for the perfect shell and governs the quantity of hoop steel which must be provided.

(b) large discrepancies exist between the predicted values of circumferential force with Croll's increase being larger by a factor as great as four compared to Al-Dabbagh.

(c) Croll's membrane solution yields no moment whereas the increase in meridional moment given by Al-Dabbagh makes a significant contribution to normal stress in the meridional direction.

(2) With respect to the published tolerances of Croll and Al-Dabbagh, the recently standardized guidelines of the ACI 334 are:

(a) conservative in the upper, less stressed regions of the shell and non conservative in the highly stressed regions near the base.

(b) conservative for 'long' imperfection lengths and non conservative for 'short' imperfection lengths.

(c) show increasing discrepancies as tower dimensions increase.

(3) A significant difference in radial deviation can arise between the tolerances set by Croll and Al-Dabbagh where for a wide range of imperfection lengths:

(a) Croll's criteria, assuming only hoop action to resist the out-of-balance moment is more conservative below the shell throat.

(b) Al-Dabbagh's criteria, attempting to prevent meridional bending failure is more conservative in the less stressed regions above the shell throat.

Chapter VI

DIRECT EVALUATION OF MERIDIONAL IMPERFECTION FORCES

6.1 VALIDITY OF PRESENT METHODS IN CALCULATING IMPERFECTION FORCES

Croll and Al-Dabbagh have proposed equations (4-1) and (4-4) respectively for calculating the maximum increase in forces associated with a local meridional imperfection having a radial deviation Δ and imperfection length H, as in Figure 4-1. The equations relate to specific shell conditions at the level of imperfection and are based on a linear elastic response of the shell assuming it to be isotropic and homogeneous. These assumptions are consistent with those used in calculating the perfect shell forces so that the two set of forces can be superposed to yield a set of design forces for a maximum imperfection tolerance $T(\Delta,H)$. This forms the basis for calculating the necessary steel requirements for the as constructed, imperfect shell.

In chapter 5, a comparison disclosed significant differences between the respective imperfection forces predicted by equations (4-1) and (4-4). This can lead to a perplexing situation for the design engineer who must calculate the force increases for some specified imperfection in a given

shell design and furthermore, questions the validity of assumptions used in their calculation. It was also demonstrated in chapter 5 that the force increases arising from meridional imperfection at a given level in the tower can be larger than the respective maximum forces in the perfect shell. Considering therefore, that these force increases are likely to influence the required steel quantities in the circumferential and meridional directions, a closer examination should be made of the methods by which they are calculated. In particular, this chapter will proceed to outline certain shortcomings in the imperfection model adopted by Croll and Al-Dabbagh and will then present a more valid closed form solution for calculating imperfection forces.

6.1.1 CYLINDRICAL IMPERFECTION MODEL

Croll and Al-Dabbagh have assumed that imperfection forces in a cooling tower shell are analogous to those arising in a cylindrical shell having the same circumferential radius and imperfection errors, and loaded with the same meridional force as the cooling tower at the level of the imperfection. Such a correspondence neglects the variation in profile of the perfect meridian which is characterized by:

(1) Curvature in the region of the tower's throat and

(2) Slope near the tower's base.

In one case, Croll analyzed the effects of an imperfection near midheight of the Ardeer tower and found the circumferential forces to be similar in value to the hoop forces in the analogous cylinder. However, because a theoretical basis for this similarity was not presented, such an observation should be considered with caution since this region of the tower does not exhibit maximum slope or curvature. Adoption of the cylindrical imperfection model, therefore, requires further justification.

6.1.2 CHARACTERISTIC LENGTH AND HEIGHT OF IMPERFECTION

Croll and Al-Dabbagh characterize a meridional imperfection in terms of radial deviation Δ and length H, Figure 4-1. This introduces error in portions of the shell where the perfect meridian displays significant slope. Consider, as example, an imperfection near the base of the Ardeer tower described by Δ = 0.3 m (0.98 ft) and H = 10 m (33 ft). Croll would proceed to calculate the curvature of such an imperfection as $16\,\Delta/H^2 = 0.048\ m^{-1}$ ($0.0147\ ft^{-1}$). But this is not the curvature with respect to the true meridian. If Δ and H are resolved perpendicular and parallel to the true meridian then

$$\frac{16\,\xi_i}{L^2} = \frac{16(\Delta \cos(1/3))}{(H/\cos(1/3))^2} = .040\ m^{-1} \quad (.0124\ ft^{-1})$$

which according to equation (4-1) yields a 16% lower circumferential force.

6.1.3 INCLUSION OF SHELL BENDING STIFFNES

Figures 6-1 show the variation in forces with meridional distance S generated by an imperfection having length H = 10 m (32.8 ft) and radial deviation Δ = 30 cm (11.8 in) in a concrete cylinder whose radius is 24.6 m (80.7 ft) and wall thickness 15.3 cm (6.02 in). For comparison, imperfection forces have been calculated using equations (4-1) and (4-3) in accordance with Croll and Al-Dabbagh respectively. These curves indicate the effect of an imperfection to be a local phenomenon restricted to a meridional distance about twice the imperfection wavelength L. The circumferential forces and meridional moments alternate in sign with a maximum value at the centre of the imperfection (S = 0) while undergoing atleast one cycle before diminishing to an insignificant value.

Figures 6-1, also illustrate the consequence of Croll's assumption whereby membrane action alone resists the out-of-balance moment generated by an imperfection. Local bending failure is not included in (4-2) which simply ensures static equiulibrium through the development of circumferential force. Furthermore, the assumed dominance of membrane action does not necessarily imply that the bending stresses in the

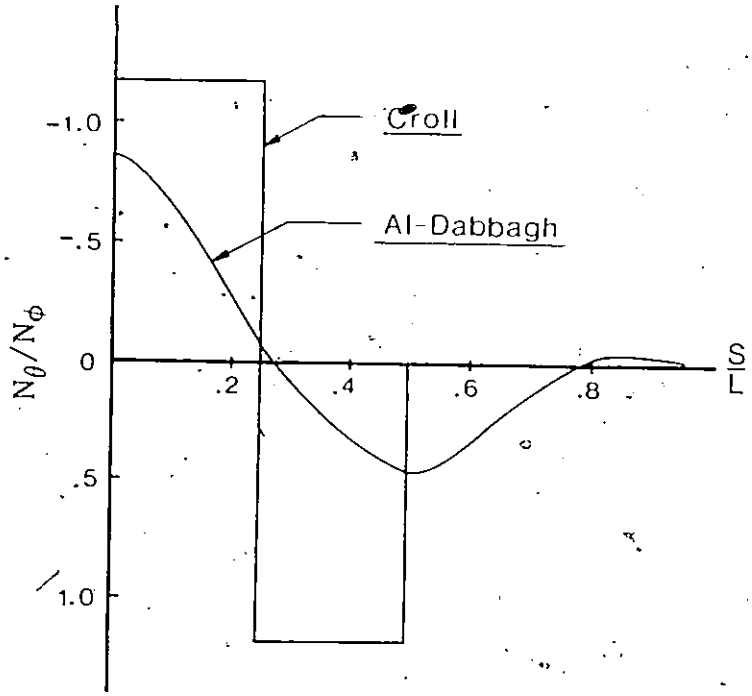

(a) Circumferential force

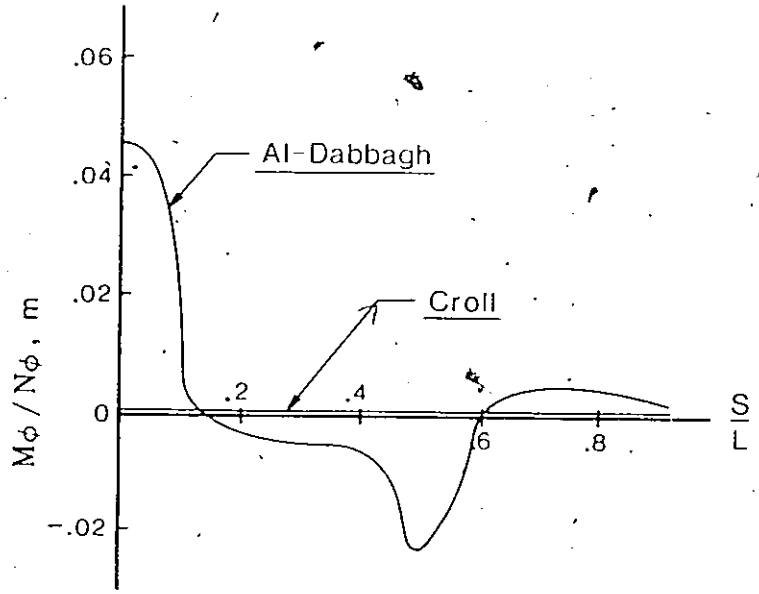

(b) Meridional moment

Figure 6-1 Meridional variation of imperfection forces based on equations (4-1) and (4-3)

meridional direction will not be large. In Figure 6-1b, the eccentricity M_ϕ/N_ϕ = 0.043 m (1.69 in) given by Al-Dabbagh accounts for 63% of the maximum meridional normal stress.

6.1.4 ASSUMED IMPERFECTION FORM

Based on Timoshenko's solution for radially loaded cylinders (1), Calladine's statically equivalent load method is readily applicable to the solution of a curvature imperfection in the form of circular arcs (Croll) or a slope imperfection in the form of conical frustrums (Al-Dabbagh). However, any symmetrical cooling tower imperfection spanning a length of five or more concrete lifts, is likely to display some intermediate geometry.

In Figures 6-2 are shown the forces arising from slope and curvature imperfections within a cylindrical concrete shell determined by a finite element analysis. The cylinder was taken to have a radius of 22 m (72.2 ft) and 15.3 cm (6.02 in) wall thickness. Both imperfections correspond to a 30 cm (11.8 in) radial deviation and 15 m (49.2 ft) imperfection length. In Figure 6-2a, the circumferential forces exhibit a similar variation with the slope imperfection giving rise to a peak force 20% higher than the curvature imperfection. In Figure 6-2b, the meridional moments show more serious discrepancies. Not only are the cyclic variations of moment out of phase, but at the centre of the imperfec-

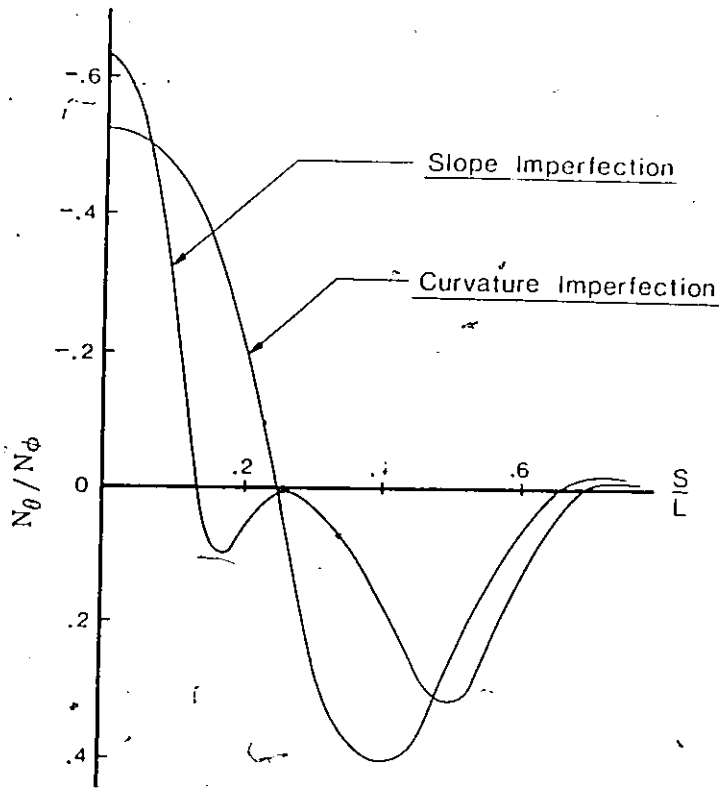

(a) Circumferential force

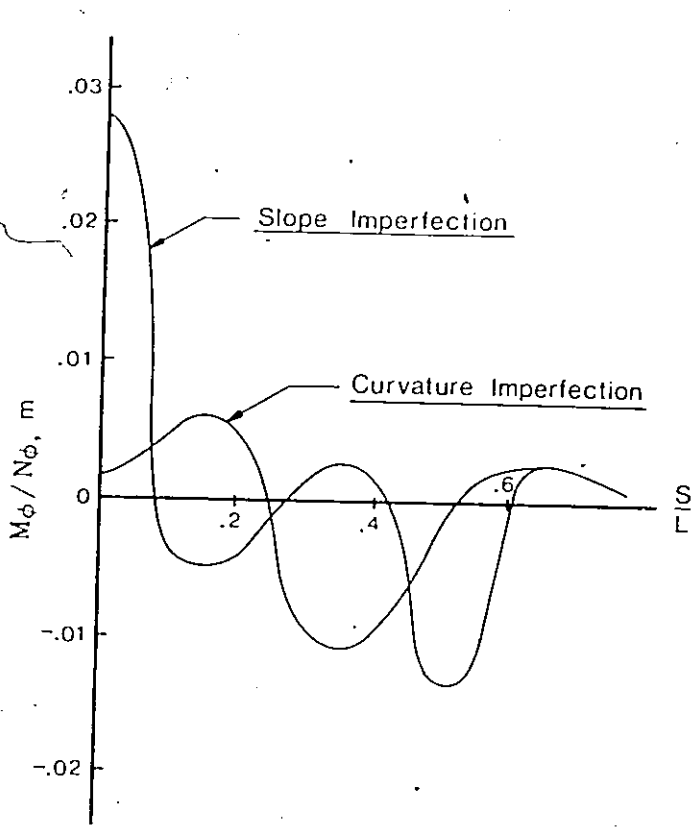

(b) Meridional moment

Figure 6-2 Meridional variation of imperfection forces based on a finite element analysis

tion a peak eccentricity of 28 mm (1.10 in) for the slope imperfection contrasts the 2 mm (0.079 in) of the curvature imperfection.

Recently, Gupta and Al-Dabbagh (25) emphasized the relation between peak imperfection force and assumed imperfection form. Their study considered varying normal pressures using the statically equivalent load method. Unfortunately, the parametric approach used is not amenable to arbitrary imperfection forms.

6.1.5 FORCE MAGNIFICATION THROUGH THE P-Δ EFFECT

Preliminary analyses of meridionally imperfect cylinders in compression, having the stiffness properties of reinforced concrete, suggest radial displacements of the order of the imperfection height. In the majority of cases, these displacements amount to a few percent of the original imperfection. However, the magnification due to the P-Δ effect is a consideration requiring closer examination.

6.2 CLOSED FORM SOLUTION

6.2.1 MATHEMATICAL FORMULATION

Calladine, has presented equations (3-5) and (3-6) for the stress resultants in an isotropic, thin shell of revolution which is loaded axisymetrically, Figure 3-4. It is possible to rework this seemingly complicated system of equa-

tions into a simpler form for the case of the hyperbolic cooling tower shell.

As a consequence of Geckeler's approximation, Calladine has suggested that the second terms on the left side of equations (3-6), representing part of the Poisson effect, have little effect on the solution for the system. Furthermore, for the hyperboloid of revolution which is characterized by a relatively mild meridional slope, the distance r_3 approaches a large value so that the terms having this quantity as part of their denominator may be ignored. Hence, the equations for the condition of equilibrium simplify to

$$N_\theta^* - N_\theta = \frac{d}{dS}(r_2 Q_\phi) \qquad (6\text{-}1a)$$

$$N_\varphi^* - N_\phi = 0 \qquad (6\text{-}1b)$$

$$\frac{dM_\phi}{dS} = Q_\phi \qquad (6\text{-}1c)$$

The corresponding force-displacement relations become

$$Q_\phi = K\frac{d^2\chi}{dS^2} \qquad (6\text{-}1d)$$

$$\frac{d^2}{dS^2}(r_2 Q_\phi) = \frac{dN_\theta^*}{dS} - \nu\frac{dN_\phi}{dS} - \frac{\chi E t}{r_2} \qquad (6\text{-}1e)$$

in which $\chi(S)$ is the meridional rotation and K is the shell's bending stiffness.

From chapter 3, the membrane stress resultants in the imperfect shell due to meridional imperfection $\xi(S)$ are

$$N_\theta^* = N_\theta^P + r_2 N_\phi^P \frac{d^2\xi}{dS^2} \qquad (6\text{-}2a)$$

$$N_\phi^* = N_\phi^P \qquad (6\text{-}2b)$$

Furthermore, it is assumed that within the localized region of an imperfection, the direct circumferential and meridional forces for the perfect shell are essentially constant so that

$$\frac{dN_\theta^P}{dS} = \frac{dN_\phi^P}{dS} = 0 \qquad (6\text{-}3)$$

Substituting (6-3) and (6-2) into (6-1) yields the following system of equations for local imperfection in the cooling tower shell.

$$\delta N_\theta = r_2 \left\{ N_\phi^P \frac{d^2\xi}{dS^2} - \frac{d^2 M_\phi}{dS^2} \right\} - \frac{dr_2}{dS} \cdot \frac{dM_\phi}{dS} \qquad (6\text{-}4a)$$

$$\delta N_\phi = 0 \qquad (6\text{-}4b)$$

$$Q_\phi = \frac{dM_\phi}{dS} \qquad (6\text{-}4c)$$

$$\frac{dM_\phi}{dS} = K\frac{d^2\chi}{dS^2} \qquad (6\text{-}4d)$$

$$\frac{d^4\chi}{dS^4} + \left(\frac{2}{r_2}\cdot\frac{dr_2}{dS}\right)\frac{d^3\chi}{dS^3} + \left(\frac{1}{r_2}\cdot\frac{d^2r_2}{dS^2}\right)\frac{d^2\chi}{dS^2} + \left(\frac{Et}{Kr_2^2}\right)\chi$$

$$= \frac{N_\phi^P}{K}\left\{\frac{d^3\xi}{dS^3} + \left(\frac{2}{r_2}\cdot\frac{dr_2}{dS}\right)\frac{d^2\xi}{dS^2}\right\} \qquad (6\text{-}4e)$$

In comparison to the statically equivalent load method proposed by Calladine (equations(3-7)) and adopted by Croll and Al-Dabbagh, the above system of equations offers the advantage in that:

(a) The slope and curvature of the perfect meridan are accounted for through the first and second derivative terms of r_2.

(b) The system is not restricted to imperfections in the form of circular arcs or conical frustrums, but instead, is equally amenable to any imperfection form which can be described by derivatives of $\xi(S)$.

(c) Two additional terms in the form of first and second derivatives of M_ϕ are included in (6-4a) which the previous authors neglected. This suggests greater accuracy for imperfections of shorter wavelength which tend to generate relatively abrupt changes in meridional moment.

6.2.2 SOLUTION

The above system can be solved by evaluating the rotations $\chi(S)$ from equation (6-4e) for some specified imperfection $\xi(S)$. Substitution into the remaining four equations then determines the force changes associated with this imperfection as would be driven by the meridional force N_ϕ^p. The general solution $\chi(S)$ is the sum of the complimentary function χ_H for the corresponding homogeneous equation and a particular integral χ_p.

The characteristic equation of (6-4e) is the quartic polymial

$$m^4 + \left(\frac{2}{r_2}\cdot\frac{dr_2}{dS}\right)m^3 + \left(\frac{1}{r_2}\cdot\frac{d^2r_2}{dS^2}\right)m^2 + \frac{Et}{Kr_2^2} = 0$$

Based on the relationships which exist among the roots and the coefficients of polynomial equations (26), it can be demonstrated (Appendix A) on the basis of the Ardeer cooling tower shell, that the second and third terms of this equation have little effect on its solution. Hence, the roots of

m are taken to be

$$m = \pm (1 \pm i)\lambda$$

where

$$\lambda = \sqrt[4]{\frac{\pm E}{4Kr_2^2}}$$

and

$$i = \sqrt{-1}$$

The complimentary function is then found to be (27)

$$\chi_H = \exp \lambda s \left[A_1 \cos \lambda s + A_2 \sin \lambda s\right] + \exp -\lambda s \left[A_3 \cos \lambda s + A_4 \sin \lambda s\right]$$

Replacing the exponential functions in this equation by the hyperbolic functions (28)

$$\exp \lambda s = \cosh \lambda s + \sinh \lambda s \ , \ \exp -\lambda s = \cosh \lambda s - \sinh \lambda s$$

and the complimentary function after some reduction becomes

$$\chi_H = B_1 \sin \lambda s \cdot \sinh \lambda s + B_2 \sin \lambda s \cdot \cosh \lambda s + B_3 \cos \lambda s \cdot \sinh \lambda s + B_4 \cos \lambda s \cdot \cosh \lambda s \qquad (6\text{-}5)$$

in which B_1 to B_4 designate real arbitrary constants.

Considering next the remainder of the solution, if the right handside of (6-4e) is a function composed of trigonometric terms, the particular integral becomes readily solvable by the method of undetermined coefficients. Figure 6-3 schematizes a meridional imperfection having height ξ_i and wavelength L in the form of a cosine wave. Such a symmetrical imperfection can be accurately represented by the first four terms of a Fourier Series on an interval 2L as

$$\xi(s) = \xi_i \left[\frac{1}{4} + \frac{4}{3\pi} \cos\left(\frac{\pi s}{L}\right) + \frac{11}{14\pi} \cos\left(\frac{2\pi s}{L}\right) + \frac{4}{15\pi} \cos\left(\frac{3\pi s}{L}\right) \right] \quad (6\text{-}6)$$

and is graphically illustrated in Figure 6-4 in relation to the two extreme imperfection forms - curvature and slope imperfection which were previously assumed by Croll and Al-Dabbagh respectively. It may be observed that the proposed 'Cosine Imperfection' lies between these two idealized imperfection forms.

For an imperfection of the type described by (6-6), the particular integral is of the form

$$\chi_p = \frac{N_\phi^P \xi_i}{KL^2} \pi \left\{ C_1 \sin\left(\frac{\pi s}{L}\right) + C_2 \sin\left(\frac{2\pi s}{L}\right) + C_3 \sin\left(\frac{3\pi s}{L}\right) + C_1^* \cos\left(\frac{\pi s}{L}\right) + C_2^* \cos\left(\frac{2\pi s}{L}\right) + C_3^* \cos\left(\frac{3\pi s}{L}\right) \right\} \quad (6\text{-}7)$$

where by substituting into (6-4e), the coefficients are found to be

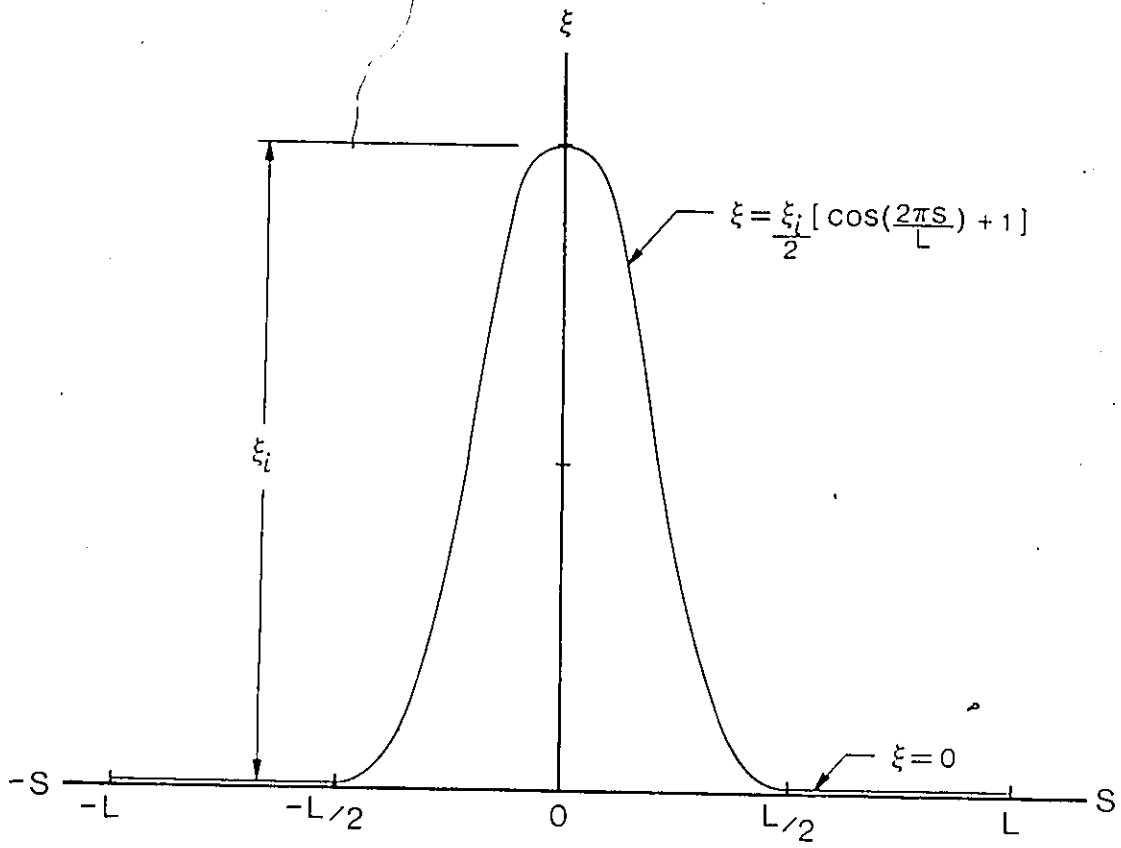

Figure 6-3 Meridional imperfection in the form of a cosine wave

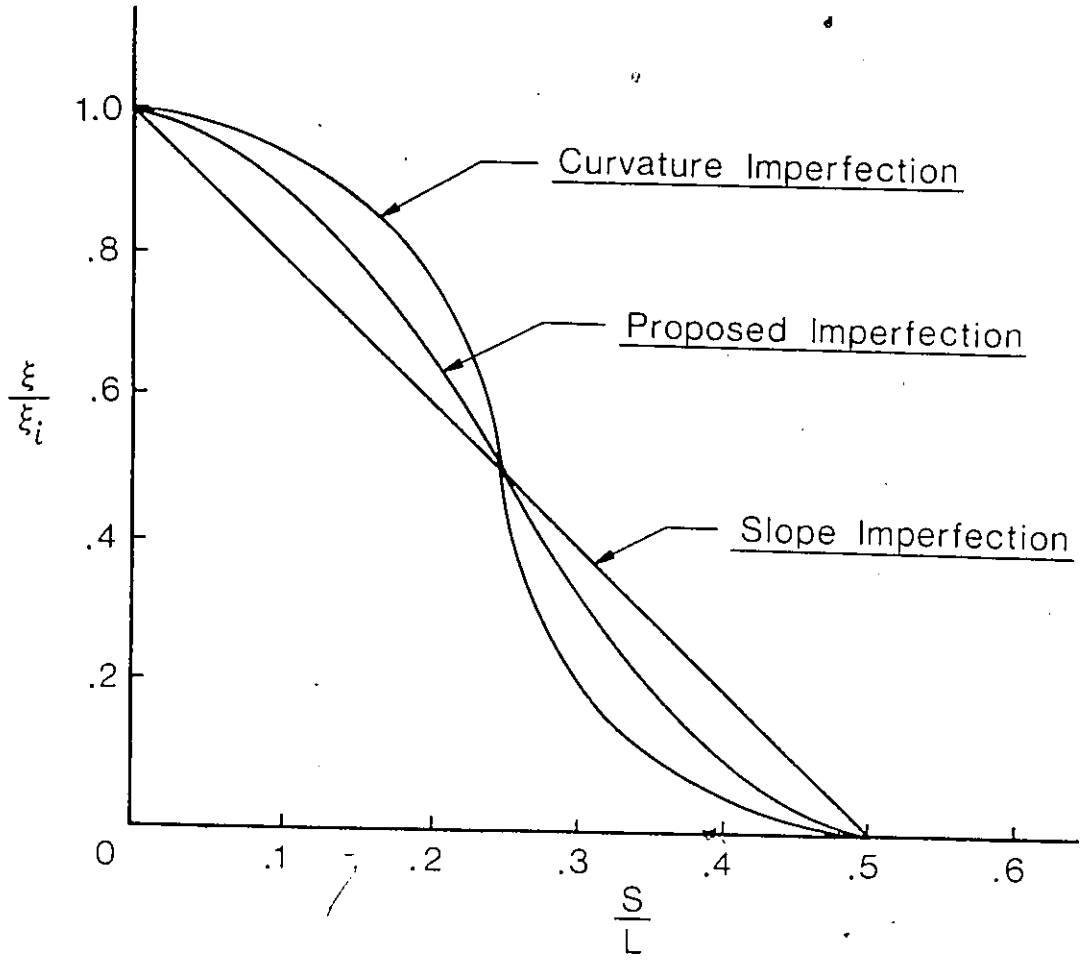

Figure 6-4 Proposed imperfection form in relation to slope and curvature imperfections

$$C_1 = \frac{4}{3}\left\{\frac{\bar{J}_0}{\bar{J}_0^4 - \bar{J}_2 + \bar{J}_3}\right\} \quad , \quad C_1^* = -\frac{\bar{J}_1}{\bar{J}_0} C_1$$

$$C_2 = \frac{44}{7}\left\{\frac{\bar{J}_0}{16\bar{J}_0^4 - 4\bar{J}_2 + \bar{J}_3}\right\} \quad , \quad C_2^* = -\frac{\bar{J}_1}{2\bar{J}_0} C_2$$

$$C_3 = \frac{36}{5}\left\{\frac{\bar{J}_0}{81\bar{J}_0^4 - 9\bar{J}_2 + \bar{J}_3}\right\} \quad , \quad C_3^* = -\frac{\bar{J}_1}{3\bar{J}_0} C_3$$

and

$$\bar{J}_0 = \frac{\pi}{L}$$

$$\bar{J}_1 = \frac{2}{r_2} \cdot \frac{dr_2}{ds}$$

$$\bar{J}_2 = \frac{\pi^2}{L^2 r_2} \cdot \frac{d^2 r_2}{ds^2}$$

$$\bar{J}_3 = \frac{12(1-\nu^2)}{(r_2 t)^2}$$

From equations (6-5) and (6-7), the complete solution is

$$\chi = B_1 \sin\lambda s \cdot \sinh\lambda s + B_2 \sin\lambda s \cdot \cosh\lambda s$$

$$+ B_3 \cos\lambda s \cdot \sinh\lambda s + B_4 \cos\lambda s \cdot \cosh\lambda s$$

$$+ \frac{N_\phi^P \xi_i \pi}{KL^2}\left\{\sum_{n=1}^{3} C_n \sin\left(\frac{n\pi s}{L}\right) + \sum_{m=1}^{3} C_m^* \cos\left(\frac{m\pi s}{L}\right)\right\} \qquad (6\text{-}8)$$

By taking appropriate derivatives of (6-8), the remainder of equations (6-4) will yield

$$\delta Q_\phi = 2K\lambda^2 \left[B_1 \cos\lambda s \cdot \cosh\lambda s + B_2 \cos\lambda s \cdot \sinh\lambda s - B_3 \sin\lambda s \cdot \cosh\lambda s - B_4 \sin\lambda s \cdot \sinh\lambda s \right] - \frac{N_\phi^p \xi_i \pi^3}{L^4} \left\{ \sum_{n=1}^{3} C_n \sin\left(\frac{n\pi s}{L}\right) + \sum_{m=1}^{3} C_m^* \cos\left(\frac{m\pi s}{L}\right) \right\} \quad (6\text{-}9a)$$

$$\delta M_\phi = K\lambda \; B_1 (\cos\lambda s \cdot \sinh\lambda s + \sin\lambda s \cdot \cosh\lambda s) + B_2 (\cos\lambda s \cdot \cosh\lambda s + \sin\lambda s \cdot \sinh\lambda s) + B_3 (\cos\lambda s \cdot \cosh\lambda s - \sin\lambda s \cdot \sinh\lambda s) + B_4 (\cos\lambda s \cdot \cosh\lambda s - \sin\lambda s \cdot \cosh\lambda s) + \frac{N_\phi^p \xi_i}{L^3} \pi^2 \left\{ \sum_{n=1}^{3} n C_n \cos\left(\frac{n\pi s}{L}\right) - \sum_{m=1}^{3} m C_m^* \sin\left(\frac{m\pi s}{L}\right) \right\} \quad (6\text{-}9b)$$

$$\delta N_\theta = -2K\lambda^2 \Big[B_1 \left(-\lambda r_2 \sin\lambda s \cdot \cosh\lambda s + \lambda r_2 \cos\lambda s \cdot \sinh\lambda s + \frac{dr_2}{ds} \cos\lambda s \cdot \cosh\lambda s\right)$$

$$+ B_2 \left(-\lambda r_2 \sin\lambda s \cdot \sinh\lambda s + \lambda r_2 \cos\lambda s \cdot \cosh\lambda s + \frac{dr_2}{ds} \cos\lambda s \cdot \sinh\lambda s\right)$$

$$- B_3 \left(\lambda r_2 \cos\lambda s \cdot \cosh\lambda s + \lambda r_2 \sin\lambda s \cdot \sinh\lambda s + \frac{dr_2}{ds} \sin\lambda s \cdot \sinh\lambda s\right)$$

$$- B_4 \left(\lambda r_2 \cos\lambda s \cdot \sinh\lambda s + \lambda r_2 \sin\lambda s \cdot \cosh\lambda s + \frac{dr_2}{ds} \sin\lambda s \cdot \sinh\lambda s\right) \Big]$$

$$+ \frac{N_\phi \sum_i^p \xi_i r_2}{L^2} \Bigg\{ -\pi \left[\frac{4}{3} \cos\left(\frac{\pi s}{L}\right) + \frac{22}{7} \cos\left(\frac{2\pi s}{L}\right) + \frac{12}{5} \cos\left(\frac{3\pi s}{L}\right) \right]$$

$$+ \frac{\pi^4}{L^3} \left[\sum_{n=1}^{3} n^3 C_n \cos\left(\frac{n\pi s}{L}\right) - \sum_{m=1}^{3} m^3 C_m^* \sin\left(\frac{m\pi s}{L}\right) \right]$$

$$- \frac{\pi^3}{L^2} \cdot \frac{1}{r_2} \cdot \frac{dr_2}{ds} \left[\sum_{n=1}^{3} n^2 C_n \sin\left(\frac{n\pi s}{L}\right) + \sum_{m=1}^{3} m^2 C_m^* \cos\left(\frac{m\pi s}{L}\right) \right] \Bigg\} \quad (6\text{-}9c)$$

Equations (6-9), express the force changes in transverse shear δQ_ϕ, meridional moment δM_ϕ and circumferential force δN_θ generated by meridional imperfection for the range $-L<S<L$ on which the truncated Fourier Series (6-6) was derived. It remains to determine the constants B_1 to B_4 so that the boundary conditions of the problem are satisfied.

6.2.3 MAXIMUM IMPERFECTION FORCES

Of interest are the maximum meridional moment and circumferential force induced in a region close to the centre of the imperfection ie S = 0. The degree to which profile variations of the true meridian influence these maximum force changes can be ascertained from the form of the coefficients C_n and C_m^*. The parameter J_1 accounts for a sloping meridian while J_2 a curved meridian at the level of imperfection.

In Figure 6-5, the ratio (J_2/J_3) and (J_1/J_0) have been plotted against imperfection wavelength for the two previously analyzed shells of chapter 5. It is seen that J_2 is three orders of magnitude less than J_3 and can therefore be eliminated from the denominators of coefficients C_n with negligible loss of accuracy. The maximum value of the ratio J_1/J_0 is 10^{-1} so that coefficients C_m^* are atleast one order of magnitude less than C_n while the term $\frac{\pi^3}{L^2} \cdot \frac{1}{r_2} \cdot dr_2/dS$ in (6-9c) represents a quantity two orders of magnitude less

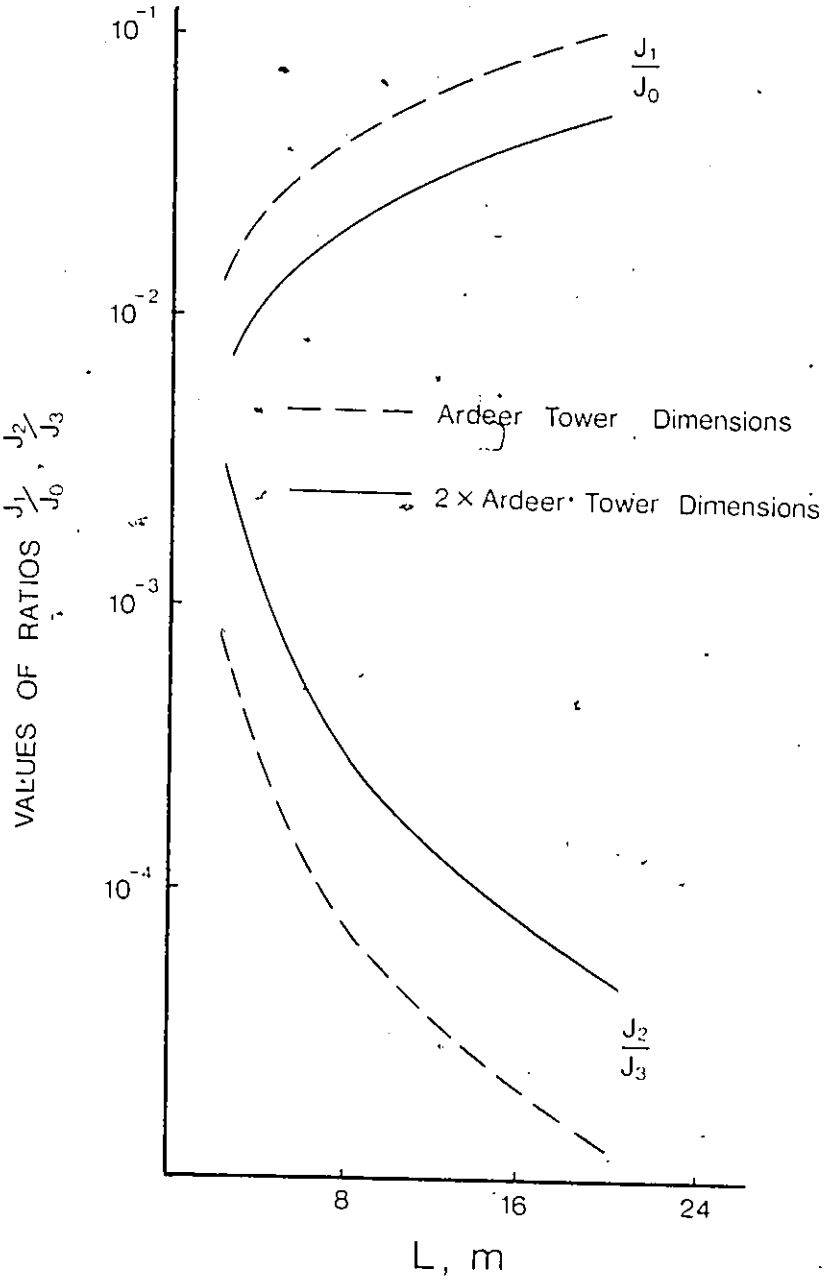

Figure 6-5 Ratios J_2/J_3 and J_1/J_0 for varying imperfection wavelength in the two cooling tower shells

than π^4/L^3. Consequently, the sine terms within the curly brackets of (6-9b) and (6-9c) have only a small influence on the force distribution. More important, the sine function ensures that these terms will make no contribution to the peak forces in the vicinity of S = 0. Thus, slope and curvature of the perfect meridian can be neglected in the particular integral (6-7). Furthermore, having previously demonstrated the second and third terms on the left side of (6-4e) to have little effect on the complimentary function (6-5), the maximum forces arising from meridional imperfection in a cooling tower shell should therefore be the same as those in an imperfect cylinder having radius r_2. In other words, when considering imperfection forces close to the centre of the imperfection

$$\chi_{\substack{\text{Cooling Tower}\\ \text{Shell}}} \cong \chi_{\substack{\text{Cylindrical Shell}\\ \text{Having } r_0 = r_2}}$$

$$= B_1 \sin\lambda s \cdot \sinh\lambda s + B_2 \sin\lambda s \cdot \cosh\lambda s$$

$$+ B_3 \cos\lambda s \cdot \sinh\lambda s + B_4 \cos\lambda s \cdot \cosh\lambda s$$

$$+ \frac{N_\phi P \xi_i}{KL^2} \sum_{n=1}^{3} \pi C_n \sin\left(\frac{n\pi s}{L}\right) \qquad (6\text{-}10)$$

Having suitably chosen the origin of the coordinate axis (S, ξ) at the centre of the imperfection, the constants B_1 to B_4 may be reduced to two in number. By symmetry of the problem, the meridional moment M_ϕ must be symmetrical about the origin ie have identical values at $\pm S$. This demands that the rotations χ in equation (6-10) be antisymmetrical about the origin. To ensure that only antisymmetric terms are present, B_1 and B_4 are set to zero. Furthermore, if it is assumed that the effects of an imperfection quickly die down over a distance equal to the imperfection wavelength, the boundary conditions for this problem can be taken as

$$\chi(L) = \left.\frac{d\chi}{dS}\right|_{S=L} = 0 .$$

The constants B_2 and B_3 satisfying these conditions are calculated to be (Appendix B)

$$B_2 = \frac{N_\phi^P \xi_i \pi^2}{KL^3}\left(-C_1 + 2C_2 - 3C_3\right)\left[\frac{-\cos\lambda L \cdot \sinh\lambda L}{\lambda \sin\lambda L \cdot \cos\lambda L - \lambda \sinh\lambda L \cdot \cosh\lambda L}\right]$$

$$B_3 = \frac{N_\phi^P \xi_i \pi^2}{KL^3}\left(-C_1 + 2C_2 - 3C_3\right)\left[\frac{\sin\lambda L \cdot \cosh\lambda L}{\lambda \sinh\lambda L \cdot \cosh\lambda L - \lambda \sin\lambda L \cdot \cos\lambda L}\right]$$

Substituting for the values of the constants B in equation (6-10) and differentiating yields

$$\delta M_\phi = \frac{N_\phi^P \xi_i \pi^2}{L^3} \left\{ \frac{-C_1 + 2C_2 - 3C_3}{\sin 2\lambda L - \sinh 2\lambda L} \times \right.$$

$$\left[(2\cos\lambda L \cdot \sinh\lambda L)(\cos\lambda s \cdot \cosh\lambda s + \sin\lambda s \cdot \sinh\lambda s) - \right.$$

$$\left. (2\sin\lambda L \cdot \cosh\lambda L)(\cos\lambda s \cdot \cosh\lambda s - \sin\lambda s \cdot \sinh\lambda s) \right] +$$

$$\left. \sum_{n=1}^{3} n C_n \cos\left(\frac{n\pi s}{L}\right) \right\} \qquad (6\text{-}11a)$$

$$\delta N_\theta = \frac{N_\phi^P \xi_i r_2}{L^2} \left\{ \frac{-2\lambda^2 \pi^2}{L} \left(\frac{-C_1 + 2C_2 - 3C_3}{\sin 2\lambda L - \sinh 2\lambda L} \right) \times \right.$$

$$\left[(2\cos\lambda L \cdot \sinh\lambda L)(\cos\lambda s \cdot \cosh\lambda s - \sin\lambda s \cdot \sinh\lambda s) + \right.$$

$$\left. (2\sin\lambda L \cdot \cosh\lambda L)(\cos\lambda s \cdot \cosh\lambda s + \sin\lambda s \cdot \sinh\lambda s) \right] -$$

$$\pi \left(\frac{4}{3} \cos\left(\frac{\pi s}{L}\right) + \frac{22}{7} \cos\left(\frac{2\pi s}{L}\right) + \frac{12}{5} \cos\left(\frac{3\pi s}{L}\right) \right) +$$

$$\left. \frac{\pi^4}{L^3} \sum_{n=1}^{3} n^3 C_n \cos\left(\frac{n\pi s}{L}\right) \right\} \qquad (6\text{-}11b)$$

As a check for the validity of equations (6-11), two meridionally loaded, imperfect shells representing truncated portions from the throat and the base of the Ardeer tower shell were analyzed. A comparison between the force changes predicted by a finite element analysis and the closed form

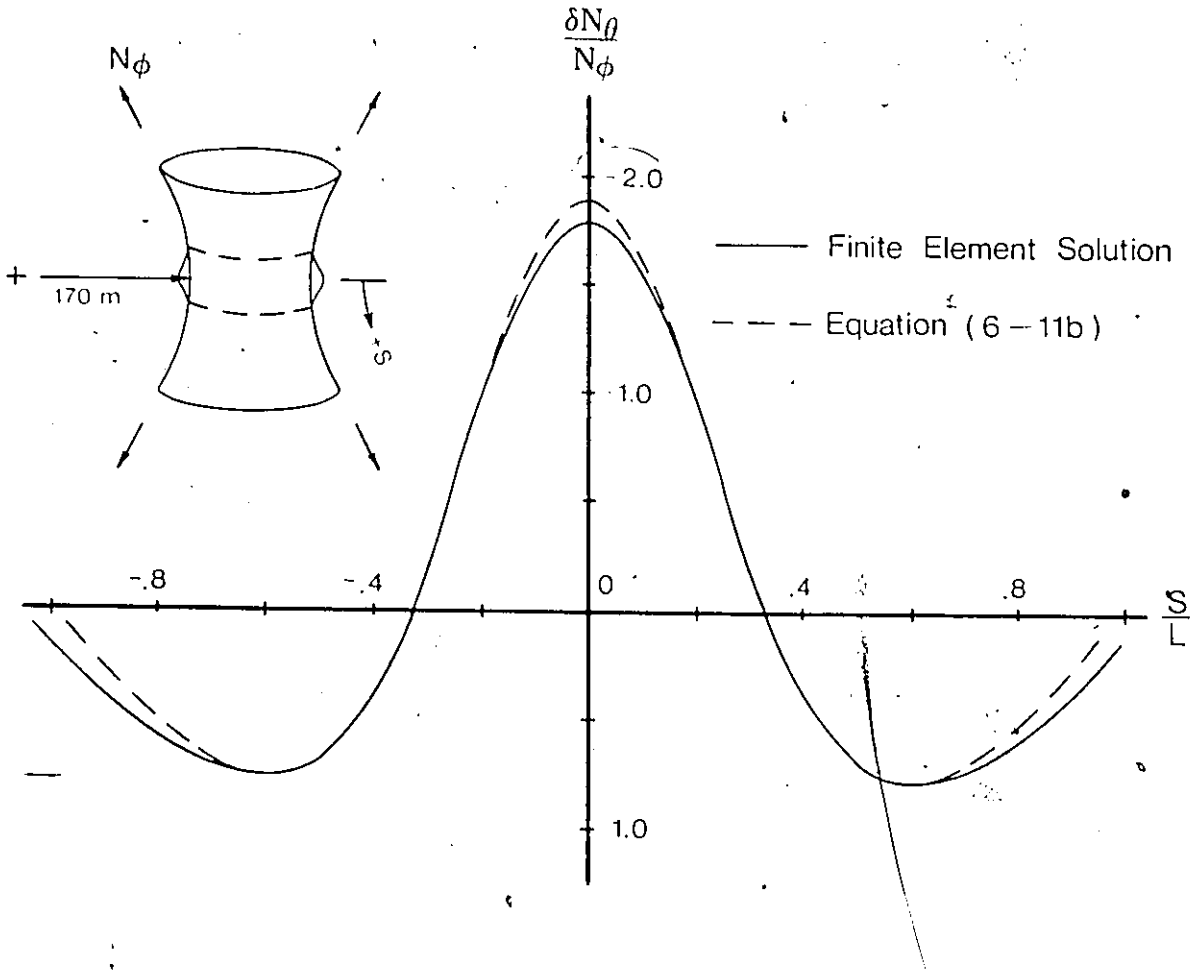

Figure 6-6a Meridional variation of circumferential force induced by an imperfection having ξ_i = 30 cm and L = 5 m

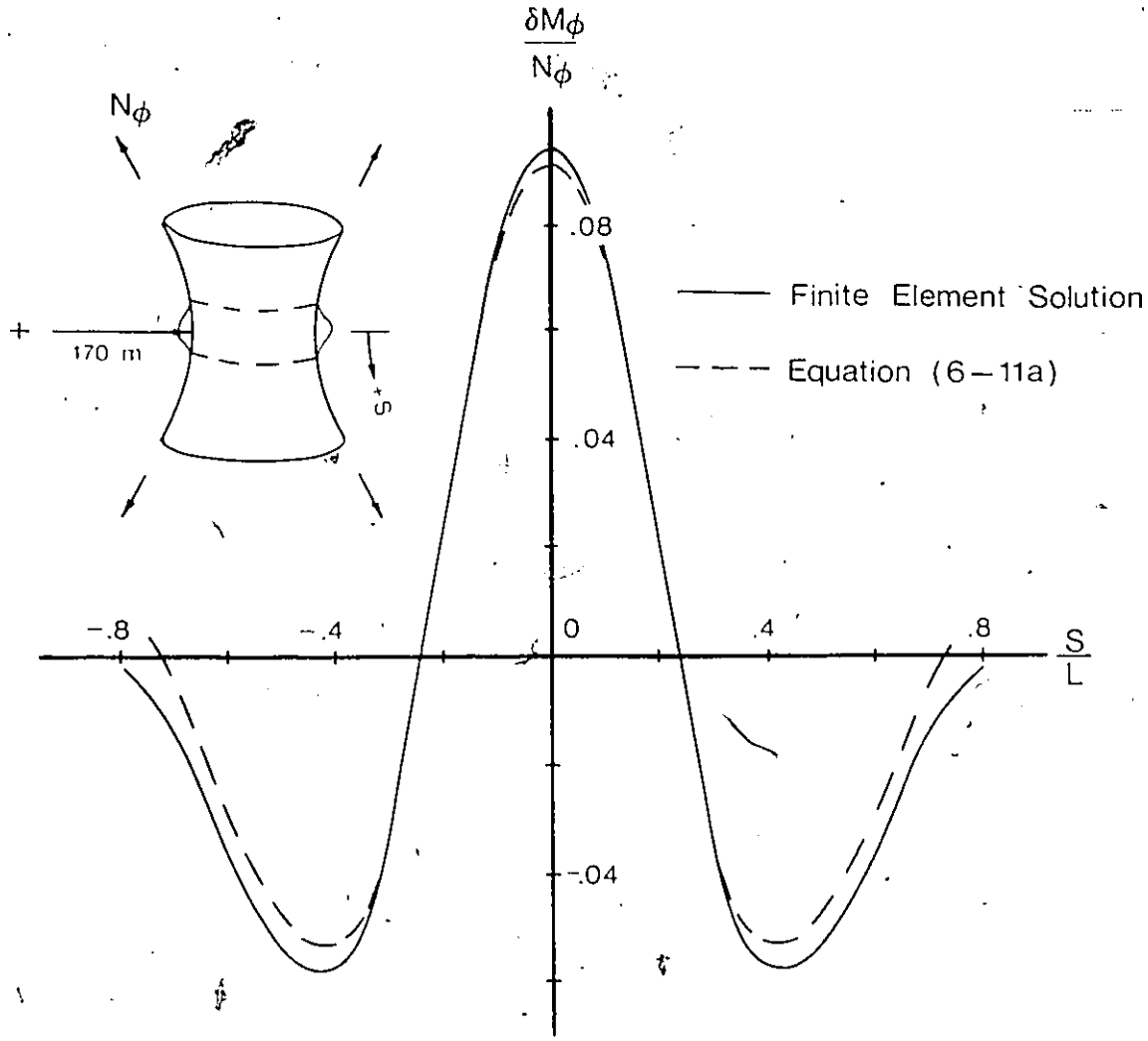

Figure 6-6b Meridional variation of meridional moment induced by an imperfection having ξ_i = 30 cm and L = 5 m

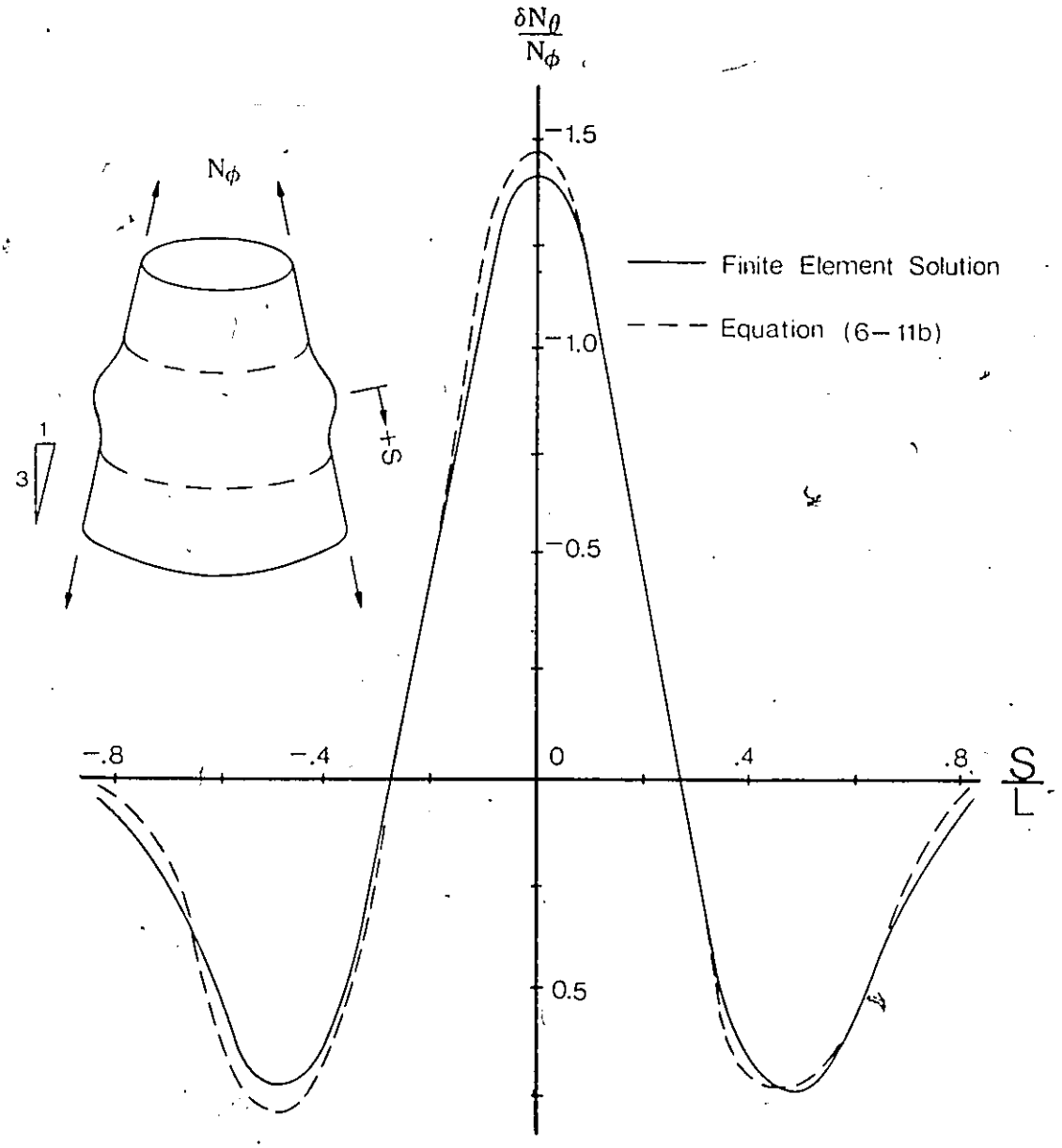

Figure 6-7a Meridional variation of circumferential force induced by an imperfection having ξ_i = 30 cm and L = 10 m

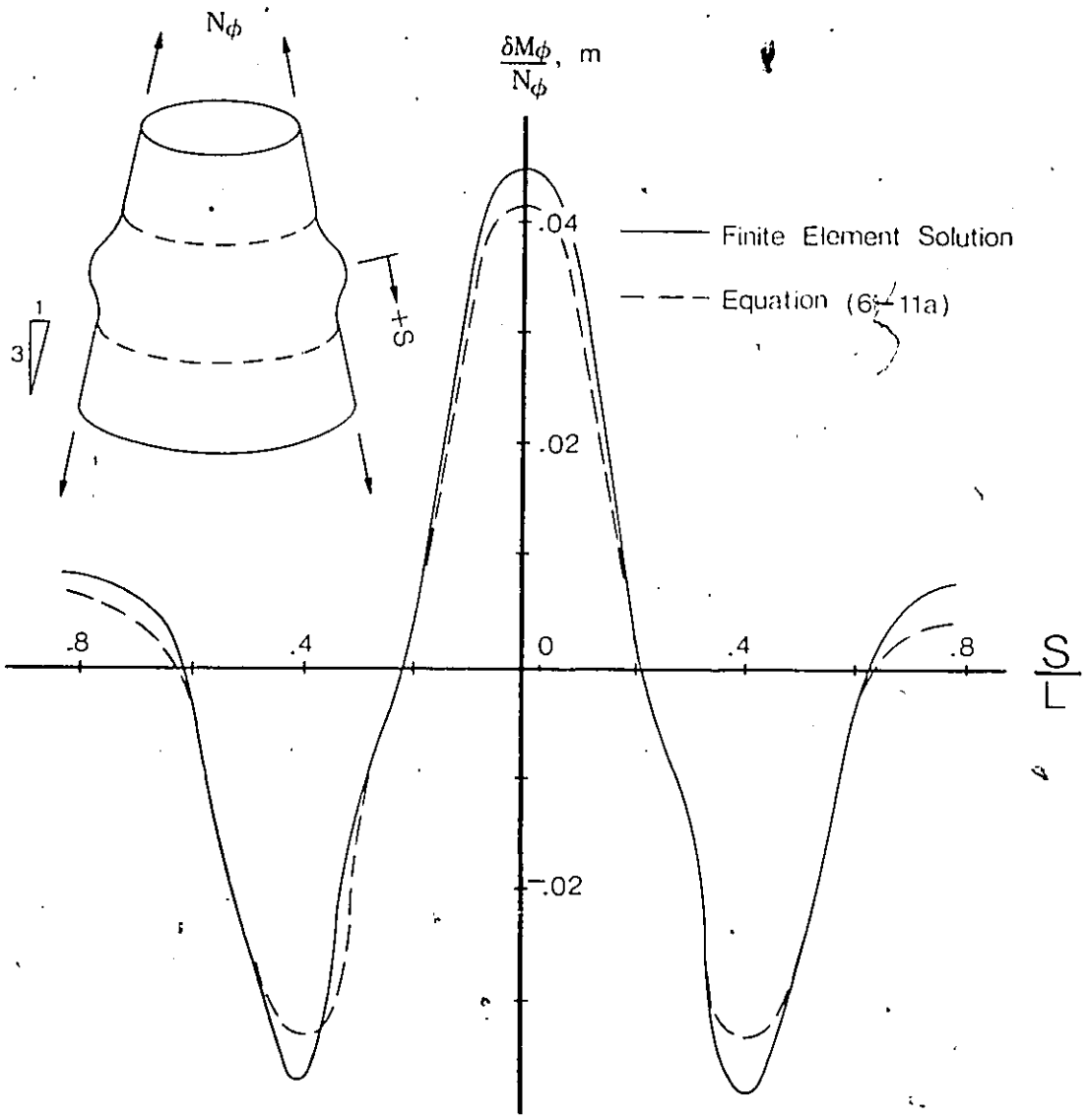

Figure 6-7b Meridional variation of meridional moment induced by an imperfection having ξ_i = 30 cm and L = 10 m

solution, shown in Figures 6-6 and 6-7, indicates close agreement within the meridional range (-.8L, .8L).

Next, setting S = 0, the maximum meridional moment and circumferential force occuring at the centre of the imperfection are determined from (6-11) to be

$$\delta M_{\phi MAX} = N_\phi^P \xi_i \left\{ \frac{4/3\,\pi^3}{\pi^4+\alpha}(1-\mu_1) + \frac{88/7\,\pi^3}{16\pi^4+\alpha}(1+\mu_1) + \frac{108/5\,\pi^3}{81\pi^4+\alpha}(1-\mu_1) \right\}$$

$$= N_\phi^P \xi_i \beta \qquad (6\text{-}12a)$$

$$\delta N_{\theta MAX} = \frac{N_\phi^P \xi_i r_2}{L^2} \left\{ \frac{4/3\,\pi^5}{\pi^4+\alpha}(1+\mu_2) + \frac{352/7\,\pi^5}{16\pi^4+\alpha}\left(1-\frac{\mu_2}{4}\right) + \frac{972/5\,\pi^5}{81\pi^4+\alpha}\left(1+\frac{\mu_2}{9}\right) - \frac{722\pi}{105} \right\}$$

$$= \frac{N_\phi^P \xi_i r_2}{L^2}\,\Gamma \qquad (6\text{-}12b)$$

where

$$\alpha = \frac{12(1-\nu^2)L^4}{(r_2 t)^2}$$

$$\mu_1 = \frac{2\cos\lambda L \cdot \sinh\lambda L - 2\sin\lambda L \cdot \cosh\lambda L}{\sin 2\lambda L - \sinh 2\lambda L}$$

$$\mu_2 = \frac{4\lambda^2 L^2}{\pi^2}\left(\frac{\cos\lambda L \cdot \sinh\lambda L + \sin\lambda L \cdot \cosh\lambda L}{\sin 2\lambda L - \sinh 2\lambda L}\right)$$

The coefficients β and Γ have been conveniently plotted in Figure 6-8 to facilitate the computation of equations (6-12). It is noted that the Poisson effect entering via the term $(1-\nu^2)$ is relatively minor for concrete and may be neglected. Furthermore, the coefficients $\mu \rightarrow 0$ and have little effect on the outcome of equations (6-12). This is to say that only the particular integral of (6-4e) need be considered so that imperfections of the type considered here, act as stress concentrators whose maximum forces are not influenced by the respective boundary conditions at $S = \pm L$.

6.2.4 MAGNIFICATION DUE TO P-Δ EFFECT

Preliminary finite element analyses of imperfect cylinders having the properties of reinforced concrete and subjected to the meridional compressive loads found near the base of cooling tower shells, indicate radial deflections to be of the order of magnitude as the height of imperfection. This implies a certain non linear magnifying effect which is proportional to the applied load and necessitates a time consuming iterative aproach on the computer. However, under the assumption that the deflected meridian is itself a cosine curve of wavelength L, an approximate but more convenient solution can be obtained.

Neglecting curvature changes in the circumferential direction, a differential change in imperfection height at the centre of the imperfection is given by

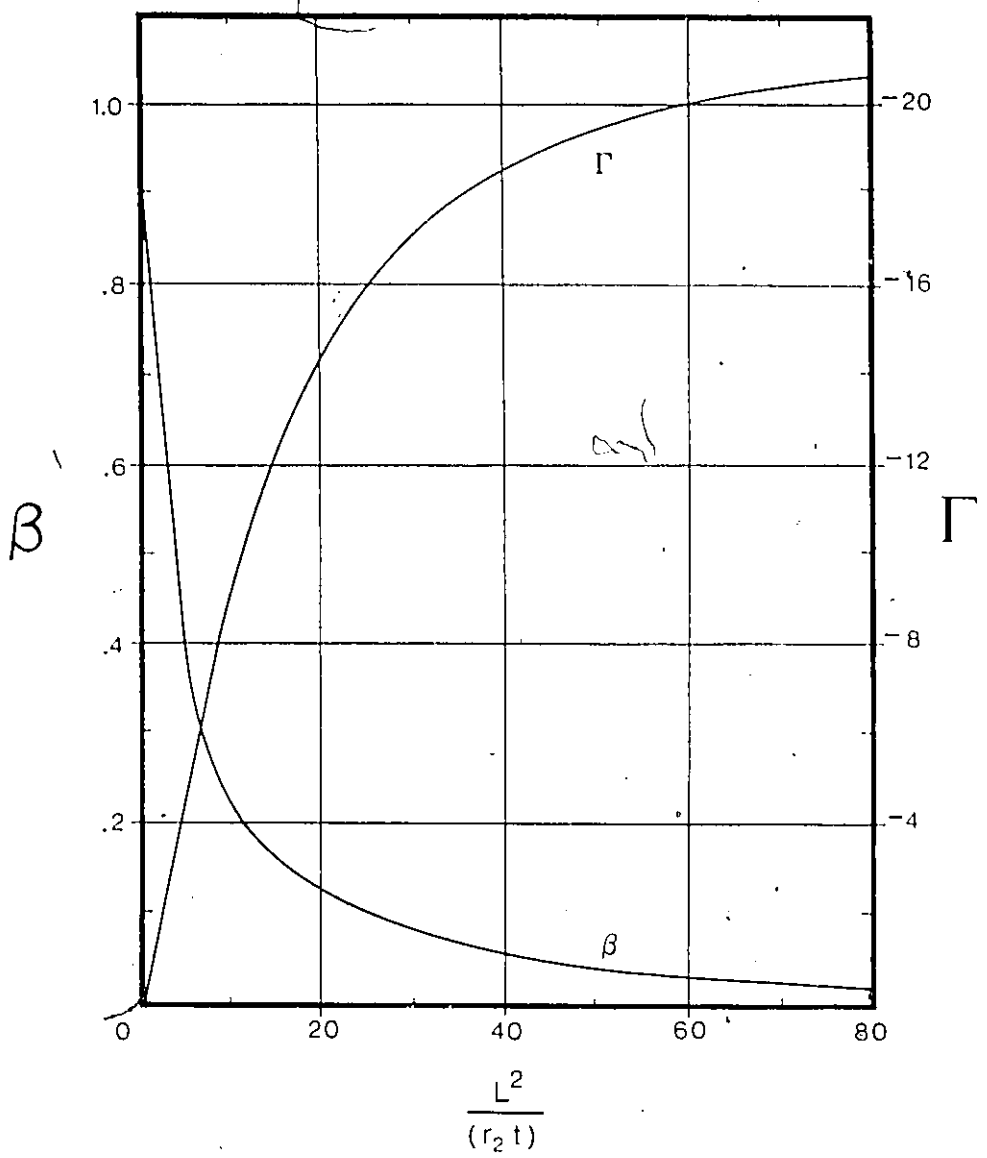

Figure 6-8 Values of β and Γ in equations (6-12) pertaining to the elastic, isotropic shell

$$d\xi = \frac{12(1-\nu^2)}{Et^3} \int_0^L (S \cdot dM_\phi)\, dS$$

Substituting for M_ϕ from (6-11a) and performing the necessary integration gives

$$d\xi = \Psi \cdot \frac{\xi_i L^2}{Et^3}\, dN_\phi \qquad (6\text{-}13)$$

where $$\Psi = \frac{12(1-\nu^2)}{L^3}\left\{-2C_1 - \frac{2}{3}C_3\right\}$$

has been plotted for convenience in Figure 6-9. In accordance with (6-11a) a differential change in imperfection moment due to a meridional force increase from N_ϕ to $N_\phi + dN_\phi$ is given by

$$d(\delta M_\phi)_{P\text{-}\Delta} = \frac{\pi^2}{L^3}\left\{\sum_{n=1}^{3} n C_n \cos\left(\frac{n\pi s}{L}\right)\right\} d\left[\left(\xi_i + \int_0^{N_\phi} d\xi\right) N_\phi\right]$$

$$= \frac{\pi^2}{L^3}\left\{\sum_{n=1}^{3} n C_n \cos\left(\frac{n\pi s}{L}\right)\right\} d\left[\left(\xi_i + \int_0^{N_\phi} \frac{\Psi \xi_i L^2}{Et^3}\, dN_\phi\right) N_\phi\right]$$

$$= \frac{\pi^2}{L^3}\left\{\xi_i \sum_{n=1}^{3} n C_n \cos\left(\frac{n\pi s}{L}\right)\right\}\left(1 + \Psi \cdot \frac{2N_\phi L^2}{Et^3}\right) dN_\phi$$

Integrating these differential changes as the meridional force progresses from 0 to N_ϕ yields

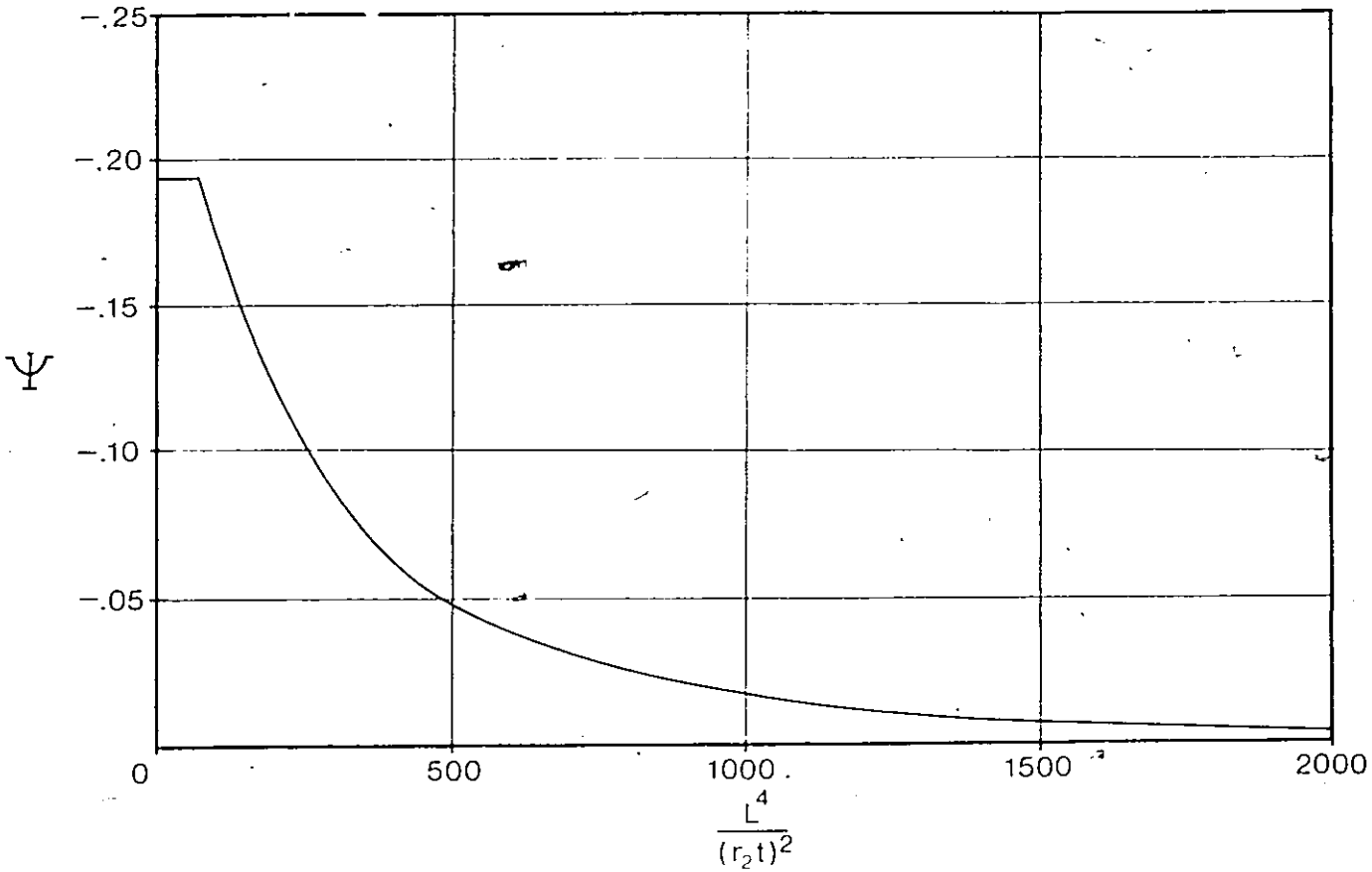

Figure 6-9 Coefficient Ψ in equations (6-13), (6-14) and (6-15)

$$\int_0^{N_\phi} d(\delta M_\phi)_{P-\Delta} = \delta M_\phi \left\{ 1 + \Psi \frac{N_\phi L^2}{E t^3} \right\} \qquad (6\text{-}14a)$$

A similar analysis for the circumferential force will yield the result

$$\int_0^{N_\phi} d(\delta N_\theta)_{P-\Delta} = \delta N_\theta \left\{ 1 + \Psi \frac{N_\phi L^2}{E t^3} \right\} \qquad (6\text{-}14b)$$

The terms within the brackets of equations (6-14) represent the magnification due to the P - Δ effect. As an example, consider an imperfection near the base of the Ardeer tower of wavelength L = 10 m (32.8 ft). In this case

$$\frac{L^4}{(r_2 t)^2} = \frac{(10\,m)^4}{(35\,m \times .15\,m)^2} = 363$$

From Figure (6-9) $\Psi \cong -.075$

$$\therefore \left\{ 1 + \Psi \frac{N_\phi L^2}{E t^3} \right\} = \left\{ 1 + (-.075) \frac{(-1.14 \times 10^6\ N/m)(10\,m)^2}{(25 \times 10^9\ Pa)(.15\,m)^3} \right\}$$

$$= 1.10$$

Hence, the P-Δ effect in this example, would increase the maximum imperfection forces by 10%.

When the above magnification effect is included in equations (6-12), the maximum change in meridional moment and circumferential force occurring at the centre of imperfection is then given by

$$\delta M_{\phi_{MAX}} = \beta N_\phi^P \xi_i \left\{ 1 + \Psi \frac{N_\phi^P L^2}{Et^3} \right\} \qquad (6\text{-}15a)$$

$$\delta N_{\theta_{MAX}} = \Gamma \frac{N_\phi^P \xi_i r_2}{L^2} \left\{ 1 + \Psi \frac{N_\phi^P L^2}{Et^3} \right\} \qquad (6\text{-}15b)$$

As previously stated, these force increases are to be superposed with the respective forces arising from an analysis of the perfect shell and forms the basis for determining the horizontal and vertical steel requirements in the as constructed, imperfect shell.

6.3 COMPARISON OF SOLUTIONS

In Figures 6-10 and 6-11, the maximum force changes arising from meridional imperfection have been plotted against imperfection length for a region near the base of the two cooling tower shells of Chapter 5. The validity of the proposed solution, equation (6-12), and those of Croll and Al-Dabbagh, equations (4-1) and (4-4), can be ascertained by comparing with the respective maximum imperfection forces as predicted by finite element analyses and which are shown as points in Figures 6-10 and 6-11.

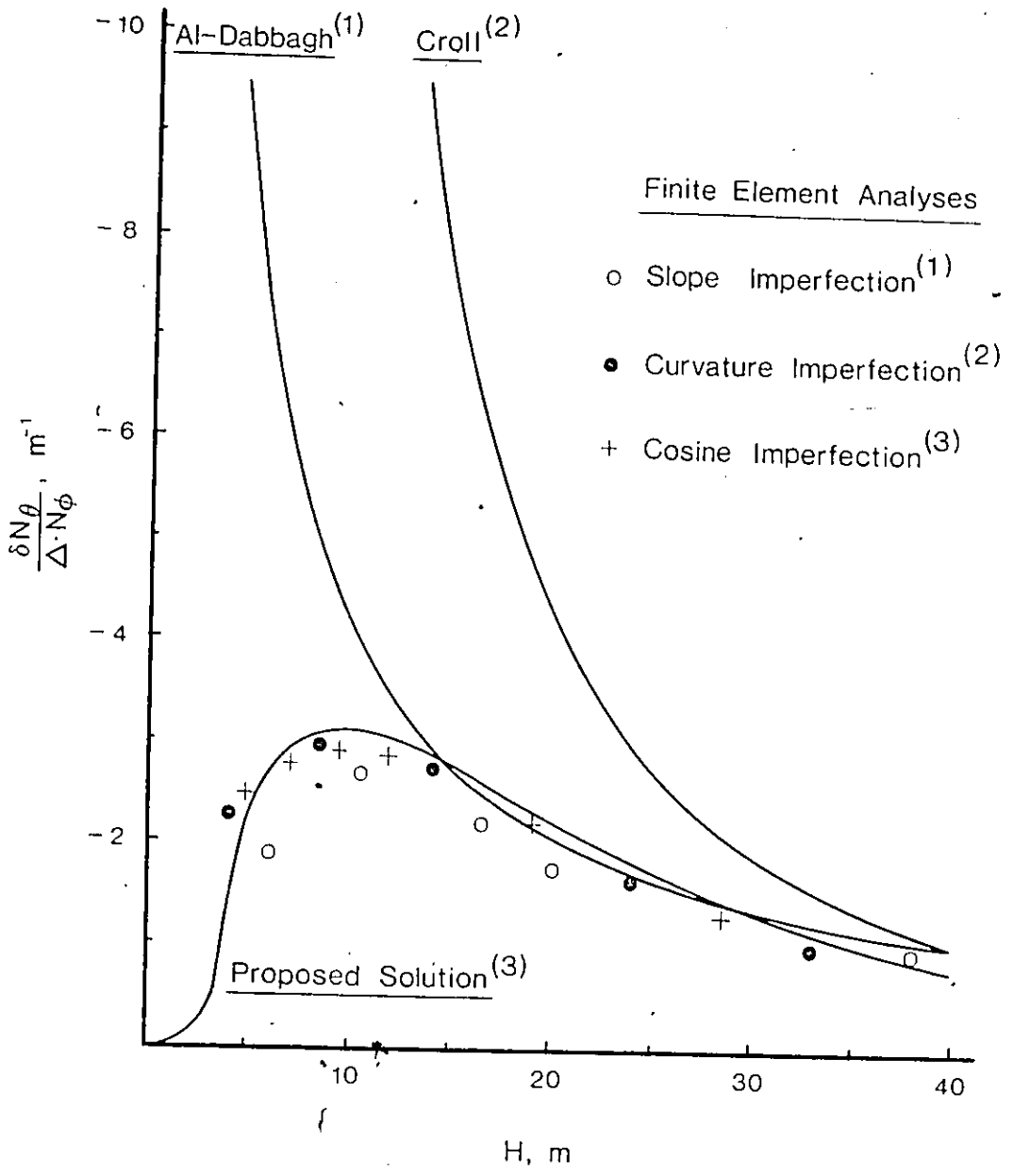

Figure 6-10a Maximum imperfection circumferential force near the base of the larger shell

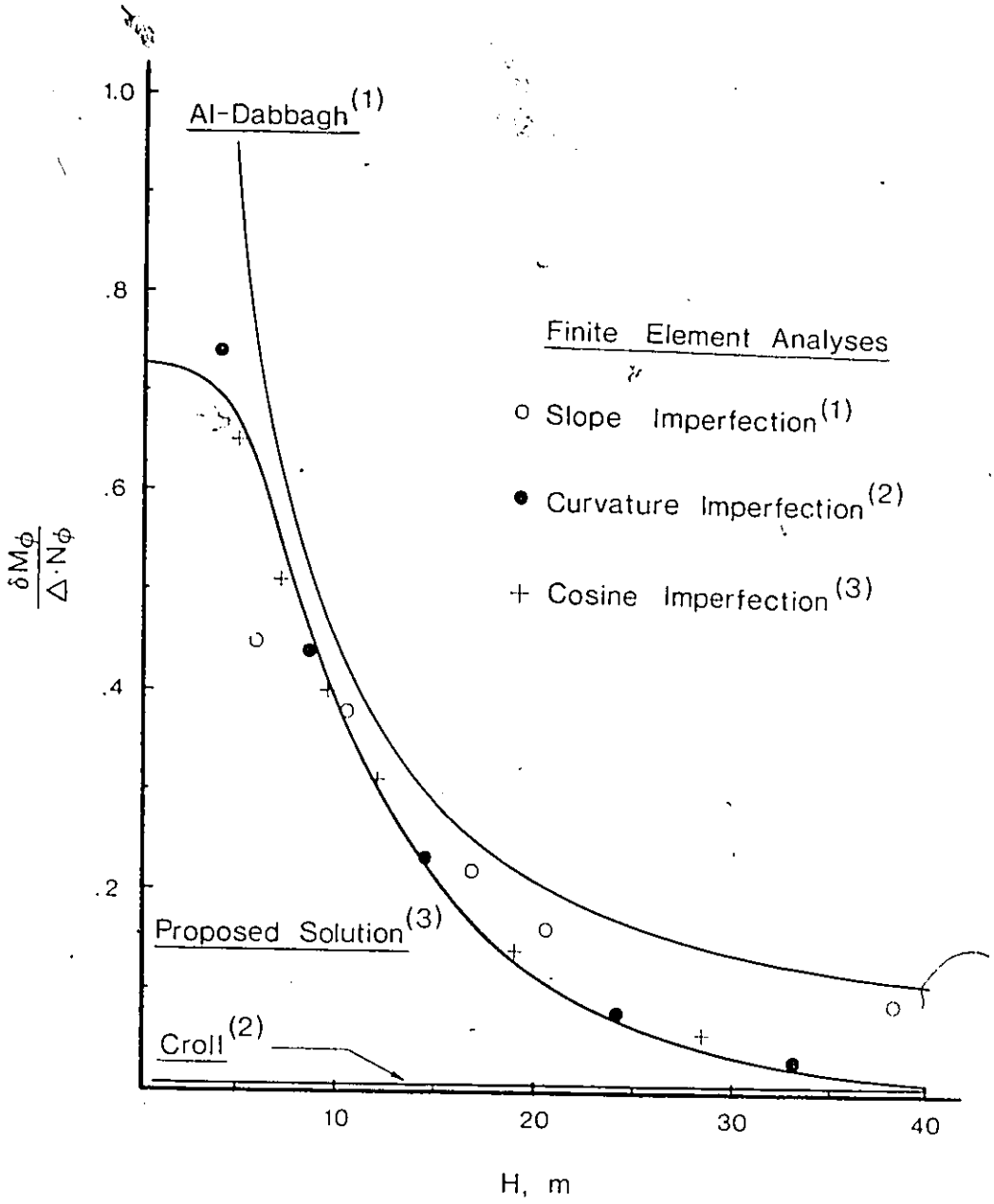

Figure 6-10b Maximum imperfection meridional moment near the base of the larger shell

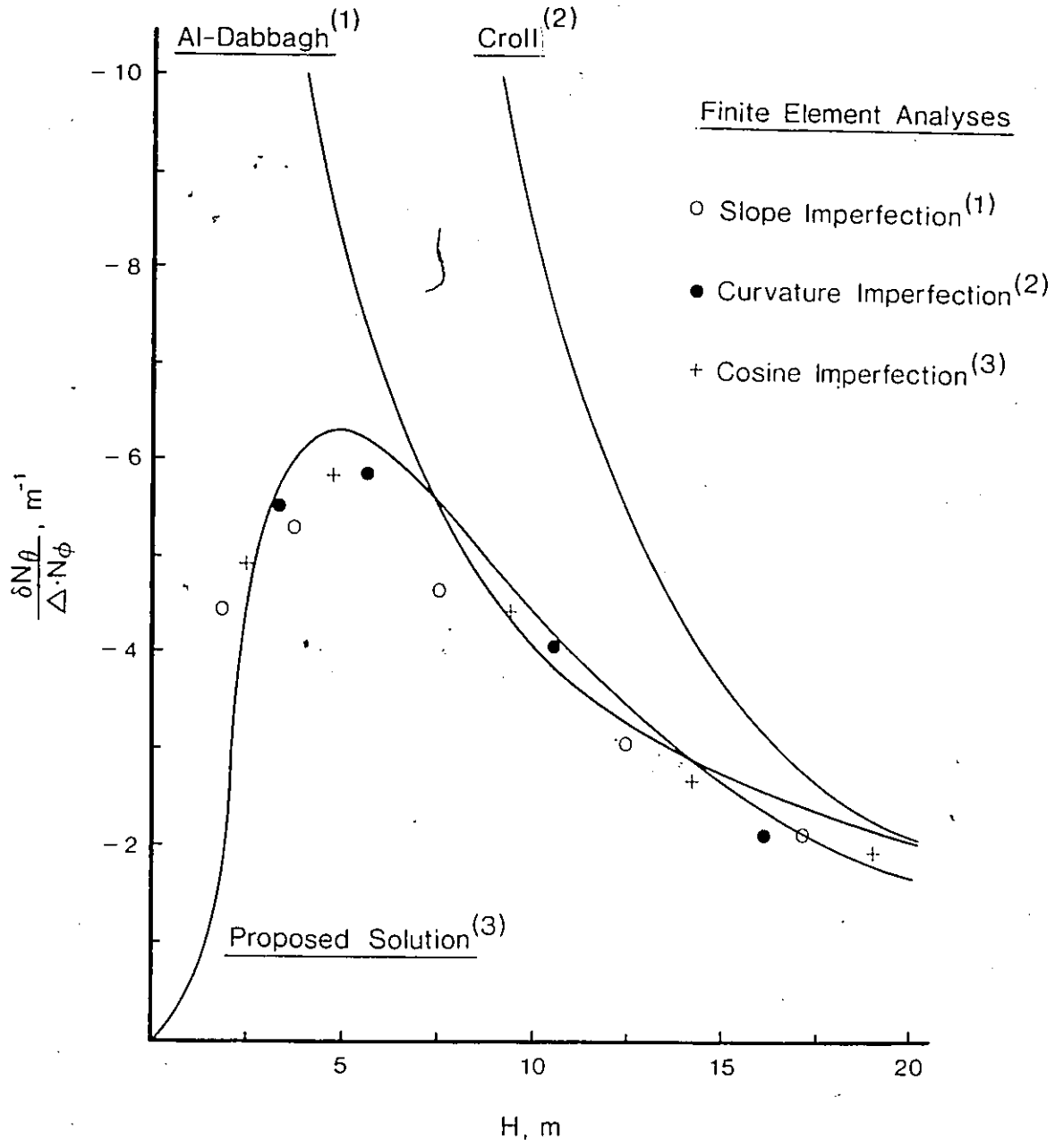

Figure 6-11a Maximum imperfection circumferential force near the base of the smaller shell

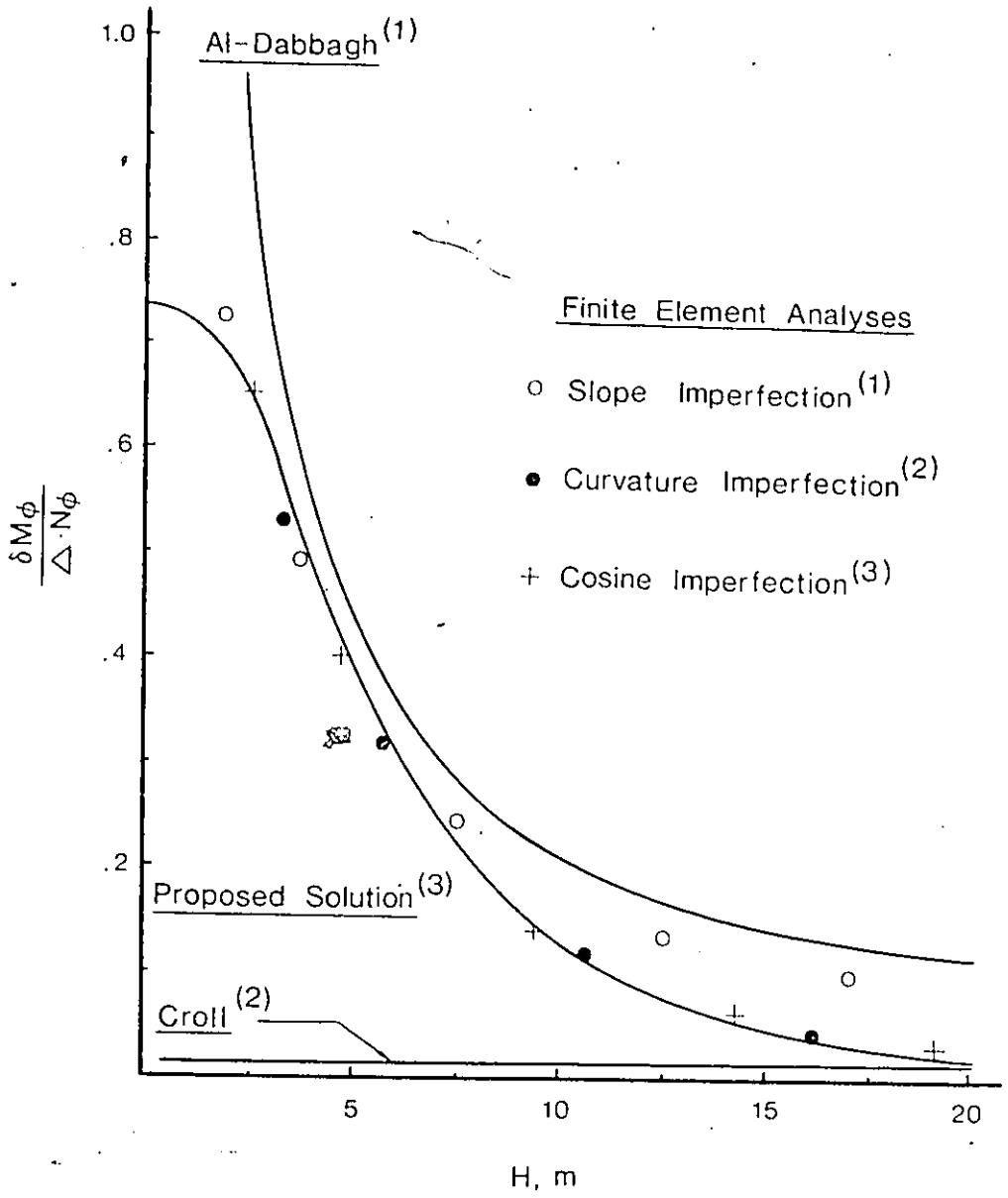

Figure 6-11b Maximum imperfection meridional moment near the base of the smaller shell

It is found that the proposed solution agrees well with the finite element analyses for a wide range of imperfection lengths; up to 20 metres (66 ft) in the smaller shell and 40 metres (131 ft) in the larger shell. For long imperfections, the shell's membrane stiffness dominates and the three solutions yield comparable forces. However, discrepancies are observed between the forces obtained from the finite element analyses and those of Croll and Al-Dabbagh for the smaller imperfection lengths as follows :

(1) With decreasing H, meridional bending becomes increasingly important in resisting the out-of-balance moment generated by an imperfection. Croll's solution, having neglected this contribution altogether, overestimates the magnitude of the circumferential force. As a consequence, for lengths $H < 9$ m (30 ft) in the smaller shell or $H < 18$ m (60 ft) in the larger shell, Croll predicts circumferential forces more than double those predicted by the finite element analyses.

(2) It is evident from the right handside of equation (6-4a) that if bending is to be included in a meridionally imperfect cylinder, the value for the statically equivalent load is not purely a function of the imperfection curvature $d^2\xi/dS^2$ as in equation (3-7a) but is also related to the change in meridional moment d^2M_ϕ/dS^2. Consequently, for meridional imperfections having a finite height but short length, neglecting the sudden variations of the meridional

moment which are induced within the region of the imperfection will cause the statically equivalent load of Figure 3-6 to increase indefinitely. ie. $d^2\xi/dS^2 \rightarrow \infty$ as $H \rightarrow 0$. Having adopted this method for evaluating imperfection forces, Al-Dabbagh inherently predicts large force changes for short imperfection lengths ($H < 7.5$ m (25 ft) in the smaller shell or $H < 15$ m (49 ft) in the larger shell). In contrast, with decreasing H, the proposed solution reverts from membrane to bending resistance where the meridional moment approaches a maximum value of $0.76\xi_i \cdot N_\phi$.

Chapter VII

TOLERANCE LIMITS FOR MERIDIONAL IMPERFECTIONS

7.1 FORCE REDISTRIBUTION IN VICINITY OF IMPERFECTION

Croll and Al-Dabbagh calculated the elastic force changes as a conseqence of a 'local' imperfection in the true meridian of a cooling tower shell. Based on assumed failure mechanisms consistent with these force changes, criteria for limiting the meridional imperfections were proposed in the form of equations (4-2) and (4-5). However, despite a common approach to the imperfection problem, a comparison of the maximum tolerable radial deviations predicted by these equations (Chapter 5), disclosed significant discrepancies between the two tolerance criteria.

In assuming a mechanism of failure, neither criterion accounts for the presence of meridional cracks in the region of an imperfection. Instead, the tolerance limits derived by Croll and Al-Dabbagh assume the shell to behave isotropically up to the instant that local failure occurs. Given such a response, Croll and Kemp assumed the shell's membrane stiffness to dominate so that the out-of-balance moment generated by an imperfection is largely resisted by membrane action. However, cooling tower shells may undergo meridional crack-

ing induced by shrinkage, thermal stresses or settlement resulting in cracks 1.6 to 3.2 mm (1/16 to 1/8 in) wide or wider (29). Such cracks would lower the membrane stiffness in the circumferential direction and render the shell orthotropic.

In the case of the Ardeer tower, the growth of vertical cracks were recorded throughout the life of the shell. Furthermore, their detrimental effect, given the presence of an imperfection, was illustrated in the calculations presented by the Committee of Inquiry. These calculations showed that the growth of a single dominant meridional crack into the zone of major imperfection was responsible for the premature failure of the tower at wind speeds lower than those which had previously been withstood.

Croll and Al-Dabbagh also neglected the effect of force redistribution during local failure induced by an imperfection. Al-Dabbagh and Gupta (23) demonstrated that the product of imperfection forces $\delta N_\theta \cdot \delta M_\phi$ is a constant and is independent of the shell's elastic properties. If the shell lacks resistance to one of them (δN_θ or δM_ϕ), there is a corresponding increase in the other so as to maintain equilibrium. Therefore, a further reduction in the membrane stiffness brought on by yielding of the circumferential steel results in a change of load resistance from circumferential membrane to meridional bending action.

Such a mechanism of force redistribution has been studied by Godoy (30) for a meridionally imperfect, reinforced concrete cylindrical shell having meridional cracks. Based on a finite element analysis, Godoy reported this shell to have significant load capacity following circumferential yield prior to exceeding the shell's meridional flexural capacity. It would appear advantageous to account for this added strength provided the shell posesses sufficient ductility to enable such a redistribution of forces to take place.

7.2 IMPERFECT CYLINDER ANALOGY

It can be concluded from a review of the literature that bending moments have only a minor effect on cooling tower shells which are properly thickened at the top and base. Provided a bending analysis is carried out for the lintel region so as to correctly model support conditions, membrane action can adequately describe the state of internal forces over most of the perfect shell.

It has been shown in chapter 6 that the effect of meridional imperfection is to induce meridional moment and circumferential force within the region of the imperfection. These force changes are driven by the meridional force N_ϕ^p which itself is unaffected by the presence of the imperfection. Furthermore, slope and curvature of the perfect merid-

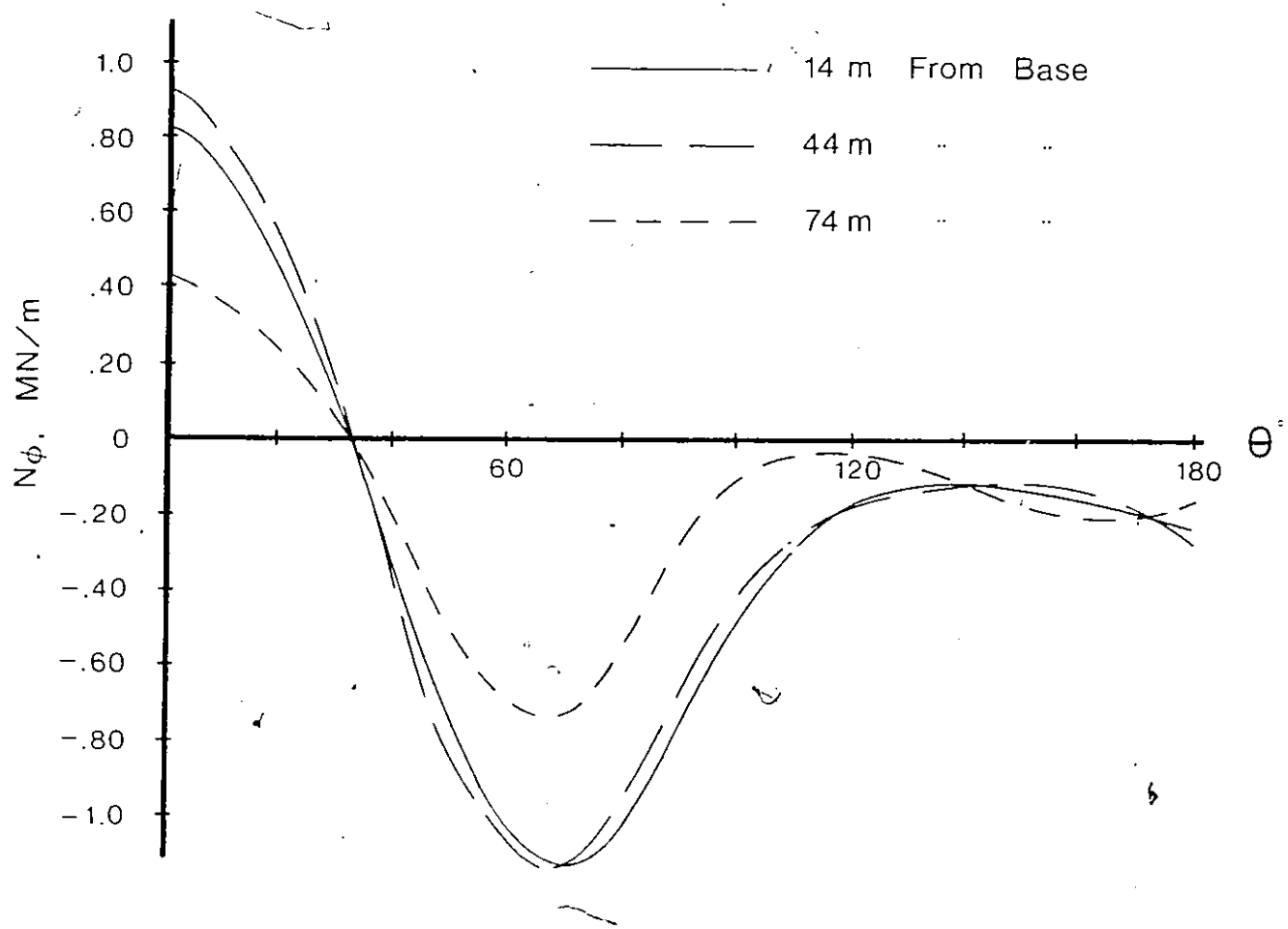

Figure 7-1a Circumferential variation of meridional force N_ϕ at three levels in the Ardeer cooling tower shell

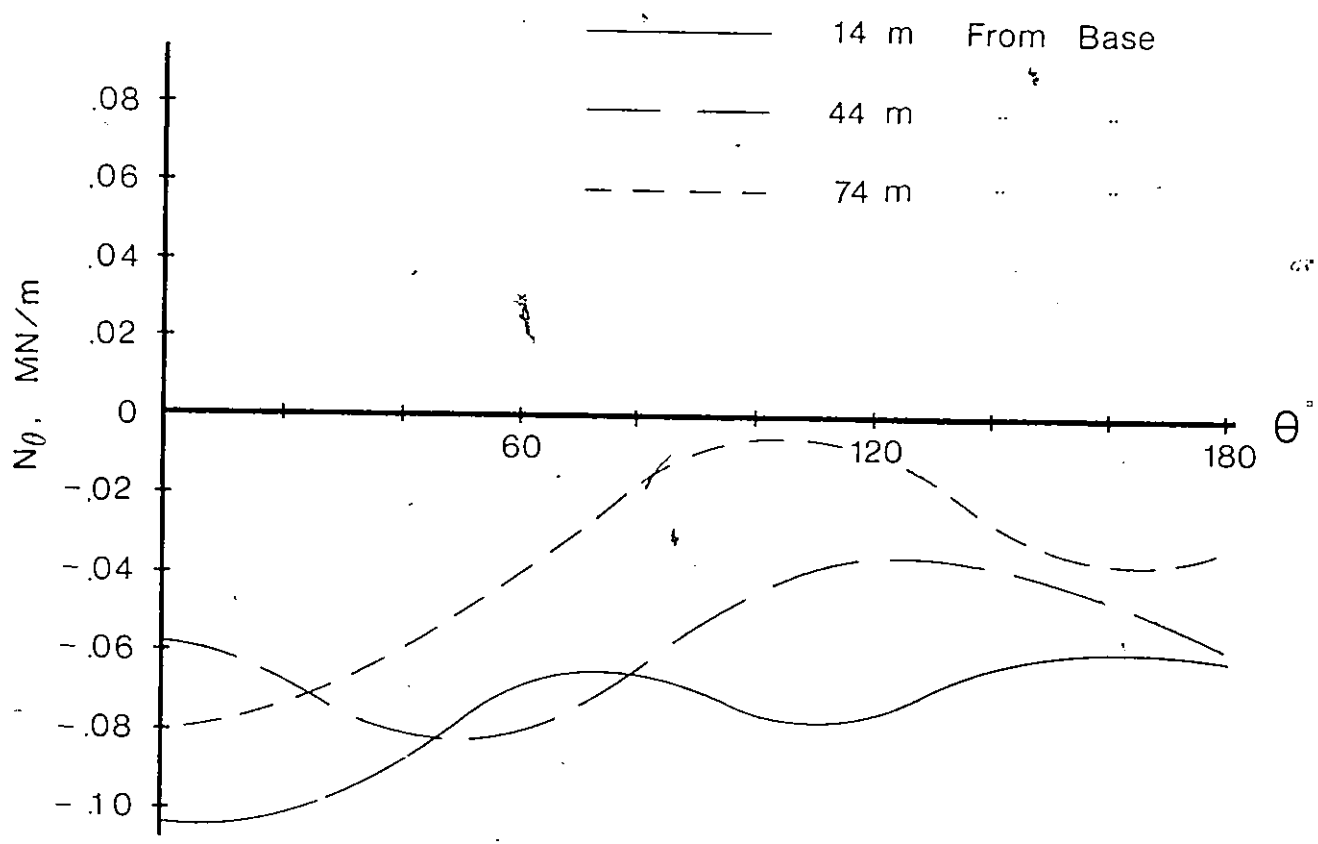

Figure 7-1b Circumferential variation of the circumferential force N_θ at three levels in the Ardeer cooling tower shell

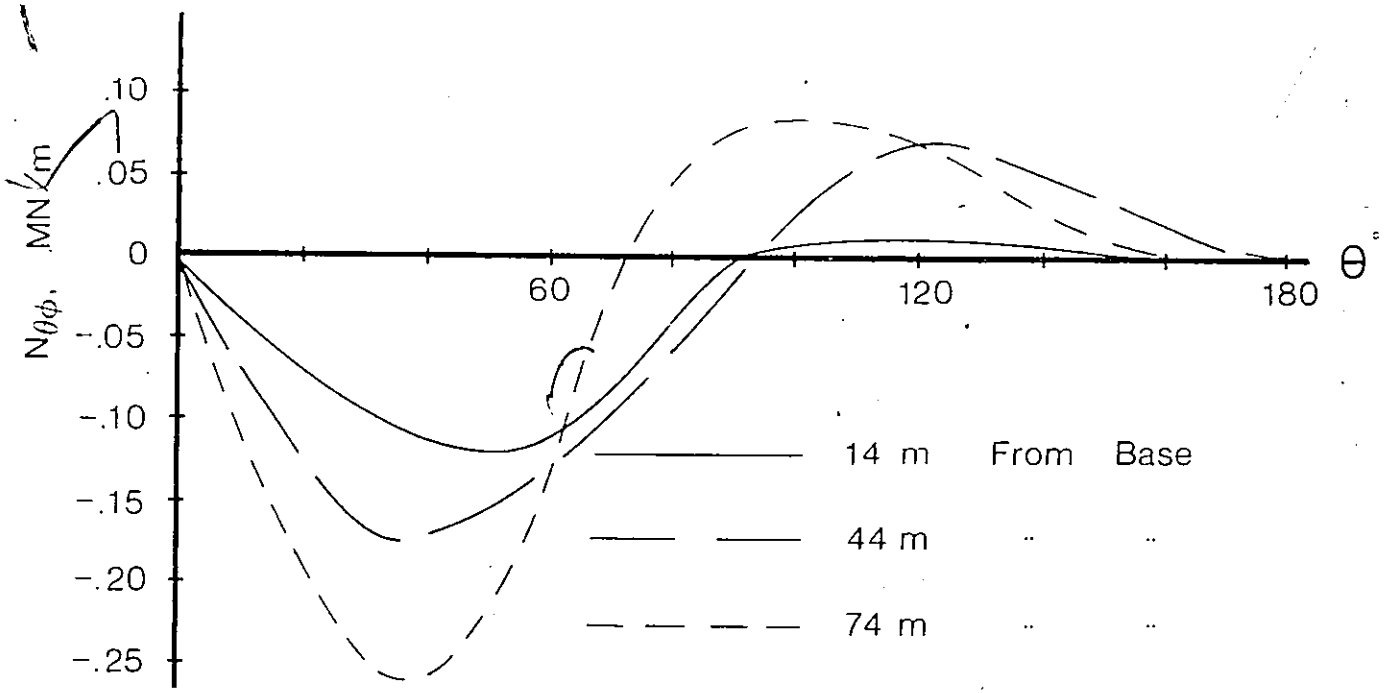

Figure 7-1c Circumferential variation of in-plane shear force $N_{\theta\phi}$ at three levels in the Ardeer cooling tower shell

ian have little influence on the maximum forces induced near the centre of the imperfection.

Figures 7-1, illustrate the circumferential variation of membrane forces at three successive levels in the Ardeer cooling tower shell subjected to gravity and a 120 mi/h wind. Figure 7-1a, suggests that failure due to a meridional imperfection would occur at circumferential locations $\theta = 0$ or $\theta = 75$ with respect to the wind direction where the driving force N_ϕ is maximum. At these same locations, in-plane shear $N_{\theta\phi}$ equals or tends to zero, Figure 7-1c. In Figure 7-1b, N_θ is seen to be one order of magnitude less than N_ϕ. Since the force change δN_θ resulting from an imperfection is expected to be within the range 1.0 to 2.0 of N_ϕ, Figure 5-2a, N_θ along with $N_{\theta\phi}$ would make a small contribution to failing the shell and may be considered negligible.

Figure 7-2, illustrates those forces contributing to failure in an element of a meridionally imperfect cooling tower shell where circumferential and in-plane shear forces N_θ and $N_{\theta\phi}$ for the perfect shell have been neglected. Since the maximum imperfection forces δM_ϕ and δN_θ are insensitive to slope and curvature of the perfect meridian, this system of forces is precisely that found in an axially loaded, meridionally imperfect cylinder. Furthermore, N_ϕ being invariant in the presence of meridional imperfection and δQ_ϕ being a function of δM_ϕ, force redistribution would take place be-

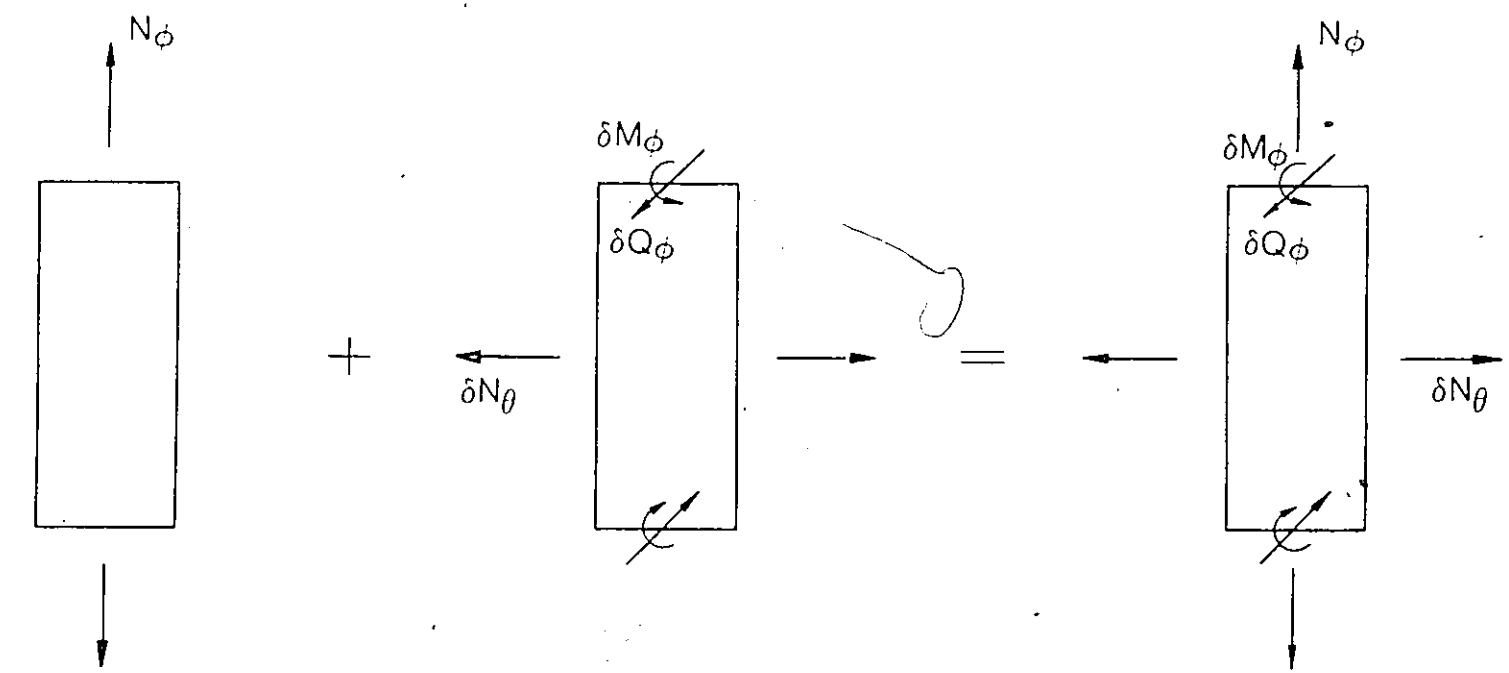

Forces in the perfect shell

Forces due to imperfection

Resultant forces in the imperfect shell

Figure 7-2 Forces contributing to failure in a meridionally imperfect cooling tower shell

tween δN_θ and δM_ϕ while the illustrated superposition of forces remains valid through the inelastic state.

7.3 CLOSED FORM SOLUTION - ORTHOTROPIC SHELL

7.3.1 GOVERNING EQUATIONS

For the stress resultants in an axially loaded cylindrical shell of radius R, equations (6-4a), (6-4b) and (6-4c) pertaining to equilibrium simplify to

$$\delta N_\theta = R\left\{ N_\phi^P \frac{d^2\xi}{dS^2} - \frac{d^2 M_\phi}{dS^2} \right\} \qquad (7\text{-}1a)$$

$$\delta N_\phi = 0 \qquad (7\text{-}1b)$$

$$Q_\phi = \frac{dM_\phi}{dS} \qquad (7\text{-}1c)$$

where $\xi(S)$ defines the deviation from the perfect meridian, Figure 3-1. Additional equations are needed to render the force system of Figure 3-4 deterministic.

For a radial displacement w(S), measured positively inwards, the circumferential strain $\epsilon(S)$ and meridional curvature $d\chi/dS$ of the middle surface are

$$\varepsilon_\theta = -\frac{W}{R}$$

$$\frac{d\chi}{dS} = -\frac{d^2W}{dS^2}$$

Combining these two equations yields a compatibility relation between the two forms of deformation

$$\frac{d^2\varepsilon_\theta}{dS^2} = \frac{1}{R}\frac{d\chi}{dS} \qquad (7\text{-}2)$$

Applying Hook's law, the constitutive relations between the stress resultants and the strain for a meridionally cracked, orthotropic shell element are taken to be

$$\frac{d\chi}{dS} = \frac{12}{E_\phi t^3} M_\phi \qquad (7\text{-}3a)$$

$$\varepsilon_\theta = \frac{1}{t}\left[\frac{N_\theta}{E_\theta} - \nu\frac{N_\phi}{E_\phi}\right] \qquad (7\text{-}3b)$$

where E_θ, E_ϕ are Young's modulii for the circumferential and meridional directions respectively and ν is Poisson's ratio for concrete.

Equations (7-1), (7-2) and (7-3) represent a solvable system of six equations. From (7-2) and (7-3)

$$M_\phi = R K_\phi \frac{d^2 \varepsilon_\theta}{dS^2} \qquad (7\text{-}4)$$

where $K_\phi = E_\phi t^3/12$ is the bending stiffness in the meridional direction for the orthotropic shell. Substituting into (7-1a) and then combining with (7-3b)

$$\frac{d^4 \varepsilon_\theta}{dS^4} + \left(\frac{t E_\theta}{R^2 K_\phi}\right) \varepsilon_\theta = \frac{N_\phi^P}{R K_\phi} \left\{ \frac{d^2 \xi}{dS^2} - \frac{\nu E_\theta}{R E_\phi} \right\} \qquad (7\text{-}5)$$

7.3.2 SOLUTION - ELASTIC ORTHOTROPIC SHELL

Prior to circumferential yield, E_θ is constant and equation (7-5), being linear, can routinely be solved for the circumferential strain ϵ_θ. Substitution into equation (7-4) then determines the associated meridional moment M_ϕ.

For the cosine imperfection illustrated in Figure 6-3 and described by equation (6-6) on the interval $S = \pm L$, the maximum circumferential force and meridional moment occurring at the centre of the imperfection ($S = 0$) are calculated to be (Appendix C)

$$\delta M_{\phi_{MAX}} = N_\phi^P \xi_i \left\{ \frac{4/3\,\pi^3}{\pi^4+\alpha}(1-\mu_1) + \frac{88/7\,\pi^3}{16\pi^4+\alpha}\left(1+\frac{\mu_1}{4}\right) + \frac{108/5\,\pi^3}{81\pi^4+\alpha}\left(1-\frac{\mu_1}{9}\right)\right\}$$

$$= N_\phi^P \xi_i \beta \qquad (7\text{-}6a)$$

$$\delta N_{\theta_{MAX}} = \frac{-N_\phi^P \xi_i R}{L^2}\left\{ \frac{4/3\,\pi\alpha}{\pi^4+\alpha}(1+\mu_2) + \frac{\pi^2\alpha}{16\pi^4+\alpha}(1-\mu_2) + \frac{12/5\,\pi\alpha}{81\pi^4+\alpha}(1+\mu_2)\right\}$$

$$= \frac{N_\phi^P \xi_i R}{L^2}\,\Gamma \qquad (7\text{-}6b)$$

where the coefficients μ corresponding to the boundary conditions $\epsilon_\theta(\pm L) = \chi(\pm L) = 0$ are

$$\mu_1 = \sqrt{\frac{4\alpha}{\pi^2}} \cdot \frac{\sin\lambda L \cdot \cosh\lambda L - \cos\lambda L \cdot \sinh\lambda L}{\sin 2\lambda L - \sinh 2\lambda L}$$

$$\mu_2 = \frac{\cos\lambda L \cdot \sinh\lambda L + \sin\lambda L \cdot \cosh\lambda L}{\sinh 2\lambda L + \sin 2\lambda L}$$

$$\lambda = \sqrt[4]{\frac{tE_\theta}{4R^2K_\phi}}, \qquad \alpha = \frac{12L^4}{R^2t^2} \cdot \frac{E_\theta}{E_\phi}$$

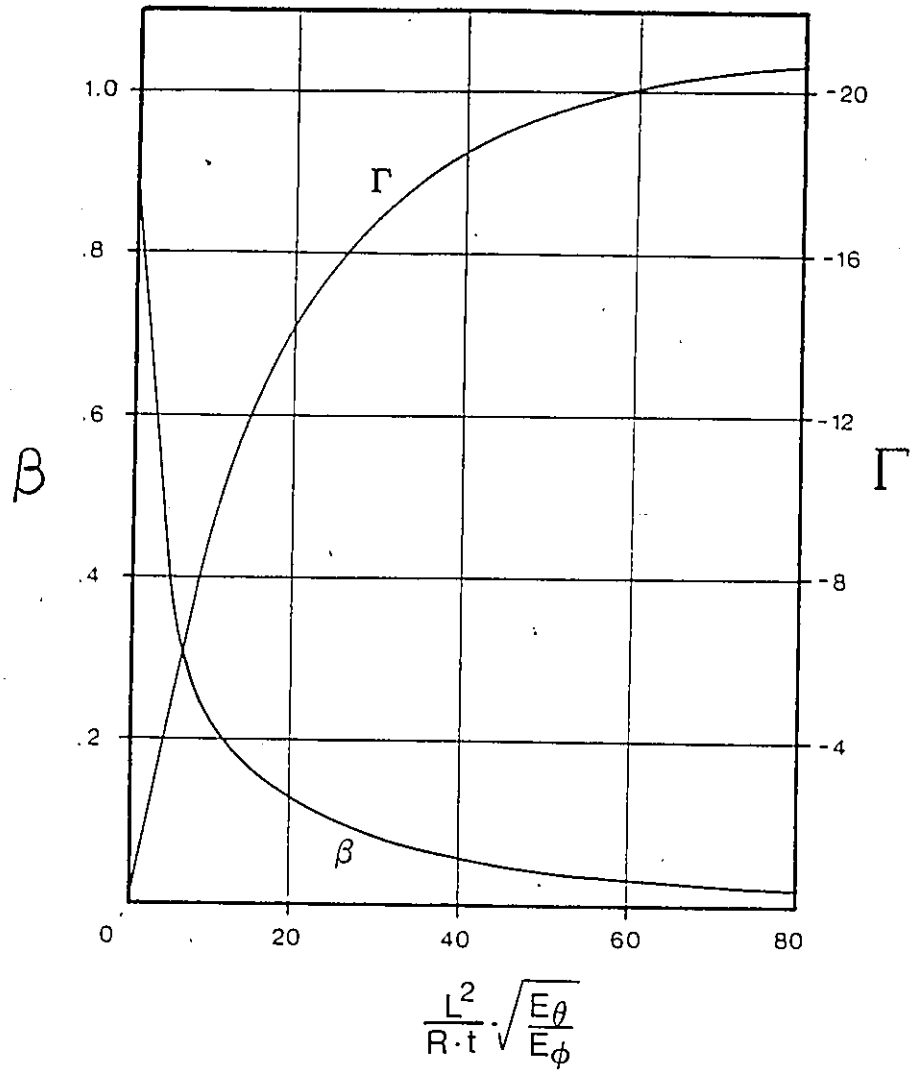

Figure 7-3 Values of β and Γ in equations (7-6) pertaining to the elastic orthotropic shell

In Figure 7-3, β and Γ pertaining to the elastic orthotropic shell have been plotted for convenience. As in the case of equations (6-12), the coefficients $\mu \rightarrow 0$ and have little effect on the outcome of equations (7-6) so that only the particular integral of (7-5) need have been considered in the analysis.

To determine the accuracy of equations (7-6) and the effect vertical cracking can have on the magnitude of the imperfection forces, the maximum circumferential force and meridional moment occurring in two meridionally imperfect, orthotropic cylinders were evaluated using the derived solution equations (7-6) and the SHORE III finite element program. The two cylinders had circumferential radii of 37.5 and 70.0 m (123 and 246 ft), and wall thicknesses of .153 and .306 m (6 and 12 in) respectively as in the regions near the base of the larger and the smaller cooling tower shells previously described in Chapter 5. For the analyses, a meridional cosine imperfection was used characterised by wavelength L = 10 m (32.8 ft) and a height ξ_i = 0.3 m (1.0 ft). Varying degrees of orthotropicity were accounted for by allowing the circumferential membrane stiffness to decrease from 100% to 5% of the meridional membrane stiffness while the modulus of elasticity in the meridional direction was assumed to have a constant value of 26 GPa (3,800 ksi); this value being representative of uncracked, reinforced concrete. It should be mentioned that for the finite element

E_θ / E_ϕ	$\delta N_\theta / N_\phi$		$\delta M_\phi / \check{N}_\phi$, m	
	Eq.(7-6b)	Finite El.	Eq.(7-6a)	Finite El.
100%	−1.200	−1.145	.02496	.02540
80	−1.146	−1.099	.02906	.02930
60	−1.072	−1.030	.03497	.03490
40	−0.966	−0.927	.04373	.04390
20	−0.770	−0.744	.06314	.06210
5	−0.436	−0.420	.10620	.10500

Table 7-1a Maximum imperfection forces in a meridionally imperfect, orthotropic cylinder having the dimensions of the base of the Ardeer tower shell

E_θ/E_ϕ	$\delta N_\theta/N_\phi$		$\delta M_\phi/N_\phi$, m	
	Eq. (7-6b)	Finite El.	Eq. (7-6a)	Finite El.
100%	-.9601	-.9348	.0989	.0976
80	-.8697	-.8434	.1062	.1047
60	-.7617	-.7346	.1159	.1140
40	-.6271	-.5988	.1301	.1268
20	-.4293	-.4128	.1557	.1482
5	-.1609*	-.1816	.1988*	.1866

Table 7-1b Maximum imperfection forces in a meridionally imperfect, orthotropic cylinder having twice the dimensions of the base of the Ardeer tower shell

analyses, the Poisson's ratio and the bending stiffness for the circumferential directions were assumed equal to zero. Several preliminary computer runs indicated this assumption to have a minor effect on the computed imperfection forces. More importantly, setting both values to zero was deemed a valid model for the state of internal forces in a shell having a large number of wide vertical cracks penetrating the full thickness of the concrete.

The results of the analyses for both cylinders are tabulated in Tables 7-1. Comparing the maximum imperfection forces reveals that the values predicted by equations (7-6) are in close agreement with the respective forces predicted by the finite element analyses. Indeed, the difference between the proposed and the numerical solution in most cases does not exceed 5% of the numerical solution while the largest discrepancy (indicated by the * symbol) is 7% for the meridional moment and 11% for the circumferential force.

In Figures 7-4, the maximum imperfection forces in both cylinders as given by equations (7-6) have been drawn for varying values of the circumferential membrane stiffness. It may be observed that for the meridional imperfection being considered, larger meridional moments are induced in the larger shell while larger circumferential forces in the smaller shell. Furthermore, with decreasing circumferential membrane stiffness, there is a reduction in the circumferen-

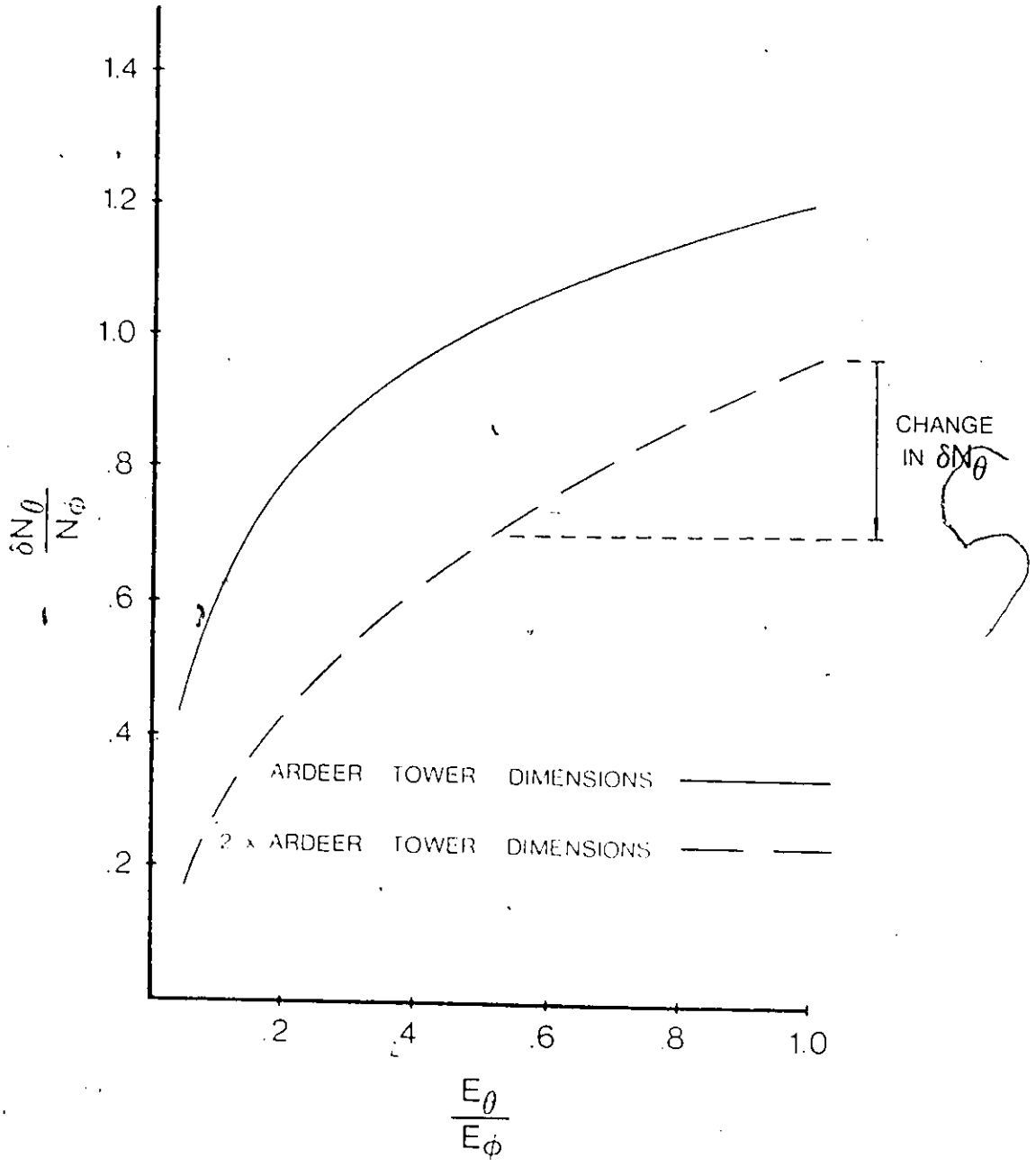

Figure 7-4a Maximum circumferential force in a meridionally imperfect, orthotropic cylinder

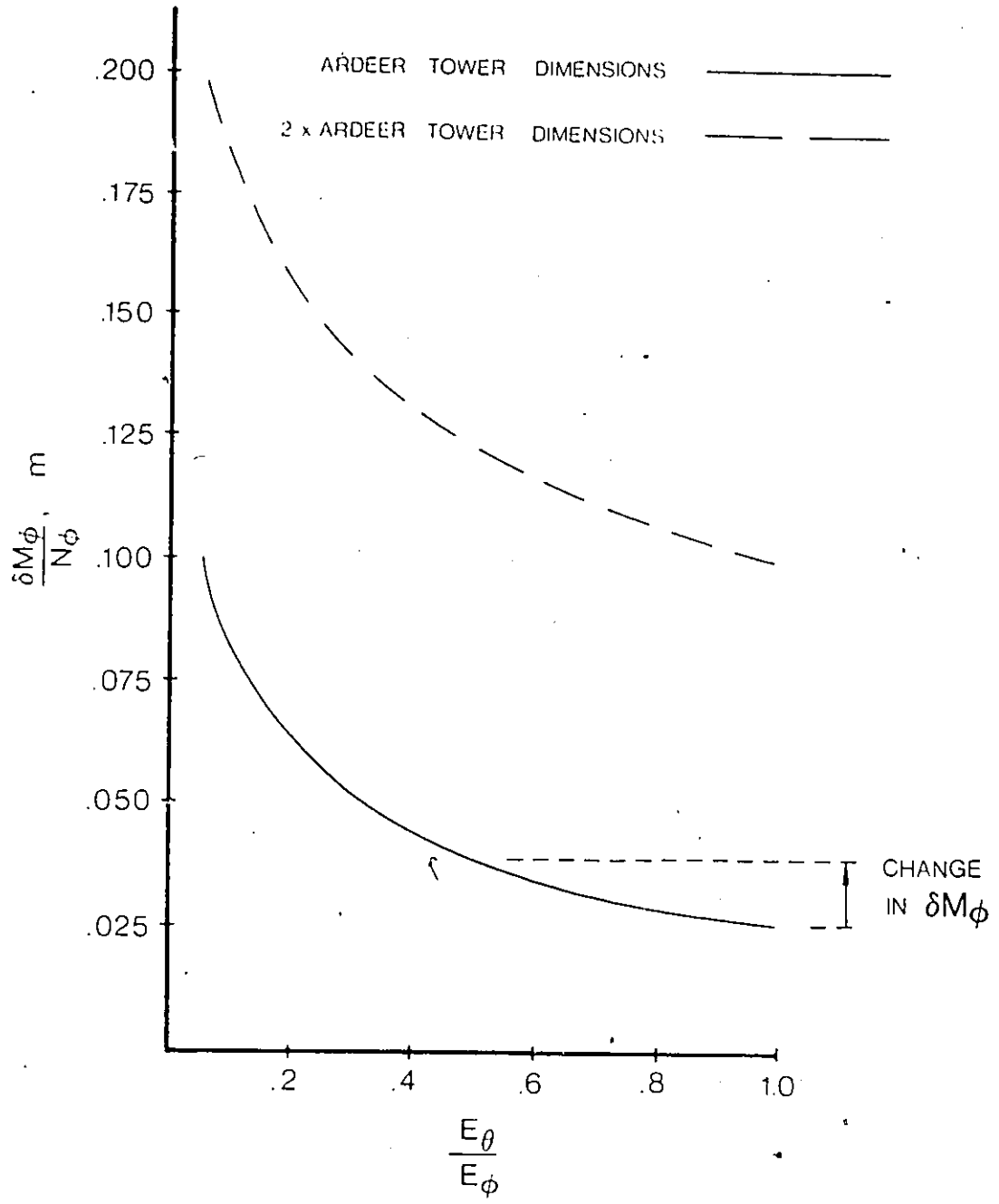

Figure 7-4b Maximum meridional moment in a meridionally imperfect, orthotropic cylinder

tial force and a corresponding increase in the meridional moment; these changes in the imperfection forces being more pronounced at the lower values of the circumferential membrane stiffness.

As an example for the degree to which orthotropicity can influence the imperfection forces, the situation is considered in which the membrane stiffness due to vertical cracking is reduced by 50%. As shown in Figures 7-4, for a cooling tower shell having twice the radius and thickness dimensions of the base of the Ardeer tower, the maximum circumferential force would decrease by 28% while for a shell having the radius and thickness dimensions of the base of the Ardeer tower, the maximum meridional moment would increase by 58%. These changes are judged sufficiently large to justify an orthotropic analysis.

7.3.3 EXTENDED SOLUTION - CIRCUMFERENTIALLY YIELDED SHELL

If the reinforcing steel is symmetrically placed over the shell's depth, the middle surface remains essentially stress free during pure bending and equations (7-1), (7-2) and (7-3) remain valid during circumferential yield. In this case, E_θ can no longer be treated as a constant. Instead, being a furction of the circumferential strain, E_θ will vary in the meridional and circumferential shell directions.

Figure 7-5a illustrates an element of shell representing a portion of the shell's circumference, bounded by two vertical cracks a distance l appart and stressed in the horizontal direction by $\sigma_\theta = N_\theta/t$. In Figure 7-5b, the membrane stiffness E_θ is shown to be a function of the circumferential distance x measured from the edge of one of the cracks. In vicinity of the crack, there is a loss of steel concrete integrity and the stiffness is assumed to vary over the distance l' in some unspecified manner. At a distance greater than l' from the crack, the full section of the concrete along with the steel acts to resist the stress σ_θ and the membrane stiffness is closely approximated by that of concrete so that $E_\theta = E_\phi = E_{concrete}$. At the crack edge, the membrane stiffness is entirely due to the action of the reinforcing steel and takes on the reduced value $\rho_\theta E_{steel}$. The resultant variation of circumferential strain would then be as in Figure 7-5c, reaching a maximum value at the crack edge given by $\sigma_\theta/\rho_\theta E_{steel}$.

From elementary strength of materials, the overall deformation of the shell element due to σ_θ is

$$\delta l = \sigma_\theta \int_0^l \frac{dx}{E_\theta}$$

The 'average' normal strain along the element is then calculated to be

$$\varepsilon_\theta = \frac{\delta l}{l} = \frac{\sigma_\theta}{l} \int_0^l \frac{dx}{E_\theta}$$

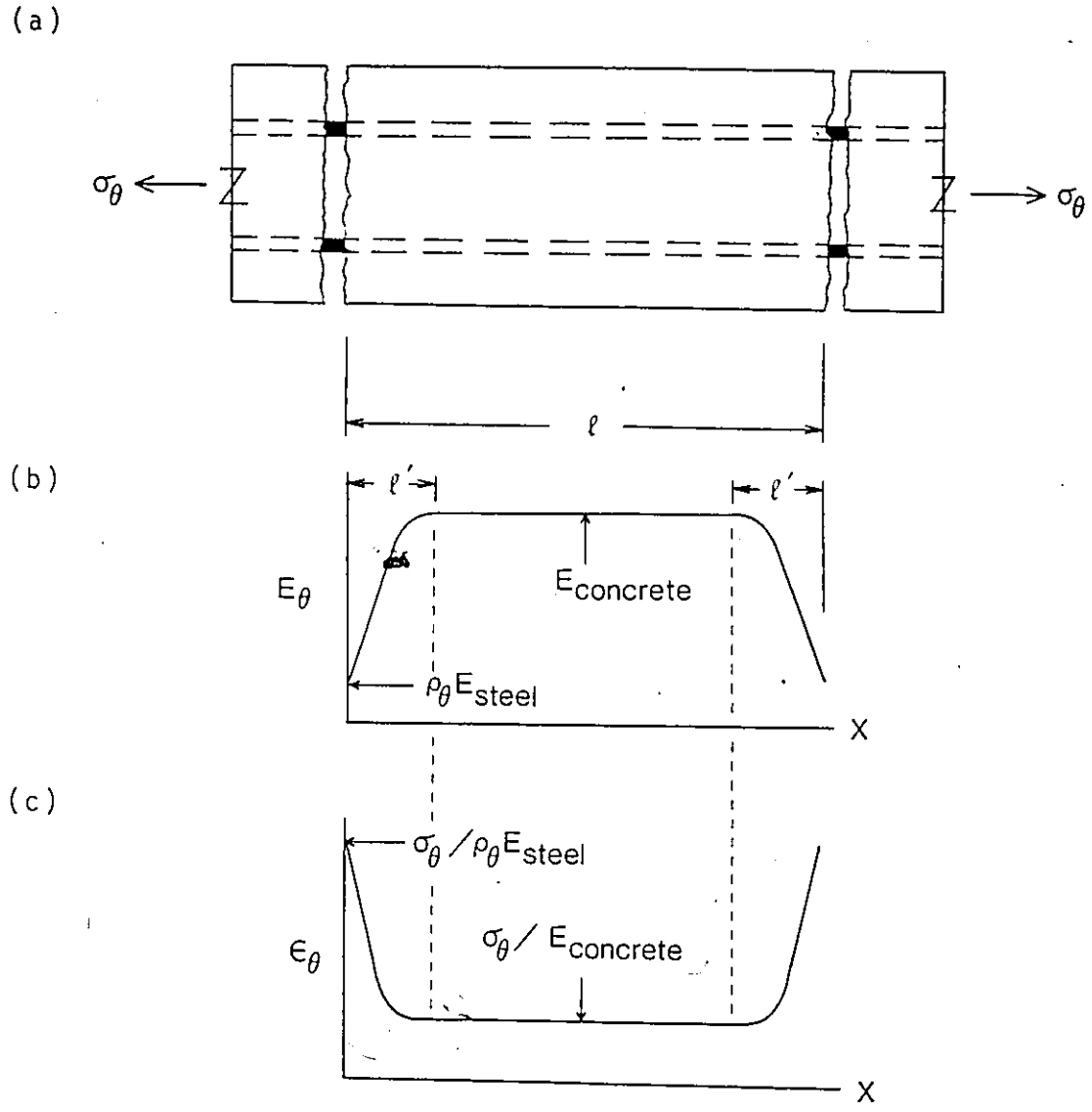

Figure 7-5 (a) Element of shell from a meridionally cracked, reinforced concrete cylinder
(b) Variation of circumferential stiffness
(c) Variation of circumferential strain

and the corresponding membrane stiffness of the element as

$$E_\theta = \frac{\sigma_\theta}{\varepsilon_\theta} = \ell \Big/ \int_0^\ell \frac{dx}{E_\theta} \qquad (7\text{-}7)$$

Considering next the full circumference of the shell, if the contribution of the concrete to the shell's hoop stiffness is reduced by the presence of meridional cracks, then the overall relation between the circumferential stress and strain would be similar to that indicated by the dashed lines in Figure 7-6 where, having previously observed the Poisson effect to be minor in the case of the elastic orthotropic shell, ν is assumed to be zero. The initial hoop stiffness E_{θ_i} (portion AB of the stress-strain relation) is taken to be that given by equation (7-7) above while the maximum circumferential stress that can be resisted by the shell (point B) is limited to the value $\rho_\theta f_y$ at which the reinforcing steel at any given crack begins to yield.

Assuming that the steel, being sufficiently ductile, is capable of undergoing additional strain beyond its yield, then the failure of the shell in the circumferential direction need not be defined as the yield point B but instead by some point C which is further to the right. Furthermore, for the purpose of analysis, the true stress-strain relation ABC may be approximated by a continuous third order curve of the form

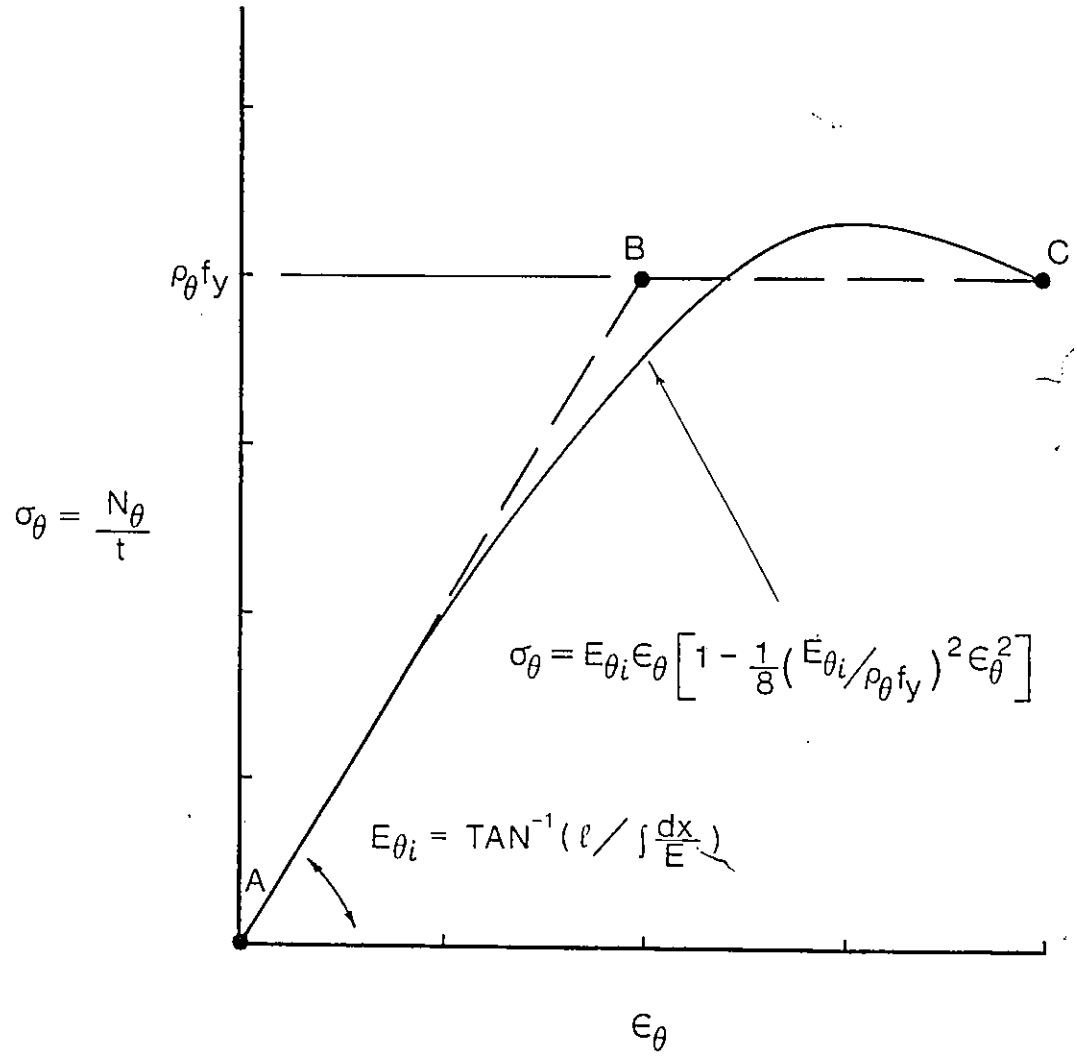

Figure 7-6 Relation between circumferential stress and strain for a meridionally cracked, reinforced concrete cylinder

$$\sigma_\theta = E_{\theta i}\varepsilon_\theta - \frac{E_{\theta i}^3}{8(\rho_\theta f_Y)^2}\varepsilon_\theta^3$$

$$= E_{\theta i}\varepsilon_\theta\left[1 - \frac{1}{8}\left(\frac{E_{\theta i}}{\rho_\theta f_Y}\right)^2\varepsilon_\theta^2\right] \qquad (7\text{-}8)$$

which is shown as a solid line in Figure 7-6.

Using (7-8) in lieu of (7-3b), equation (7-5) pertaining to the elastic orthotropic shell can be generalised to include the effect of circumferential yield as

$$\frac{d^4\varepsilon_\theta}{dS^4} + \frac{tE_{\theta i}}{R^2K_\phi}\varepsilon_\theta\left[1 - \lambda'\varepsilon_\theta^2\right] = \frac{N_\phi^P}{RK_\phi}\left\{\frac{d^2\xi}{dS^2}\right\} \qquad (7\text{-}9)$$

in which the non-linear term λ' represents a perturbation factor whose value is

$$\lambda' = \frac{1}{8}\left(\frac{E_{\theta i}}{\rho_\theta f_Y}\right)^2$$

The simplest representation of the solution to the differential equation (7-9) is a power series of the form

$$\varepsilon_\theta = \varepsilon_{\theta_0} + \lambda'\varepsilon_{\theta_1} + \lambda'^2\varepsilon_{\theta_2} + \ldots. \qquad (7\text{-}10)$$

Substituting this assumed solution into the differential equation yields

$$\frac{d^4}{dS^4}\left(\varepsilon_{\theta_o} + \lambda'\varepsilon_{\theta_1} + \lambda'^2\varepsilon_{\theta_2} + \dots\right) +$$

$$\frac{tE_{\theta i}}{R^2 K_\phi}\left(\varepsilon_{\theta_o} + \lambda'\varepsilon_{\theta_1} + \lambda'^2\varepsilon_{\theta_2} + \dots\right)\left[1 - \lambda'\left(\varepsilon_{\theta_o} + \lambda'\varepsilon_{\theta_1} + \lambda'^2\varepsilon_{\theta_2} + \dots\right)^2\right]$$

$$= \frac{N_\phi^P}{RK_\phi}\left\{\frac{d^2\xi}{dS^2}\right\}$$

If the coefficients of powers of λ' in this equation are balanced, then the following system of differential equations must be satisfied:

$$\frac{d^4\varepsilon_{\theta_o}}{dS^4} + \frac{tE_{\theta i}}{R^2 K_\phi}\varepsilon_{\theta_o} = \frac{N_\phi^P}{RK_\phi}\left\{\frac{d^2\xi}{dS^2}\right\} \qquad (7\text{-}11a)$$

$$\frac{d^4\varepsilon_{\theta_1}}{dS^4} + \frac{tE_{\theta i}}{R^2 K_\phi}\varepsilon_{\theta_1} = \frac{tE_{\theta i}}{R^2 K_\phi}\left(\varepsilon_{\theta_o}^3\right) \qquad (7\text{-}11b)$$

$$\frac{d^4\varepsilon_{\theta_2}}{dS^4} + \frac{tE_{\theta i}}{R^2 K_\phi}\varepsilon_{\theta_2} = \frac{tE_{\theta i}}{R^2 K_\phi}\left(3\varepsilon_{\theta_1}\varepsilon_{\theta_o}^2\right) \qquad (7\text{-}11c)$$

$$\vdots$$

In this system of equations, similarity between equation (7-11a) and equation (7-5) indicates that ϵ_{θ_o} is the elastic solution for the orthotropic shell having circumferential membrane stiffness E_{θ_i}.

For the remainder of the solution, the assumption is made that in addition to ϵ_{θ_o}, the inclusion of one more term will suffice for an accurate description of the deformed state of the circumferentially yielded shell. Hence, the complete solution is taken to be

$$\varepsilon_\theta \cong \varepsilon_{\theta_o} + \lambda' \varepsilon_{\theta_1} \qquad (7\text{-}12)$$

where, as was discussed in section 7.3.2 and is shown in Appendix C

$$\varepsilon_{\theta_o} = \sum_{n=1}^{3} U_n \cos\left(\frac{n\pi s}{L}\right) \qquad (7\text{-}13)$$

and

$$U_1 = -\frac{N_\phi^P \xi_i R}{L^2 t E_{\theta i}} \left\{ \frac{4/3\,\pi\alpha}{\pi^4 + \alpha} \right\}$$

$$U_2 = -\frac{N_\phi^P \xi_i R}{L^2 t E_{\theta i}} \left\{ \frac{22/7\,\pi\alpha}{16\pi^4 + \alpha} \right\}$$

$$U_3 = -\frac{N_\phi^P \xi_i R}{L^2 t E_{\theta i}} \left\{ \frac{12/5\,\pi\alpha}{81\pi^4 + \alpha} \right\}$$

Furthermore, it is assumed that ϵ_{θ_1} can accurately be described by the first nine terms of a cosine series as

$$\varepsilon_{\theta_1} = \sum_{n=0}^{9} A_n \cos\left(\frac{n\pi s}{L}\right) \qquad (7\text{-}14)$$

Substituting for ϵ_{θ_0} and ϵ_{θ_1} in equation (7-11b) and equating cosine terms of equal wavelength, the coefficients A in (7-14) are calculated to be

$$A_0 = \frac{3U_1^2U_2 + 6U_1U_2U_3}{4}$$

$$A_1 = \frac{3U_1^3 + 6U_1U_2^2 + 6U_1U_3^2 + 3U_1^2U_3 + 3U_2^2U_3}{4(\pi^4/\alpha + 1)}$$

$$A_2 = \frac{3U_2^3 + 6U_1^2U_2 + 6U_2U_3^2 + 6U_1U_2U_3}{4(16\pi^4/\alpha + 1)}$$

$$A_3 = \frac{U_1^3 + 3U_3^3 + 3U_1U_2^2 + 6U_1^2U_3 + 6U_2^2U_3}{4(81\pi^4/\alpha + 1)}$$

$$A_4 = \frac{3U_1^2U_2 + 3U_2U_3^2 + 6U_1U_2U_3}{4(256\pi^4/\alpha + 1)}$$

$$A_5 = \frac{3U_1U_2^2 + 3U_1U_3^2 + 3U_1^2U_3}{4(625\pi^4/\alpha + 1)}$$

$$A_6 = \frac{U_2^3 + 6U_1U_2U_3}{4(1296\pi^4/\alpha + 1)}$$

$$A_7 = \frac{3U_1U_3^2 + 3U_2^2U_3}{4(2401\pi^4/\alpha + 1)}$$

$$A_8 = \frac{3U_2U_3^2}{4(4096\pi^4/\alpha + 1)}$$

$$A_9 = \frac{U_3^3}{4(6561\pi^4/\alpha + 1)}$$

Equation (7-12) describes the variation of the circumferential strain in the meridional direction for a meridionally imperfect, circumferentially yielded cylinder. This solution is the sum of the linear term ϵ_{θ_0} given by (7-13) and the non-linear term ϵ_{θ_1} given by (7-14). In accordance with equation (7-4), the moment which is simultaneously induced in the meridional direction is obtained by twice differentiating equation (7-12). Thus, for the yielded shell

$$M_\phi = RK_\phi \frac{d^2}{dS^2}\left[\varepsilon_{\theta_0} + \lambda'\varepsilon_{\theta_1}\right]$$

$$= M_{\phi_0} + \lambda' M_{\phi_1} \qquad (7\text{-}15)$$

in which

$$M_{\phi_0} = -RK_{\phi} \cdot \frac{\pi^2}{L^2} \sum_{n=1}^{3} n^2 U_n \cos\left(\frac{n\pi s}{L}\right) \qquad (7\text{-}16)$$

and

$$M_{\phi_1} = -\frac{L^2 t E_{\theta i}}{R} \cdot \frac{\pi^2}{\alpha} \sum_{n=1}^{9} n^2 A_n \cos\left(\frac{n\pi s}{L}\right) \qquad (7\text{-}17)$$

Near the centre of the imperfection (S = 0), the cosine terms approach unity so that the maximum circumferential strain and the meridional moment which are induced in the yielded shell are given by

$$\delta\varepsilon_{\theta_{MAX}} = \varepsilon_{\theta_{0MAX}} + \lambda' \sum_{n=0}^{9} A_n \qquad (7\text{-}18a)$$

$$\delta M_{\phi_{MAX}} = M_{\phi_{0MAX}} + \lambda' \frac{L^2 t E_{\theta i}}{R} \cdot \frac{-\pi^2}{\alpha} \sum_{n=1}^{9} n^2 A_n \qquad (7\text{-}18b)$$

The solution of equations (7-18) is made complicated by having to compute the coefficients A_n. Therefore, the ensueing tolerance equations which include the effect of circumferential yield would not be amenable to hand calculation. Instead, a lengthy iterative process would be necessary requiring the aid of a computer; a situation to be avoided by the construction engineer. Furthermore, if the shell is to be allowed to fail locally in the circumferential direction,

it is imperative not to underestimate the magnitude of the meridional moment which otherwise could lead to a progressive type failure in the shell. Consequently, reduction of (7-18) to a simpler but conservative pair of relations was deemed more suitable from which to proceed to derive the necessary tolerance limits.

Setting $\alpha \to \infty$ so as to maximize coefficients A_n

$$\sum_{n=0}^{9} A_n = U_1^3 + U_2^3 + U_3^3 + 6U_1U_2U_3 +$$

$$+ 3U_1U_2^2 + 3U_1U_3^2 + 3U_1^2U_2 +$$

$$+ 3U_1^2U_3 + 3U_2^2U_3 + 3U_2U_3^2$$

$$= (U_1 + U_2 + U_3)^3$$

$$= \varepsilon_{\theta_0 MAX}^3$$

and

$$\sum_{n=1}^{9} n^2 A_n = 3\left[U_1^3 + 4U_2^3 + 9U_3^3 + 28U_1U_2U_3 \right.$$

$$\left. + 9U_1U_2^2 + 19U_1U_3^2 + 6U_1^2U_2 \right.$$

$$+ \; 11 U_1^2 U_3 + 17 U_2^2 U_3 + 20 U_2 U_3^2$$

$$= (U_1 + U_2 + U_3)^2 (U_1 + 4U_2 + 9U_3)$$

$$= \varepsilon_{\theta_{o_{MAX}}}^2 \cdot \frac{-3L^2}{\pi^2 R K_\phi} M_{\phi_{o_{MAX}}}$$

Substituting these results into (7-18), the maximum circumferential strain and meridional moment is conservatively given by

$$\delta\varepsilon_{\theta_{MAX}} = \varepsilon_{\theta_{o_{MAX}}} + \lambda' \varepsilon_{\theta_{o_{MAX}}}^3$$

$$= \varepsilon_{\theta_{o_{MAX}}} \left[1 + \lambda' \varepsilon_{\theta_{o_{MAX}}}^2 \right]$$

$$= \frac{N_\phi^p \xi_i R\Gamma}{L^2 t E_{\theta_i}} \left[1 + \lambda' \left(\frac{N_\phi^p \xi_i R\Gamma}{L^2 t E_{\theta_i}} \right)^2 \right] \qquad (7\text{-}19a)$$

$$\delta M_{\phi_{MAX}} = M_{\phi_{o_{MAX}}} + 3\lambda' \varepsilon^2_{\theta_{o_{MAX}}} \cdot M_{\phi_{o_{MAX}}}$$

$$= M_{\phi_{o_{MAX}}} \left[1 + 3\lambda' \varepsilon^2_{\theta_{o_{MAX}}} \right]$$

$$= N^p_\phi \xi_i \beta \left[1 + 3\lambda' \left(\frac{N^p_\phi \xi_i R\Gamma}{L^2 t E_{\theta i}} \right)^2 \right] \qquad (7\text{-}19b)$$

where, due to the yielding process, the terms within the square brackets being greater than unity act so as to magnify the elastic strain and moment.

To study the effect arising from a loss in the circumferential membrane stiffness, the maximum circumferential strain and meridional moment in two meridionally imperfect, orthotropic cylinders were computed by means of equations (7-19) and the SHORE 111 finite element program using a stepwise non-linear analysis. The two cylinder radii were 22.5 and 45 m (74 and 148 ft) while the wall thicknesses were .153 and .306 m (6 and 12 in) respectively representing the throat regions of the smaller and larger cooling tower shells of Chapter 5. The assumed imperfection, in the form of a cosine wave, had wavelength L = 10 m (32.8 ft) and height ξ_i = 0.3 m (1.0 ft).

For the linear analyses of the two shells, orthotropicity was included by taking the circumferential membrane stiffness to be 80 percent that of the meridional direction. For the stepwise non-linear analyses, this value was reduced from 80 percent to zero in those regions of the shells, where during the loading process, the circumferential membrane force exceeded the value $t\rho_\theta f_y$. Thus, the stress-strain characteristics in the horizontal direction were modelled according to the dashed line ABC of Figure 7-6. The elastic modulus in the meridional direction was assigned a constant value of 26 GPa (3,800 Ksi) representing uncracked, reinforced concrete. The circumferential steel ratio was taken to be 0.35 percent in conformity with present ACI practice while the steel was assumed to yield at a stress level of 340 MPa (49,000 Psi).

According to equation (7-6b), the driving force necessary to induce tensile yield in the throat region of the smaller shell is $N_\phi^p = -1.662 \times 10^5$ N/m and in the larger shell $N_\phi^p = -4.223 \times 10^5$ N/m. Thus, for the non-linear analyses, the meridional membrane force was considered to increase from 0 to 1.6 times that required to yield the shell. At the higher stress level, the circumferential strain is approximately twice that at yield and corresponds to point C of Figure 7-6.

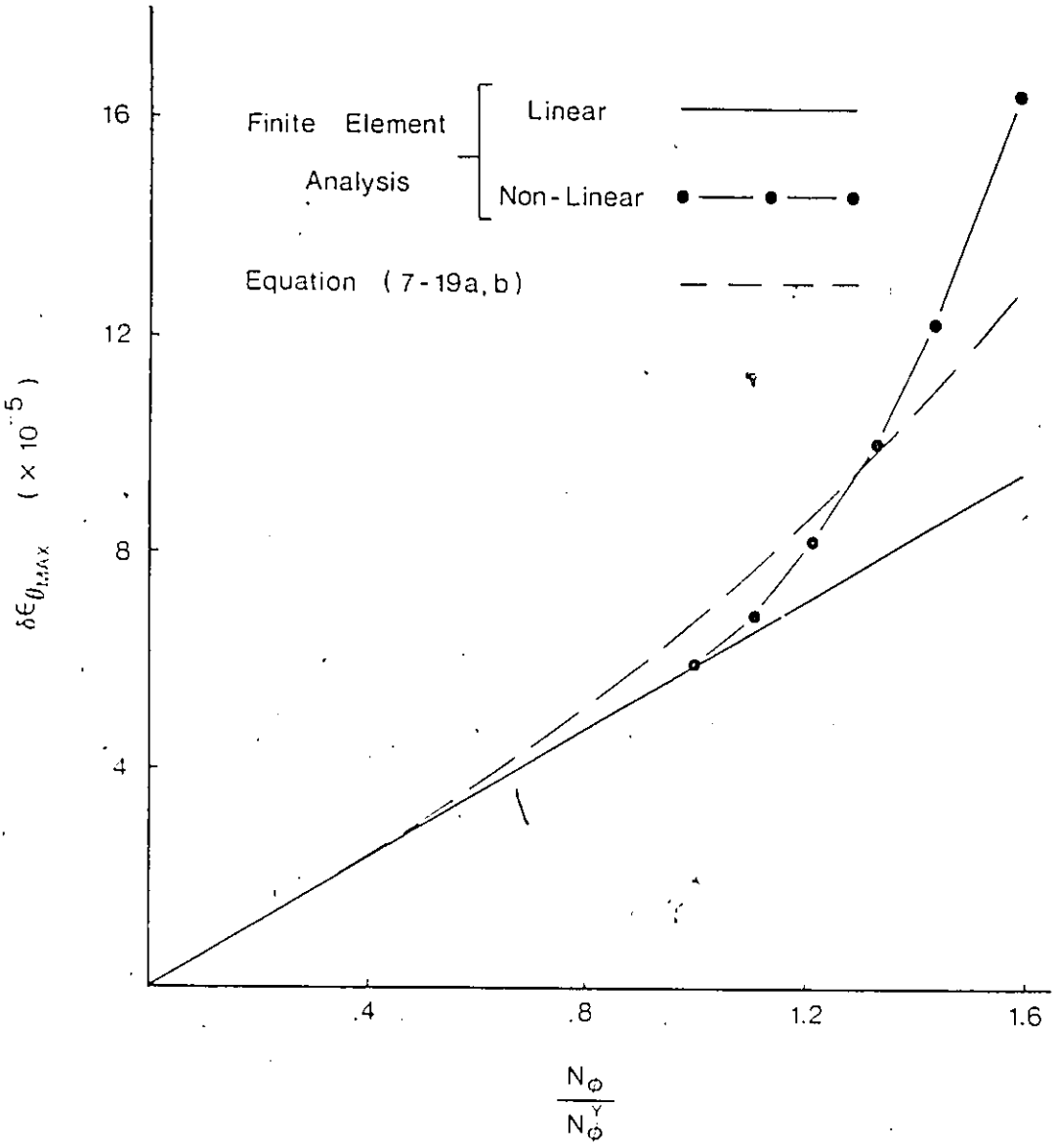

Figure 7-7a Maximum circumferential strain in a meridionally imperfect, circumferentially yielded, orthotropic cylinder having the dimensions of the throat of the Ardeer tower shell

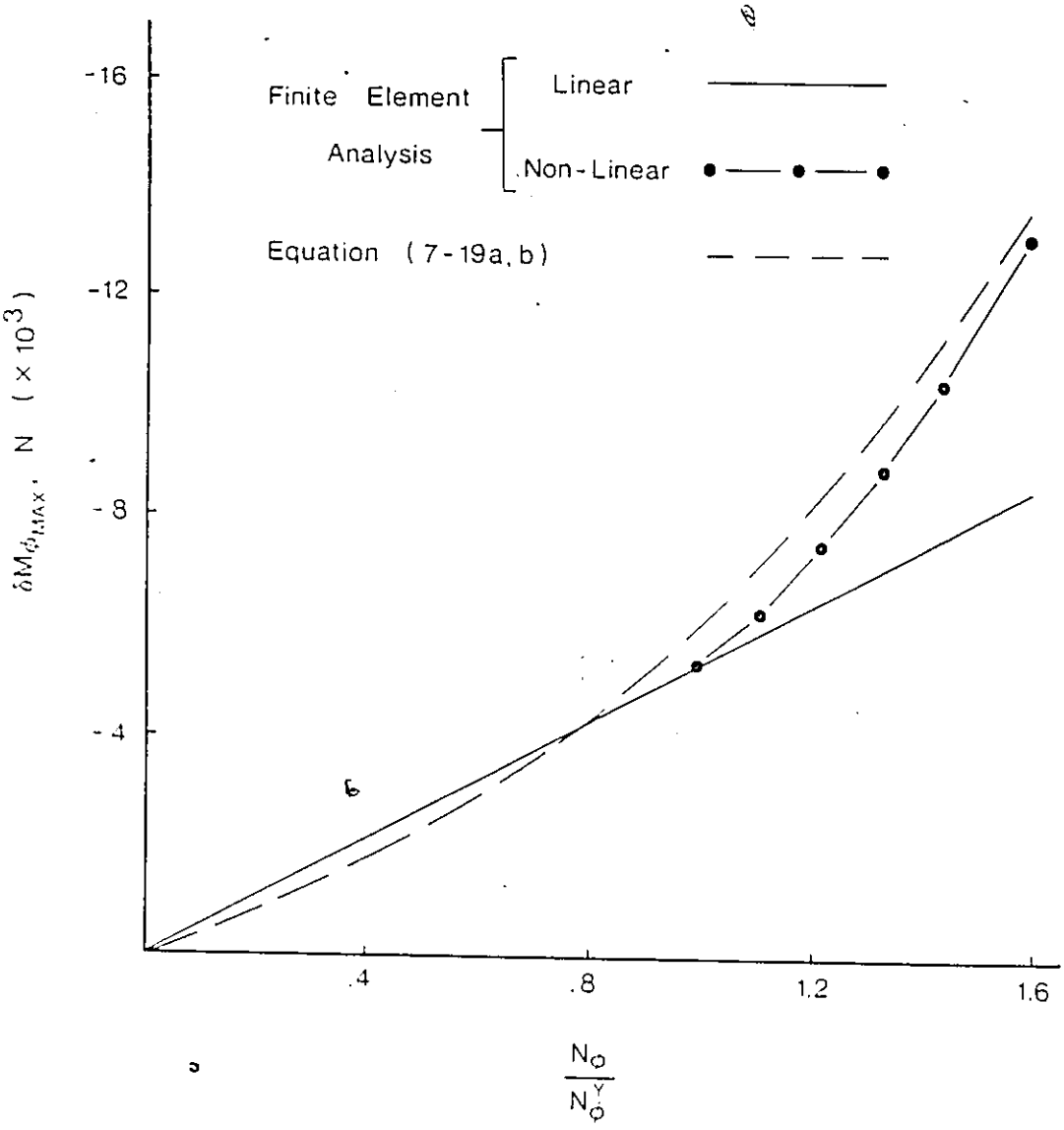

Figure 7-7b Maximum meridional moment in a meridionally imperfect, circumferentially yielded, orthotropic cylinder having the dimensions of the throat of the Ardeer tower shell

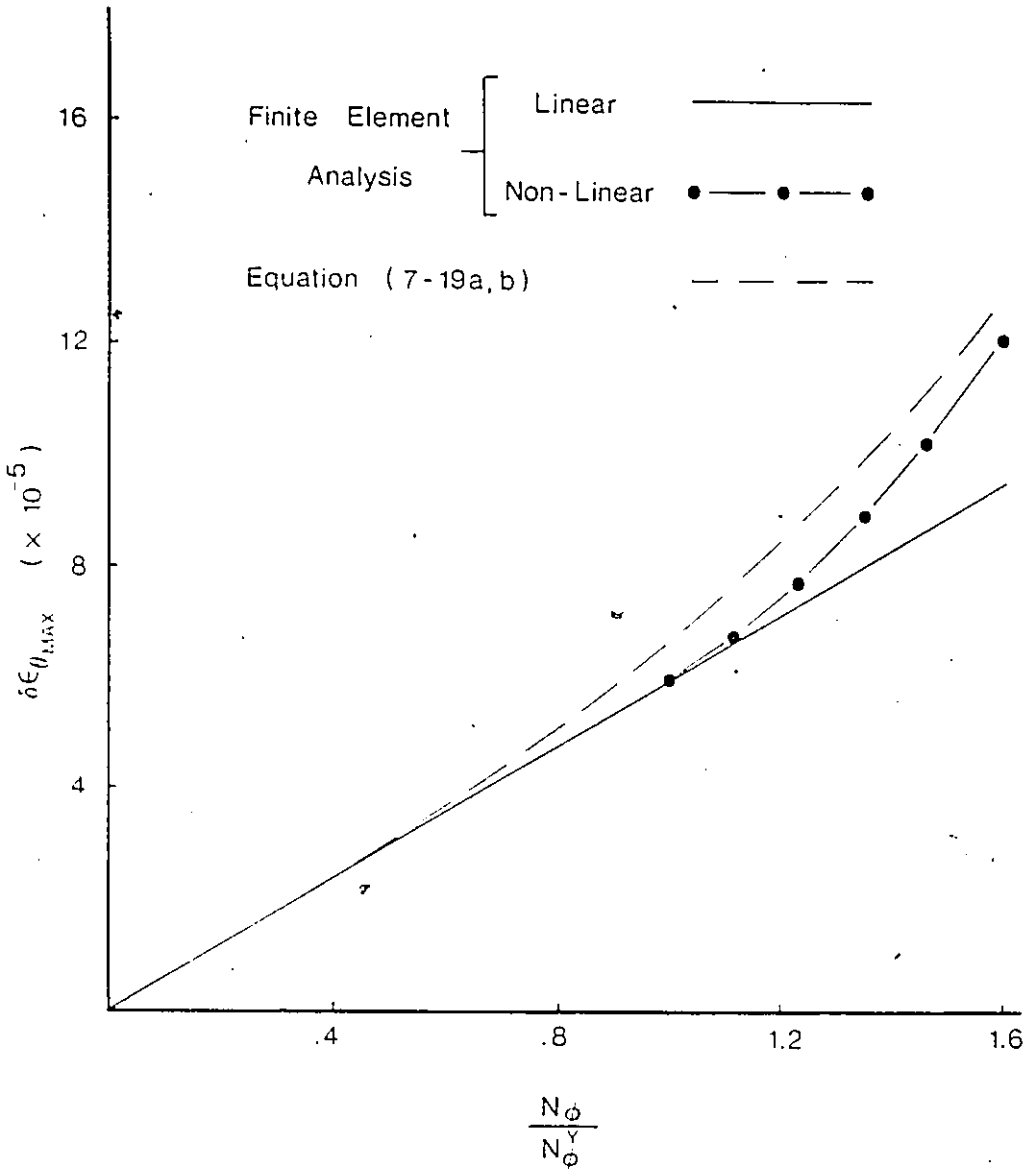

Figure 7-8a Maximum circumferential strain in a meridionally imperfect, circumferentially yielded, orthotropic cylinder having twice the dimensions of the throat of the Ardeer tower shell

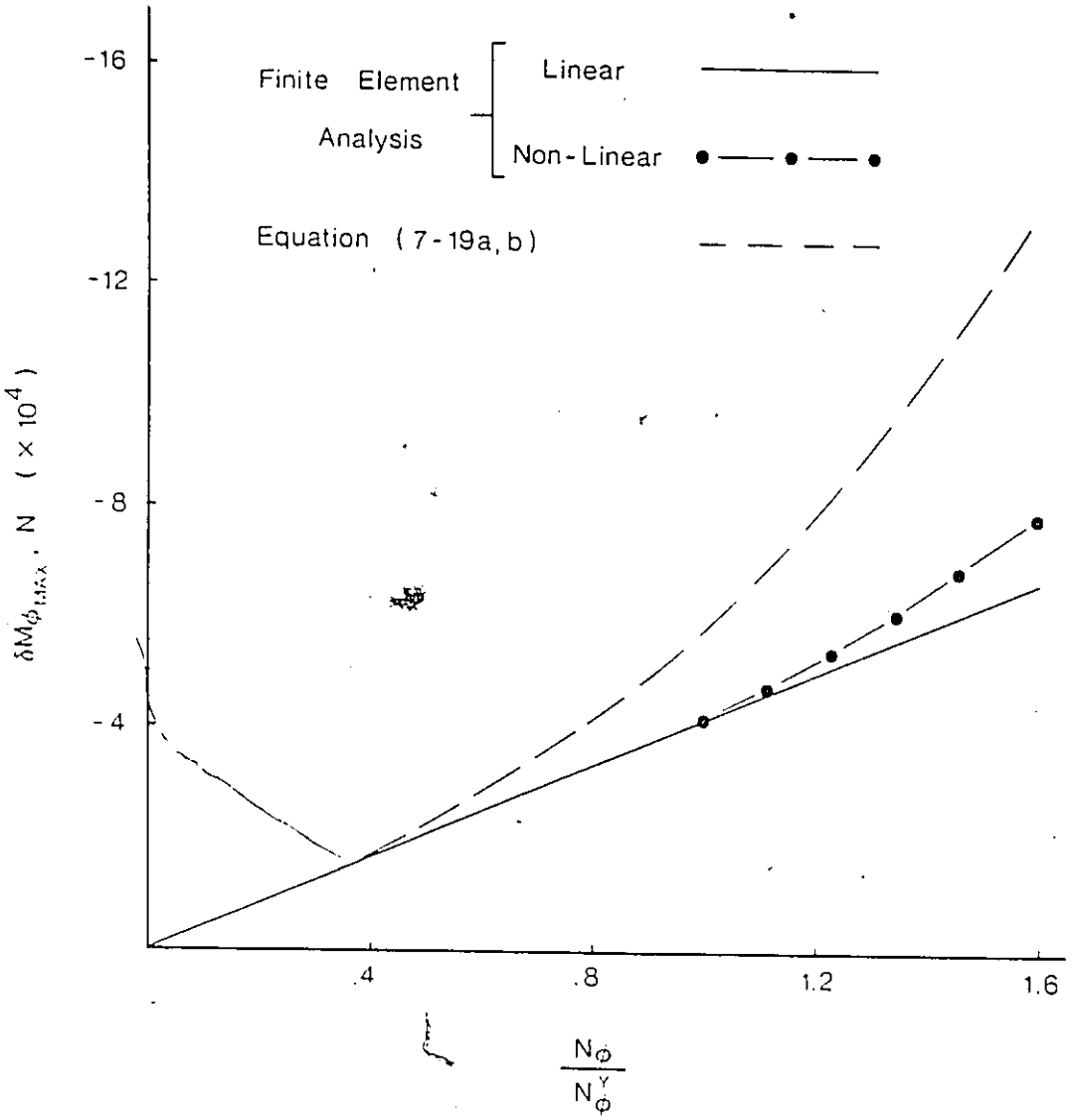

Figure 7-8b Maximum meridional moment in a meridionally imperfect, circumferentially yielded, orthotropic cylinder having twice the dimensions of the throat of the Ardeer tower shell

For the meridional imperfection being considered, the maximum circumferential strains and meridional moments obtained from the non-linear analyses of the two cylinders are illustrated in Figures 7-7 and 7-8 for varying values of the meridional membrane force. The derived solution (7-19) and the finite element analyses show that the effect of circumferential yield is to increase both the maximum circumferential strain and meridional moment. Furthermore, the loss in membrane stiffness following circumferential yield results in greater strain and moment increases for the smaller shell. This is explained by the fact that membrane action in the smaller shell plays a more important role in resisting the out-of-balance moment generated by the imperfection and is evidenced by the elastic moments which are approximately ten times greater in the larger than in the smaller shell. As example, at the highest stress level considered in the two analyses ($N_\phi/N_\phi^y = 1.6$), circumferential yield in the smaller shell leads to a strain increase which is 82% of the maximum elastic circumferential strain. This contrasts the 27% strain increase in the larger shell. Similarly, for the vertical moment there is an increase of 54% of the maximum elastic meridional moment in the smaller shell compared to 18% in the larger shell.

Comparing the strains and moments predicted by equations (7-19) with those obtained from the stepwise non-linear finite element analyses, it is found that both display

similar trends with increasing meridional membrane force. In the case of the maximum circumferential strain, there is close agreement; the largest discrepancy being a 22% lower strain predicted by the proposed solution at the highest stress level in the smaller shell. It is further noted that for the two shells, the maximum meridional moments predicted by the proposed solution are conservative. In particular, at the highest stress level in the larger shell, equation (7-19b) yields a maximum meridional moment which is 70% higher than that obtained by the respective finite element analysis.

7.4 MAXIMUM ALLOWABLE IMPERFECTION HEIGHT

A cooling tower shell designed on the basis of perfect geometry can accomodate a degree of local meridional imperfection on the assumption that the shell posesses sufficient capacity to resist both the perfect shell forces and a rise in the circumferential force and meridional moment due to the imperfection. Thus, for a specified shell geometry and a reinforcing steel schedule, the derived equations (7-6) and (7-19) offer a means for setting tolerance limits for meridional imperfection in terms of a maximum allowable imperfection height ξ_{MAX}.

7.4.1 ELASTIC ORTHOTROPIC SHELL

Equation (7-6b) expresses the maximum change in circumferential force arising from a meridional imperfection while taking into account the orthotropic behaviour of the shell as a result of vertical cracking within the region of imperfection. For this case, the driving force N_ϕ^p is assumed equal to the maximum meridional force arising from the action of wind and gravity. Furthermore, on the assumption that it is equally probable to have a positive and negative imperfection $\xi(S)$, the resultant force change $\delta N_{\theta_{MAX}}$ is taken to be tensile in nature and must therefore be resisted by the the horizontal steel at that level in the tower. Thus, if the horizontal steel reinforcement is $\rho_\theta t$ with a yield stress of f_y then

$$\delta N_{\theta_{MAX}} = \frac{N_\phi^p \xi_i R\Gamma}{L^2} \leq \rho_\theta t f_Y$$

which after re-arranging gives

$$\xi_{MAX} = \frac{\rho_\theta t L^2 f_Y}{N_\phi^p R\Gamma} \qquad (7\text{-}20a)$$

Next, consideration is given to the rise in meridional moment at a point on the circumference where the driving force N_ϕ^p has a maximum tensile value. Therefore, neglecting the action of the concrete, this moment must be resisted by the vertical steel alone which is assumed to be in two lay-

ers. Considering the vertical reinforcement to be designed so as to resist the uplift force N_ϕ^p during the overturning action of the wind and that an overstress η can be permitted in the vertical steel, then the maximum allowable meridional moment is calculated to be

$$M_{\phi_{Allowable}} = 0.4\eta t N_\phi^p$$

in which the distance between the two layers of reinforcement is taken to be 0,8t. Combining this result with equation (7-6a)

$$\delta M_{\phi_{MAX}} = N_\phi^p \xi_i \beta \leq 0.4\eta t N_\phi^p$$

and after re-arranging gives

$$\xi_{MAX} = \frac{0.4\eta t}{\beta} \qquad (7\text{-}20b)$$

Equations (7-20) define the maximum height of imperfection for any desired level in a cooling tower shell. Adopting the lesser of the two values implies that the shell will remain elastic by ensuring that the capacity of the horizontal and the vertical steel in the tower is not exceeded in terms of its yield strength.

7.4.2 CIRCUMFERENTIALLY YIELDED SHELL

In regions of the elastic, orthotropic shell where the permissible height of imperfection is limited by the yield strength of the horizontal steel ie. equation (7-20a), it is advantageous to re-define failure as having exceeded both the capacity of the horizontal and the vertical steel. Thus, if the shell is permitted to strain beyond its yield in the circumferential direction, a progressive type failure can be prevented by simply ensuring sufficient bending resistance in the shell's meridional direction while making due account of the re-distribution of forces which takes place during the yielding process.

The strain given by equation (7-19a) includes the effect of circumferential yield up to a strain value twice that necessary to yield the horizontal steel (point C of Figure 7-6). Furthermore, noting from Figure 7-6 that

$$\lambda' = \frac{1}{8}\left(\frac{E_{\theta i}}{\rho_\theta f_Y}\right)^2 = \frac{1}{8}\left(\frac{1}{\varepsilon_\theta^Y}\right)^2$$

equation (7-19a) can be re-written as

$$\delta\varepsilon_{\theta_{MAX}} = \varepsilon_{\theta o_{MAX}}\left[1 + \frac{1}{8}\left(\frac{\varepsilon_{\theta o MAX}}{\varepsilon_\theta^Y}\right)^2\right]$$

Further simplification results when the maximum circumferential strain in the yielded and elastic shells are approximately equal so that

$$\delta\varepsilon_{\theta MAX} = \varepsilon_{\theta_o MAX}\left[1 + \frac{1}{8}\left(\frac{\delta\varepsilon_{\theta MAX}}{\varepsilon_\theta^Y}\right)^2\right]$$

If the shell can safely accomodate twice the circumferential strain necessary to yield the horizontal steel, then, by setting $\delta\epsilon_{\theta_{MAX}} = 2\epsilon_\theta^y$ in the above equation

$$\varepsilon_{\theta_o MAX} \leq \frac{4}{3}\varepsilon_\theta^Y$$

$$= \frac{4}{3}\left(\frac{\rho_\theta f_Y}{E_{\theta i}}\right)$$

Finally, recalling that $\epsilon_{\theta_{o MAX}}$ denotes the maximum circumferential strain in the elastic orthotropic shell, this value is equated to (7-6b) so that

$$\frac{4}{3}\frac{\rho_\theta f_Y}{E_{\theta i}} = \frac{N_\phi^P \xi_i R\Gamma}{L^2 t E_{\theta i}}$$

Re-arrangement then leads to the tolerance equation

$$\xi_{MAX} = \frac{4}{3}\frac{\rho_\theta t L^2 f_Y}{N_\phi^P R\Gamma} \qquad (7\text{-}21a)$$

Similarly, for the vertical steel, equation (7-19) pertaining to the maximum meridional moment in the circumferentially yielded shell can be re-written in the form

$$\delta M_{\phi_{MAX}} = M_{\phi_{o_{MAX}}} \left[1 + \frac{3}{8} \left(\frac{\delta \varepsilon_{\theta_{MAX}}}{\varepsilon_{\theta}^{Y}} \right)^2 \right]$$

Setting the circumferential strain to twice the strain value necessary to yield the horizontal steel leads to

$$\delta M_{\phi_{MAX}} = \frac{5}{2} M_{\phi_{o_{MAX}}}$$

Assuming, as in the case of the elastic orthotropic shell, that the maximum vertical moment be limited to the value

$$\delta M_{\phi_{MAX}} \leq 0.4 \eta t N_{\phi}^{P}$$

and recalling that $M_{\phi_{o_{MAX}}}$ denotes the maximum meridional moment in the elastic orthotropic shell then

$$0.4 \eta t N_{\phi}^{P} = \frac{5}{2} N_{\phi}^{P} \xi_i \beta$$

This equation can be re-arranged to give the tolerance limit

$$\xi_{MAX} = \frac{2}{5} \cdot \frac{0.4 \eta t}{\beta} \qquad (7\text{-}21b)$$

Equations (7-21) define the maximum height of imperfection in those levels of a cooling tower shell which would yield circumferentially as a result of tensile hoop forces.

Using the lesser of the two values restricts the circumferential strains to twice the strain value needed to yield the horizontal steel while at the same time ensuring that the capacity of the vertical steel is not exceeded.

7.4.3 PROPOSED LIMITS OF TOLERANCE

Thus far, equations (7-20) and (7-21) have been derived for calculating a certain maximum height of imperfection at any point in a cooling tower shell. Together, these equations take into account the effect arising from the development of vertical cracks following the tower's construction and the redistribution of forces associated with yielding of the circumferential steel. Furthermore, their solution involves quantities which are determined at the design stage and are therefore known to the construction engineer.

In establishing limits of tolerance for meridional imperfection, it is now possible for the construction engineer, using (7-20) and (7-21), to distinguish between two limiting criteria based on assumed failure modes:

(1) If the sum of forces in the perfect shell and those arising from an imperfection are limited so that all points in the as constructed shell remain within the elastic limit, then, only equations (7-20) need be applied to establish the maximum permissible radial deviation at any level in the

tower. Thus, as was demonstrated by the comparative study of Chapter 5 and is illustrated in Figure 7-9, equation (7-20a) pertaining to the horizontal steel would govern the permissible radial deviation in the highly stressed regions near the base of the tower while (7-20b) pertaining to the vertical steel would govern in the upper, less stressed regions of the tower.

(2) Alternatively, if allowance is made for local circumferential yield to take place in vicinity of the imperfection, then, for the lower regions of the tower which would initially undergo circumferential yield, equations (7-21) in lieu of (7-20a) can be used to determine the maximum permissible radial deviation, Figure 7-9. Furthermore, to reduce the uncertainty of where the change from elastic to non elastic limits occurs, the application of equations (7-21) can be extended to include the upper regions of the tower resulting in a more conservative tolerance limit for those regions where (7-20b) would normally govern. Thus, equations (7-21) can be used to establish the maximum permissible radial deviation at all levels in the tower.

For the solution of equations (7-20b) and (7-21b) it is suggested that the value 0.5 be assigned to the overstress factor η. This value is chosen on the basis that, for an im-

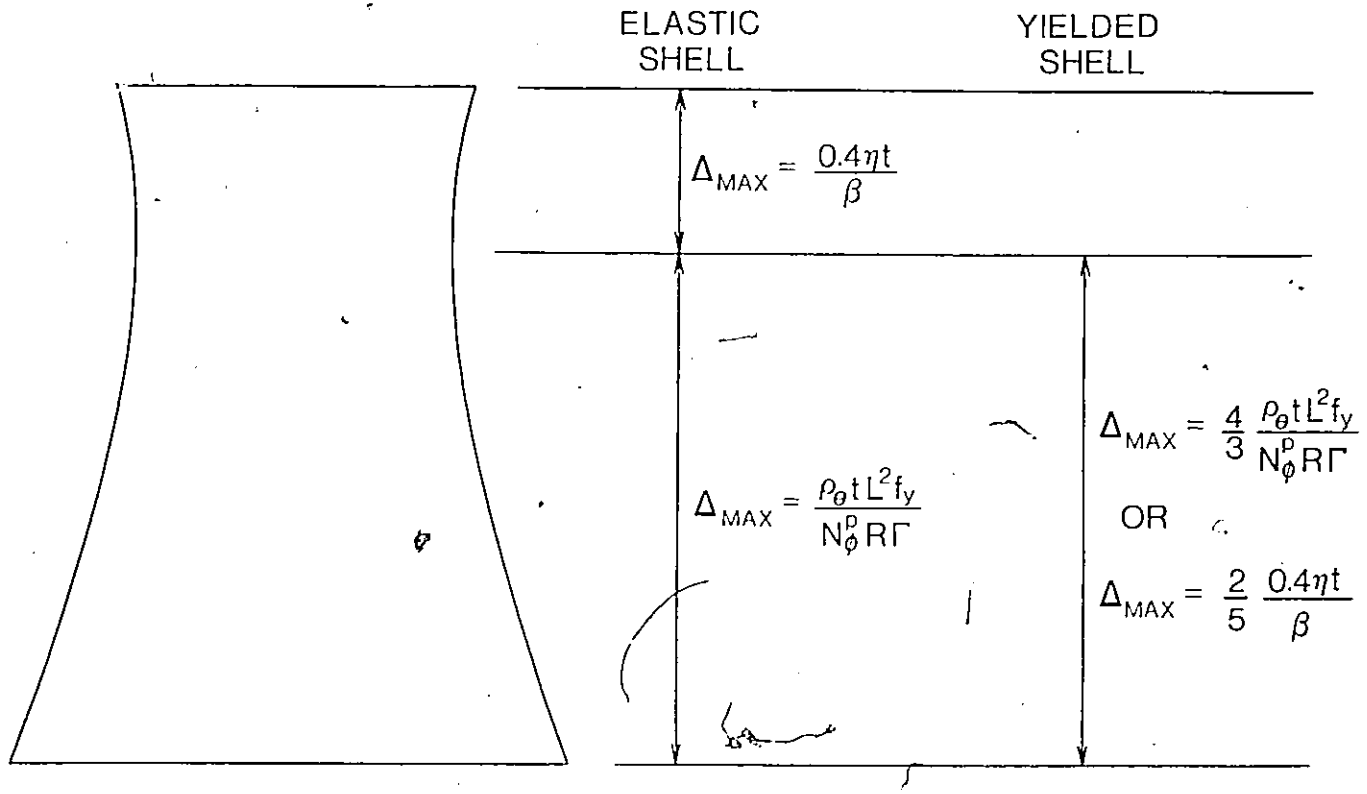

Figure 7-9 Maximum permissible radial deviation for different levels in a cooling tower shell

perfection which acts as a local stress concentrator, the full strength of the shell can be utilized to resist the resultant imperfection forces. Considering that in the design of concrete structures, sufficient steel reinforcement is generally specified so as to limit steel stresses to within two thirds of the yield value, a 50 percent increase in stress for the vertical steel could then be accomodated.

7.5 COMPARISON BETWEEN PUBLISHED AND PROPOSED LIMITS OF TOLERANCE

Finally, as an indication for the type of imperfection tolerances obtained when the effects due to vertical cracking and circumferential yield are taken into account, the maximum radial deviations permitted by the presently proposed method (equations (7-21)) were evaluated for the two cooling tower shells who's dimensions were described in Chapter 5. Further, as a basis for comparison, the recommended tolerances of the ACI and the published limitations of Croll and Al-Dabbagh were used as standards of reference for discussing the proposed limits.

To determine the degree of influence of vertical cracking, two 'extreme' cases were considered for calculating the permissible radial deviations. In the absence of vertical cracking, as would occur during or shortly proceeding the tower's construction, the shell was considered to behave isotropically. Otherwise, for the case of significant verti-

cal cracking within the region of the imperfection, the shell's circumferential membrane stiffness was reduced to 50 percent that of the meridional direction. As was done for the comparative study of Chapter 5, a uniform distribution of circumferential steel was assumed having steel ratio 0.35 percent and a yield stress of 340 MPa (49,400 Psi).

Figures 7-10 illustrate the maximum permissible radial deviations calculated for varying heights Z by considering an imperfection of length 12 m (39.4 ft). Figures 7-11 show the maximum permissible radial deviations Δ for a region close to the base of each shell as the length H varies from 0 to 25 m (82.0 ft). In both sets of Figures, the recommended tolerances of the ACI and the published limitations of Croll and Al-Dabbagh are shown as solid lines while the presently proposed tolerances are drawn as broken lines; the degree of orthotropicity being indicated by the ratio of the circumferential to the meridional membrane stiffness.

From Figures 7-10 and 7-11, the following observations concerning the maximum permissible radial deviations are made:

(1) Because the tolerance limits recommended by the ACI are empirical in form and do not relate to the geometry or stresses in the tower, the 4.5 cm (1.77 in) radial deviation permitted in both shells is conserva-

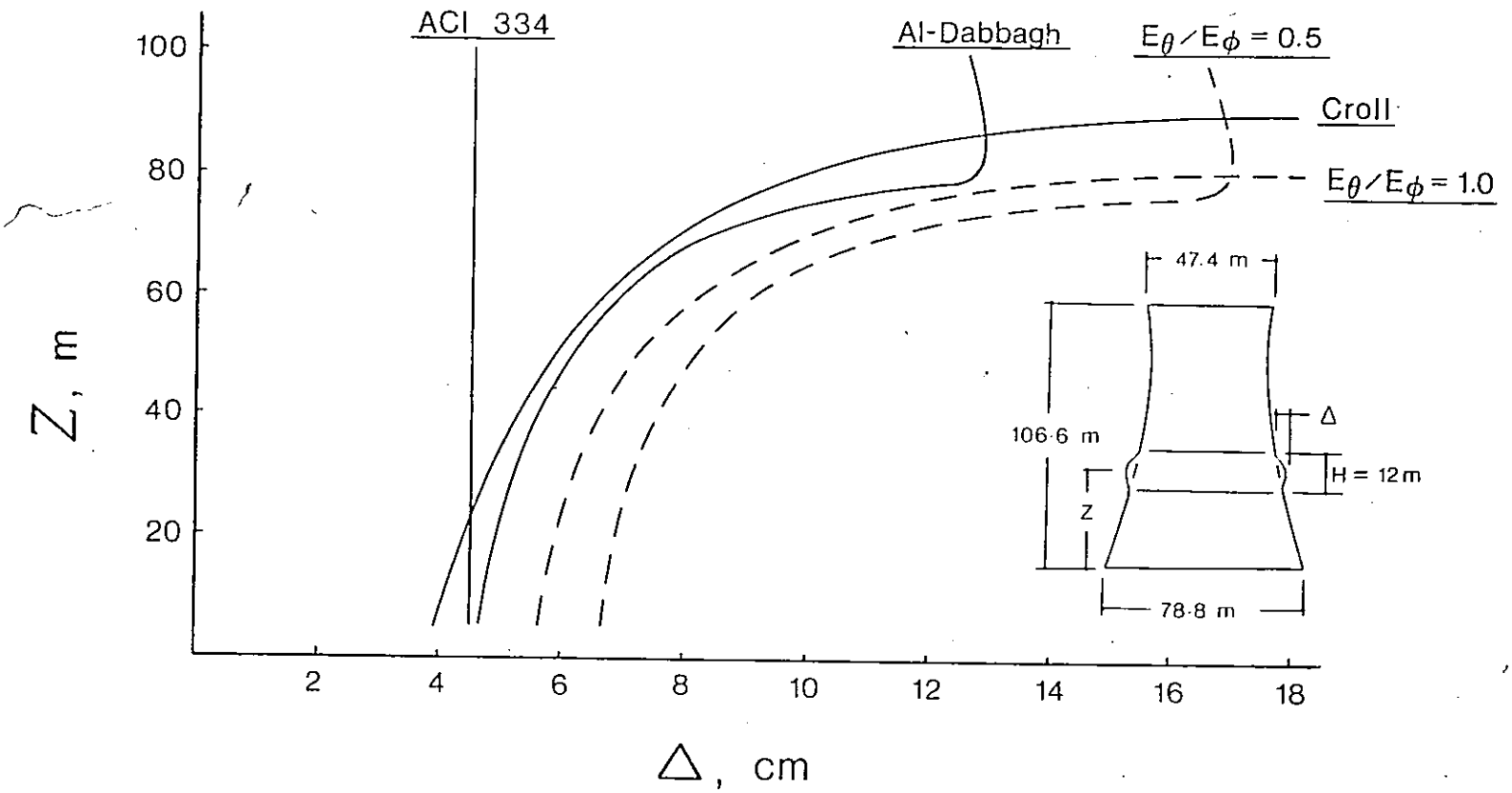

Figure 7-10a Maximum tolerable radial deviation at varying levels in the smaller shell

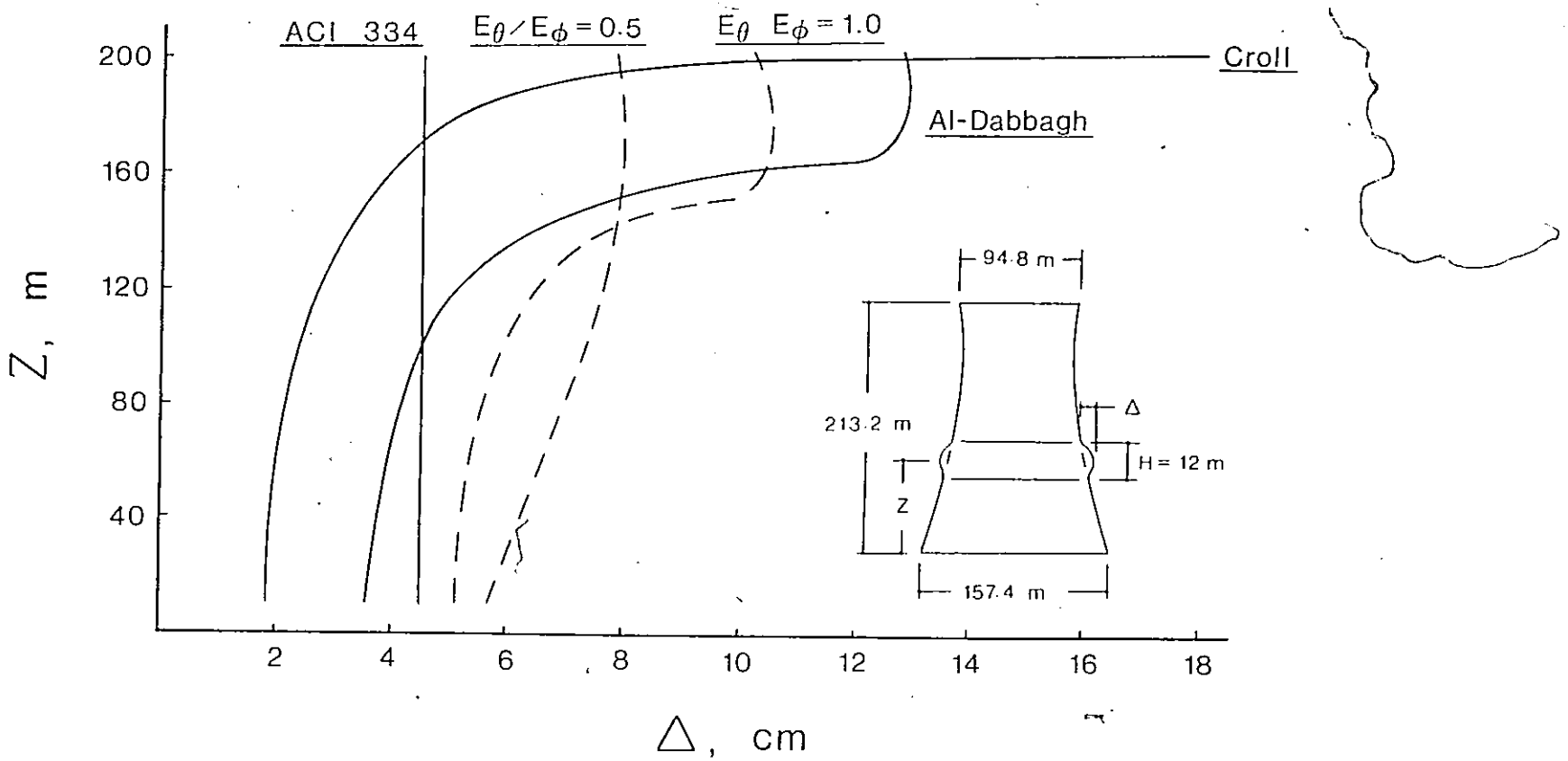

Figure 7-10b Maximum tolerable radial deviation at varying levels in the larger shell

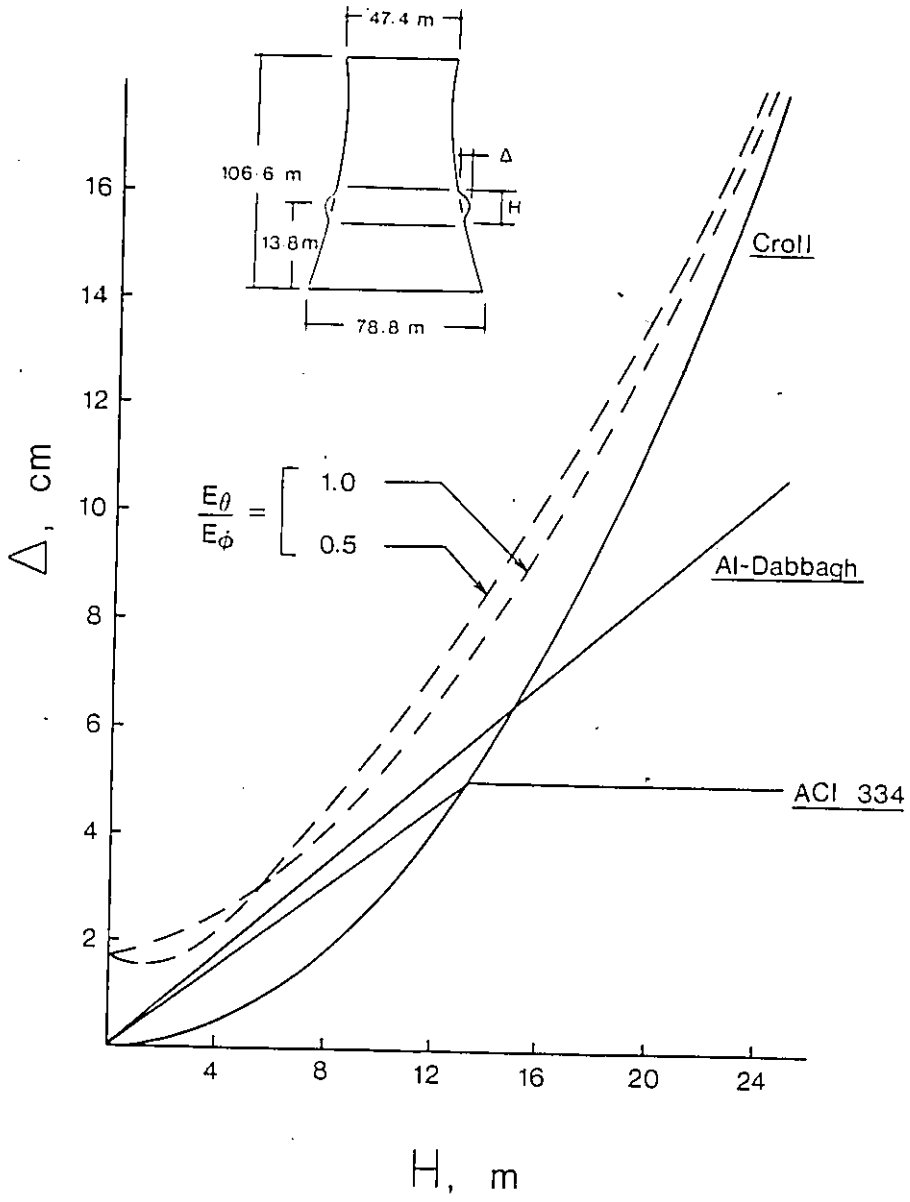

Figure 7-11a Maximum tolerable radial deviation for varying imperfection length near the base of the smaller shell

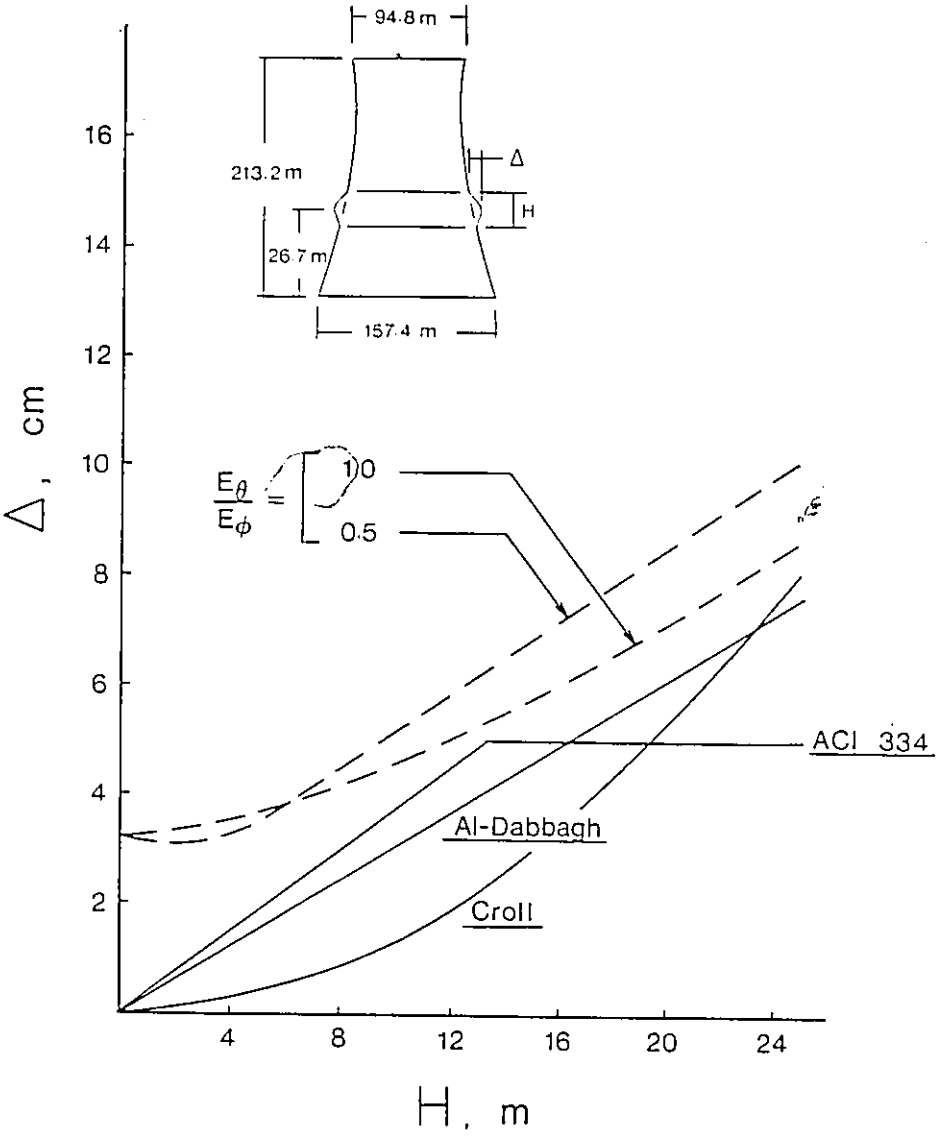

Figure 7-11b Maximum tolerable radial deviation for varying imperfection length near the base of the larger shell

tive, particularly in the upper levels of both towers. Consequently, near the throat region of the shell having dimensions as the Ardeer tower, Figure 7-10a, the 16.8 cm (6.61 in) radial deviation permitted by the proposed method is approximately four times greater than that permitted by the ACI. Similarly, for the larger cooling tower shell of Figure 7-10b, the 7.8 cm (3.07 in) radial deviation allowed by the proposed method is almost twice that given by the ACI. Furthermore, in Figures 7-11, the ACI restriction of 5 cm (2.0 in) on radial deviation tends to be conservative for 'long' imperfections whereas the 1.3 to 1.7 percent slope restriction leads to conservative tolerances for 'short' imperfections.

(2) The tolerances for imperfection set by the proposed method exhibit trends similar to those of Croll and Al-Dabbagh by permitting larger radial deviations in the upper regions of both shells while becoming more stringent as tower dimensions increase, Figures 7-10. Furthermore, near the base region of both shells, Figures 7-11, the proposed method allows increasingly larger radial deviations for the longer imperfection lengths as does Croll and Al-Dabbagh. However, some discrepancy is evident for the very short imperfections characteristic of a 'kink' in the perfect meridian which is probably the most frequent imperfection

in practice. For the limiting case where $H \rightarrow 0$, Croll and Al-Dabbagh do not permit such imperfections to occur, whereas the proposed method tolerates radial deviations in the larger and the smaller cooling tower shells of 3.2 cm and 1.7 cm (1.26 in and .67 in) respectively, Figures 7-11.

(3) Excepting the upper regions of the larger shell where the shell's bending capacity limits the maximum radial deviation, Figure 7-10b, the proposed method which allows the shell to circumferentially strain beyond its yield, generally permits larger radial deviations in both shells. Specifically, near the base of the larger shell, Croll and Al-Dabbagh permit radial deviations of 1.9 cm and 3.5 cm (.75 in and 1.4 in) contrasting the 5.1 cm to 5.7 cm (2.00 in to 2.20 in) permitted by the proposed method. Further, this observation holds true for a wide range of imperfection lengths near the base of the two shells - up to 25 m (82 ft), Figures 7-11. As example, consider an imperfection of length 12 m (39 ft) in the smaller shell 55 metres above its base, Figure 7-10a. At this level, the maximum radial deviations permitted by Croll and Al-Dabbagh are 5.8 and 6.1 cm (2.28 and 2.40 in) respectively. In contrast, the proposed method permits larger radial deviations from 7.2 to 8.1 cm (2.83 to 3.19 in) depending on the degree to which vertical cracking has occured.

It is interesting to note that these values are significantly smaller than the 20 cm (7.87 in) radial deviation found to have occurred at this level in the Ardeer tower and believed to have been the cause for its collapse.

(4) The proposed method, Figures 7-10 and 7-11, suggests that a reduction in circumferential membrane stiffness due to vertical cracking will result in larger permissible radial deviations at levels where imperfection tolerances are governed by circumferential yield. This occurs because in an uncracked shell, the out-of-equilibrium forces induced by an imperfection are largely resisted by membrane action. Following the formation of vertical cracks, a greater portion of the out-of-equilibrium forces is resisted by the development of meridional moments, thus, reducing the magnitude of the hoop forces in vicinity of the imperfection. However, the shell's tensile capacity (which governs the permissible radial deviation and is related to the hoop reinforcement) remains unaffected by the presence of the cracks.

Chapter VIII

CONCLUSIONS

Based on the present study, the following conclusions are made:

(1) The recently standardized guidelines of ACI 334 relating to tolerances for cooling tower imperfections limit both circumferential and meridional imperfections the effects of which are very different. Because the ACI guidelines do not relate to shell geometry, reinforcement or magnitude of stresses at the level of imperfection, no variation in tolerance occurs through-out the shell height. Consequently, compared to the tolerances for meridional imperfection published by Croll and Al-Dabbagh, the ACI tolerances are found conservative in the upper, less stressed zones of the shell and non conservative for the highly stressed zones near the shell base. Further, the ACI restriction of 5 cm (2 in) on radial deviation tends to a conservative tolerance for 'long' imperfections whereas the 1.3 to 1.7 percent slope restriction leads to non conservative tolerances for 'short' imperfections. These discrepancies increase as tower dimensions increase.

(2) The published criteria of Croll and Al-Dabbagh for meridional imperfection offer a more rational approach to specifying tolerance limits than does ACI 334. Croll's criterion for preventing yield of the circumferential steel is the more conservative tolerance below the shell throat. Al-Dabbagh, attempting to prevent meridional bending failure, provides more stringent tolerances in certain regions above the shell throat.

(3) For a specified tolerance $T(\Delta,H)$ characterized by a height ξ_i and wavelength L with respect to the true meridian, the maximum imperfection forces at any level in a tower can be superposed with the design forces arising from an analysis of the perfect shell. Provided construction errors are within this specified tolerance, the imperfect shell should adequately resist all internal forces. In this respect, this study presents a closed form solution for imperfection forces. For an imperfection in the form of a cosine curve, the maximum increases in meridional moment and circumferential force are

$$\delta M_{\phi_{MAX}} = \beta N_\phi^P \xi_i \left[1 + \Psi \frac{N_\phi^P L^2}{E t^3} \right] \qquad (8\text{-}1a)$$

$$\delta N_{\theta_{MAX}} = \frac{\Gamma N_\phi^P \xi_i r_2}{L^2} \left[1 + \Psi \frac{N_\phi^P L^2}{E t^3} \right] \qquad (8\text{-}1b)$$

where the parameters β, Γ and Ψ are given in Figures 6-8 and 6-9. This solution closely agrees with the results from a finite element analysis, Figures 6-10 and 6-11. Furthermore, the closed form solution offers an advantage in that, compared to Croll and Al-Dabbagh, it more closely approximates the forces from the finite element analysis over the whole range of possible imperfection lengths.

(4) A maximum meridional imperfection may be permitted without a cooling tower shell having been explicitly designed for it. This is justified on the basis of a certain amount of steel always being present and capable of resisting the additional forces due to imperfection. For this purpose; equations (8-1) can be generalized to include the effect of vertical cracking which causes the shell to behave orthotropically and to also include the redistribution of forces from circumferential membrane to meridional bending which occurs during yielding of the circumferential steel. Assuming that a cooling tower shell can safely accomodate twice the yield strain of steel in the circumferential direction while retaining sufficient bending resistance in the meridional direction to prevent a progressive type failure, the generalized form of equations (8-1) can be reworked to give the following set of tolerance limits

$$\Delta_{MAX} = \frac{4}{3} \frac{\rho_e t L^2 f_y}{N_\phi^r R \Gamma} \qquad (8\text{-}2a)$$

$$\Delta_{MAX} = \frac{2}{5} \cdot \frac{0.4\eta t}{\beta} \qquad (8\text{-}2b)$$

where the lesser of the two values defines the maximum allowable radial deviation in a cooling tower shell. Compared to the published limitations of Croll and Al-Dabbagh, the derived limits of tolerance generally permit larger radial deviations in the more critically stressed zones near the base of a cooling tower shell, Figures 7-10 and 7-11. Furthermore, unlike Croll and Al-Dabbagh, the derived tolerance limits permit imperfections of very short length characteristic of a kink in the perfect meridian.

(5) The effect of vertical cracking is to reduce the shell's circumferential membrane stiffness. This in turn, reduces the magnitude of the hoop forces in vicinity of an imperfection and allows a greater portion of the out-of-balance forces induced by an imperfection to be resisted through the development of meridional moments. Because the shell's tensile capacity is related to the hoop reinforcement and remains unaffected by the presence of vertical cracks, the derived tolerance limits, equations (8-2), permit larger radial deviations at levels where imperfection

tolerances are governed by circumferential yield. This suggests that, from an imperfection point of view, vertical cracking is not detrimental to a shell's integrity and therefore, need not be considered when calculating tolerance limits for meridional imperfection.

BIBLIOGRAPHY

(1) FLUGGE, W., 'Stresses In Shells'. Springer Verlag N.Y., 1960.

(2) TIMOSHENKO, S., WOINOWSKY-KRIEGER, S., 'Theory Of Plates And Shells'. McGraw - Hill, 1959.

(3) GIBSON, J. E., 'Linear Elastic Theory Of Thin Shells'. Pergamon Press, 1965.

(4) ZERNA, W., MUNGAN, I., 'Construction And Design Of Large Cooling Towers'. ASCE Journ. Of The Struc. Div., Feb. 1980.

(5) ACI-ASCE COMMITTEE 334, 'Reinforced Concrete Cooling Tower Shells'. Journal Of The Am. Conc. Inst., November-December, 1984.

(6) 'Ferrybridge Inquiry'. Electricity, Jan/Feb 1966.

(7) 'What Lessons From Ferrybridge'. Engineering, 2 Sept. 1966.

(8) 'Report Of The Committee Of Inquiry Into Collapse Of Cooling Towers At Ferrybridge', Monday 7 November 1965. Central Electricity Generating Board, 1966.

(9) 'Building Code Requirements For Minimum Design Loads In Buildings And Other Structures (ANSI A58-1 1982)', American Standards Institute, New York, 1982.

(10) NIEMANN, H. J., 'On The Stationary Wind Loading Of Axisymmetric Structures In The Region Beyond The Critical Reynolds Number'. Technical-Scientific Communication No. 71-2, Institute For Structural Engineering, Ruhr University, Bochum, Germany, 1971.

(11) IASS WORKING GROUP No. 3, 'Recommendations For The Design Of Hyperbolic Or Other Similarly Shaped Cooling Towers'. International Association For Shell And Spatial Structures, Madrid, 1979.

(12) ZERNA, W., KRATZIG, W. B., MUNGAN, I., 'Cooling Tower Practice In Germany: State Of The Art'. ASCE Journal Of The Energy Division, Vol. 108, No. EY1, March 1982.

(13) KEMP, K. O., CROLL, J. G. A., 'The Role Of Geometric Imperfections In The Collapse Of A Cooling Tower'. The Structural Engineer, No. 1, V. 54, January 1976.

(14) 'Strongest Tower Collapses In Gale'. New Civil Engineer, 4 October, 1973.

(15) 'Cooling Tower Collapse Exposes Calculated Gamble'. New Civil Engineer, 19 January, 1984.

(16) 'Report Prompts Cooling Tower Scare'. Construction Today, November 1985.

(17) 'Report Of The Committee Of Inquiry Into The Collapse Of The Cooling Tower At Ardeer Nylon Works, Ayrshire On Thursday, 27th September 1973.' ICI Ltd., Petrochemicals Division, 1974.

(18) BS4485: PART 4: 1975, 'Structural Design Of Cooling Towers'. British Standards Institute, 1975.

(19) SOARE, M., 'Cooling Towers With Constructional Imperfections'. Concrete, November 1967.

(20) CALLADINE, C. R., 'Structural Consequences Of Small Imperfections In Elastic Thin Shells Of Revolution'. Int. J. Solids Structures, Vol. 8, 1972.

(21) CROLL, J. G. A., KEMP, K. O., 'Specifying Tolerance Limits For Meridional Imperfections In Cooling Towers'. ACI Journal, Vol. 76, January 1979.

(22) CROLL, J. G. A., KALELI, F., KEMP, K. O., 'A Simplified Approach To The Analysis Of Geometrically Imperfect Cooling Tower Shells'. Eng. Struct., Vol. 1, January 1979.

(23) AL-DABBAGH, A., GUPTA, A. K., 'Meridional Imperfection In Cooling Tower Design'. ASCE Journ. Of The Struc. Div., Vol. 105, No. ST6, June 1979.

(24) BASU, P. K., GOULD, P. L., 'SHORE III Shell Of Revolution Finite Element Program - Theoretical Manual'. Structural Engineering Research Report No. 48, Dept. Of Civil Engineering, Washington University, St. Louis, Sept. 1977.

(25) GUPTA, A. K., AL-DABBAGH, A., 'Meridional Imperfection In Cooling Tower Design: Update'. ASCE Journ. Of The Struc. Div., Vol. 108, No. ST8, August 1982.

(26) A STANTON.R. G., FRYER, K. D., 'Algebra And Vector Geometry'. Holt, Rinehart And Winston Of Canada Ltd., 1965, Chapter 5.

(27) KREYSZIG, E., 'Advanced Engineering Mathematics'. Wiley And Sons Ltd., 1972, Chapter 2.

(28) SELBY, S., 'Standard Mathematical Tables'. The Chemical Rubber Co., 1971, (Hyperbolic And Related Functions).

(29) GUEDELHOEFER, O. C., KRAUKLIS, A. T., 'Crack Repair Techniques - To Bond Or Not To Bond'. Concrete International, Vol. 8, No. 8, August 1986.

(30) GODOY, L. A., 'On The Collapse Of Cooling Towers With Structural Imperfections'. Proceedings Of The Institute Of Civil Engineers, Part 2 Research And Theory, Vol. 77, Dec. 1984.

(31) ELLINAS, CHARLES P., CROLL, J. G. A., KEMP, K. O., 'Cooling Towers With Circumferential Imperfections'. Journal Of The Structural Division, Proceedings of the American Society of Civil Engineers, Vol. 106, No. ST12, December, 1980.

(32) CROLL, J. G. A., KALELI, F., KEMP, K. O., 'Meridionally Imperfect Cooling Towers'. Journal Of The Engineering Mechanics Division, Proceedings of the American Society of Civil Engineers, Vol. 105, No. EM5, October, 1979.

(33) GOULD, PHILLIP L., HAYASHI, K., 'Cracking Load for a Wind-Loaded Reinforced Concrete Cooling Tower'. ACI Journal, July-August, 1983.

APPENDIX A

If m_1, m_2, m_3 and m_4 are the roots of the quartic polynomial

$$m^4 + b_3 m^3 + b_2 m^2 + b_1 m + b_0 = 0$$

then the relations that exist between the roots and the coefficients are

$$m_1 + m_2 + m_3 + m_4 = -b_3$$

$$m_1m_2 + m_2m_3 + m_3m_4 + m_1m_4 + m_1m_3 + m_2m_4 = b_2$$

$$m_1m_2m_3 + m_2m_3m_4 + m_1m_3m_4 + m_1m_2m_4 = -b_1$$

$$m_1m_2m_3m_4 = b_0$$

For the quartic polynomial pertaining to the cooling tower shell

$$m^4 + \left(\frac{2}{r_2} \cdot \frac{dr_2}{dS}\right) m^3 + \left(\frac{1}{r_2} \cdot \frac{d^2r_2}{dS^2}\right) m^2 + \frac{Et}{Kr_2^2} = 0$$

the roots may be written in the form

$$m_1 = (1 + \varphi_1) \sqrt[4]{\frac{Et}{4Kr_2^2}} \left[(1 + \varphi_2) + i\right]$$

$$m_2 = (1 + \varphi_1) \sqrt[4]{\frac{Et}{4Kr_2^2}} \left[(1 + \varphi_2) - i\right]$$

$$m_3 = (1+\varphi_3)\sqrt[4]{\frac{Et}{4Kr_2^2}}\left[(-1+\varphi_4)+i\right]$$

$$m_4 = (1+\varphi_3)\sqrt[4]{\frac{Et}{4Kr_2^2}}\left[(-1+\varphi_4)-i\right]$$

For the case in which the parameters $\varphi = 0$, the roots are those for the equation

$$m^4 + \frac{Et}{Kr_2^2} = 0$$

where (dr_2/ds) and (d^2r_2/ds^2) are zero

Assuming the parameters φ to be small quantities with respect to unity, the relations between the roots and the coefficients reduce to

$$2\varphi_1 + \varphi_2 + 2\varphi_3 - \varphi_4 = 0$$

$$\varphi_3 - \varphi_1 = 0$$

$$\varphi_1 + \varphi_2 - \varphi_3 + \varphi_4 = \lambda$$

$$\varphi_4 - \varphi_2 = \mu$$

where

$$\lambda = \frac{-1}{4\sqrt{3}} \cdot \sqrt{\frac{t}{r_2}} \cdot \frac{dr_2}{ds}$$

$$\mu = \frac{t}{2\sqrt{3}} \cdot \frac{d^2r_2}{ds^2}$$

This system of equations is satisfied when

$$\varphi_1 = \mu/8$$

$$\varphi_2 = \lambda/2 - \mu/4$$

$$\varphi_3 = \mu/8$$

$$\varphi_4 = \lambda/2 + \mu/4$$

Considering the Ardeer tower geometry, it can be shown that the φ parameters are indeed small quantities as initially assumed. Thus, in vicinity of the tower's throat where curvature is maximum

$$\lambda = 0$$

$$\mu = \frac{.153}{2\sqrt{3}} \cdot \frac{1}{90} = 4.9 \times 10^{-4}$$

and

$$\varphi_1 = 6.13 \times 10^{-5}$$

$$\varphi_2 = -1.23 \times 10^{-4}$$

$$\varphi_3 = 6.13 \times 10^{-5}$$

$$\varphi_4 = 1.23 \times 10^{-4}$$

Near the tower's base where slope is maximum

$$\lambda = \frac{-1}{4\sqrt{3}} \cdot \sqrt{\frac{.153}{39}} \cdot \frac{1}{3} = -1.6 \times 10^{-2}$$

$$\mu = 0$$

and

$$\varphi_1 = 0$$

$$\varphi_2 = -7.9 \times 10^{-3}$$

$$\varphi_3 = 0$$

$$\varphi_4 = 7.9 \times 10^{-3}$$

Seeing how the φ parameters are three orders of magnitude less than unity, the slope and curvature of the perfect meridian can be neglected and the roots of the quartic polynomial being considered are closely approximated by

$$m = \pm \sqrt{\frac{tE}{4Kn_2^2}} \; (1 \pm i)$$

APPENDIX B

Applying the boundary conditions

$$\chi(\pm L) = B_2 \sin\lambda L \cdot \cosh\lambda L + B_3 \cos\lambda L \cdot \sinh\lambda L$$

$$= 0 \qquad \text{(B1)}$$

$$\left.\frac{d\chi}{dS}\right|_{\pm L} = B_2\lambda\left[\cos\lambda L \cdot \cosh\lambda L + \sin\lambda L \cdot \sinh\lambda L\right]$$

$$+ B_3\lambda\left[-\sin\lambda L \cdot \sinh\lambda L + \cos\lambda L \cdot \cosh\lambda L\right]$$

$$+ \frac{N\phi \sum_i^p \xi_i}{KL^2} \cdot \frac{\pi^2}{L}\left\{-C_1 + 2C_2 - 3C_3\right\} \qquad \text{(B2)}$$

$$= 0$$

From equation (B1)

$$B_3 = -B_2 \frac{\sin\lambda L \cdot \cosh\lambda L}{\cos\lambda L \cdot \sinh\lambda L}$$

Substituting into equation (B2) and expanding

$$B_2\left[(\sin^2\lambda L + \cos^2\lambda L)\sinh\lambda L \cdot \cosh\lambda L\right.$$

$$\left. + (\sinh^2\lambda L - \cosh^2\lambda L)\sin\lambda L \cdot \cos\lambda L\right]$$

$$+ \frac{N\phi \sum_i^p \xi_i}{KL^2} \cdot \frac{\pi^2}{\lambda L}(-C_1 + 2C_2 - 3C_3)\cos\lambda L \cdot \sinh\lambda L = 0$$

from which

$$B_2 = \frac{N\phi^P \xi_i \pi^2}{\lambda K L^3} (-C_1 + 2C_2 - 3C_3) \frac{\cos \lambda L \cdot \sinh \lambda L}{\sin \lambda L \cdot \cos \lambda L - \sinh \lambda L \cdot \cosh \lambda L}$$

and by substituting for B2 into equation (B1)

$$B_3 = \frac{N\phi^P \xi_i \pi^2}{\lambda K L^3} (-C_1 + 2C_2 - 3C_3) \frac{\sin \lambda L \cdot \cosh \lambda L}{\sinh \lambda L \cdot \cosh \lambda L - \sin \lambda L \cdot \cos \lambda L}$$

APPENDIX C

The general solution of equation (7-5) for a symmetrical imperfection in the form of a cosine curve is

$$\varepsilon_\theta = A_1 \sin\lambda s \cdot \sinh\lambda s + A_4 \cos\lambda s \cdot \cosh\lambda s + U_1 \cos\frac{\pi s}{L} + U_2 \cos\frac{2\pi s}{L} + U_3 \cos\frac{3\pi s}{L} \qquad (C1)$$

in which

$$U_1 = \frac{-N_\phi^P \xi_i L^2}{RK_\phi} \left\{ \frac{4/3\,\pi}{\pi^4 + \alpha} \right\}$$

$$U_2 = \frac{-N_\phi^P \xi_i L^2}{RK_\phi} \left\{ \frac{22/7\,\pi}{16\pi^4 + \alpha} \right\}$$

$$U_3 = \frac{-N_\phi^P \xi_i L^2}{RK_\phi} \left\{ \frac{12/5\,\pi}{81\pi^4 + \alpha} \right\}$$

and

$$\lambda = \sqrt[4]{\frac{tE_\theta}{4R^2K_\phi}}$$

$$\alpha = \frac{12L^4}{R^2t^2} \cdot \frac{E_\theta}{E_\phi}$$

Applying the boundary conditions

$$\varepsilon_\theta(\pm L) = A_1 \sin\lambda L \cdot \sinh\lambda L + A_4 \cos\lambda L \cdot \cosh\lambda L - U_1 + U_2 - U_3$$

$$= 0 \qquad (C2)$$

$$\left.\frac{d\varepsilon_\theta}{dS}\right|_{\pm L} = A_1 \left[\cos\lambda L \cdot \sinh\lambda L + \sin\lambda L \cdot \cosh\lambda L\right] + A_4 \left[\cos\lambda L \cdot \sinh\lambda L - \sin\lambda L \cdot \cosh\lambda L\right]$$

$$= 0 \qquad (C3)$$

From equation (C2)

$$A_1 = \frac{-A_4 \cos\lambda L \cdot \cosh\lambda L + U_1 - U_2 + U_3}{\sin\lambda L \cdot \sinh\lambda L}$$

Substituting into equation (C3) and expanding

$$-A_4 \left[(\cos^2\lambda L + \sin^2\lambda L)(\cosh\lambda L \cdot \sinh\lambda L) + (\cos\lambda L \cdot \sin\lambda L)(\cosh^2\lambda L - \sinh^2\lambda L)\right]$$

$$+ (U_1 - U_2 + U_3)(\cos\lambda L \sinh\lambda L + \sin\lambda L \cosh\lambda L)$$

$$= 0$$

from which

$$A_4 = 2(U_1 - U_2 + U_3)\left[\frac{\cos\lambda L \cdot \sinh\lambda L + \sin\lambda L \cdot \cosh\lambda L}{\sinh 2\lambda L + \sin 2\lambda L}\right]$$

and by substituting for A_4 into equation (C2)

$$A_1 = 2(U_1 - U_2 + U_3)\left[\frac{\sin\lambda L \cdot \cosh\lambda L - \cos\lambda L \cdot \sinh\lambda L}{\sin 2\lambda L + \sinh 2\lambda L}\right]$$

Substituting the values for A_1 and A_4 into equation (C1) and setting S = 0, the maximum circumferential force and meridional moment are given by

$$\delta N_{\theta MAX} = tE_\theta \varepsilon_{\theta MAX}$$

$$= -\frac{N_\phi^P \xi_i R}{L^2}\left\{\frac{4/3\,\pi\alpha}{\pi^4+\alpha}(1+\mu_2) + \frac{\pi^2\alpha}{16\pi^4+\alpha}(1-\mu_2) + \frac{12/5\,\pi\alpha}{81\pi^4+\alpha}(1+\mu_2)\right\}$$

$$\delta M_{\phi MAX} = RK\phi \frac{d^2\varepsilon_\theta}{dS^2}$$

$$= N_\phi^P \xi_i \left\{\frac{4/3\,\pi^3}{\pi^4+\alpha}(1-\mu_1) + \frac{88/7\,\pi^3}{16\pi^4+\alpha}\left(1+\frac{\mu_1}{4}\right) + \frac{108/5\,\pi^3}{81\pi^4+\alpha}\left(1-\frac{\mu_1}{9}\right)\right\}$$

where

$$\mu_1 = \sqrt{\frac{4\alpha}{\pi^2}} \cdot \frac{\sin\lambda L \cdot \cosh\lambda L - \cos\lambda L \cdot \sinh\lambda L}{\sin 2\lambda L - \sinh 2\lambda L}$$

$$\mu_2 = \frac{\cos\lambda L \cdot \sinh\lambda L + \sin\lambda L \cdot \cosh\lambda L}{\sinh 2\lambda L + \sin 2\lambda L}$$